THE UNIVERSITY OF HULL

EVAPORATION OF LIQUIDS FROM STRUCTURED AND NON-STRUCTURED MIXTURES

being a thesis submitted in partial fulfillment of the requirements for the Degree of

Doctor of Philosophy

in the University of Hull

by

Katharine Jane Beverley B.Sc

ABSTRACT

The work presented in this thesis describes the evaporation rates of a wide variety of samples obtained under a controlled gas flow using a gravimetric technique. Evaporation rates for pure liquids with vapour pressures ranging from 0.1 to 500 Torr, water contained in silica particles, alkane/squalane mixtures, hexane gelled with silica particles, surfactant/water mixtures, immiscible layered liquid mixtures and emulsions have been determined. For pure liquids and simple unstructured liquid mixtures, the evaporation rate is limited by diffusion through a stagnant vapour layer at the liquid surface. As the degree of structure within the liquid mixture increases, the time taken for concentration gradients developing in the evaporation process to relax becomes longer relative to the time taken for diffusion through the stagnant vapour layer. For highly structured liquid mixtures, the rate limiting process switches to diffusion and convection within the liquid mixture. In the case of creamed oil-in-water emulsions, evaporation of the continuous water phase is limited by diffusion through the stagnant vapour layer, whilst the evaporation rate of the emulsified oil is consistent with a mechanism in which the oil drops remain separated from the vapour phase by a thin water film. Oil transport from the drops to the vapour occurs by diffusion of dissolved oil across this film.

ACKNOWLEDGEMENTS

A number of people deserve a special mention.

Firstly, I would like to thank my two supervisors, Dr. John Clint, and particularly Professor Paul Fletcher, both of whom have offered me advice and support, and have shown an incredible amount of patience throughout my three years of experimental work and the protracted writing-up period!

The generosity of the University of Hull and Reckitt Benckiser is gratefully acknowledged. Particular thanks go to Dr. Malcolm McKechnie for useful discussions.

Thanks to the members of the Surfactant Science and Colloid Group (past and present) for helping me through the many long dark teatimes of the soul with the odd pint. In particular, thanks to Steven Bird, Richard Nicholls, Sally Rippon, Elayne Carroll, Alex Bismarck, Simon Lumsdon, Chris Bottrill, Ibon Aranberri, Tim Dunstan, Berndt Neumann and Matt Haynes. Thanks also to my final year project students, Sarah Thubron and Luke Ireland, who had a significant input to some of the work presented here.

I am very appreciative of the support offered by my friends. Thanks to Dr. I., Adam, Warren, Janice, Fletch, Tina N., Tina O., Jean, Richard, Tucky, Vince, Beckie, Mark, Mo, Stevie T. and the two Grahams (in Hull) and to Alex, Greg. Neil and especially Stewart (in Ireland).

My family has been extremely supportive throughout my university career and I owe them a great deal. This thesis is dedicated to them.

Last, but very definitely not least, a special vote of thanks to Dr. Bernie Binks, whose own inimitable brand of encouragement kept me going when it got tough.

PUBLICATIONS AND CONFERENCE PARTICIPATIONS ARISING FROM THIS THESIS

The work presented in this thesis has resulted in the following publications and conference papers;

Publications

1. "Evaporation rates of pure liquids measured using a gravimetric technique." K. J. Beverley, J. H. Clint and P. D. I. Fletcher, *Phys. Chem. Chem. Phys.*, 1999, **1**, 149.
2. "Evaporation rates of water contained within porous silica particles." K. J. Beverley, J. H. Clint, P. D. I. Fletcher and S. Thubron, *Phys. Chem. Chem. Phys.*, 1999, **1**, 909.
3. "Evaporation rates of structured and non-structured liquid mixtures." K. J. Beverley, J. H. Clint and P. D. I. Fletcher, *Phys. Chem. Chem. Phys.*, 2000, **2**, 4173.
4. "How do emulsion drops evaporate?" I. Aranberri, K. J. Beverley, B. P. Binks, J. H. Clint and P. D. I. Fletcher, *Langmuir*, 2002, **18**, 3471.

Conference Papers

1. "Evaporation from non-structured and structured liquids." *International Association of Colloid and Interface Scientists Conference*, Bristol, 2000.

INDEX OF FIGURES AND TABLES

FIGURES

CHAPTER 1 INTRODUCTION

CHAPTER 2 EXPERIMENTAL MATERIALS AND METHODS

CHAPTER 3 EVAPORATION RATES OF PURE LIQUIDS

CHAPTER 4 EVAPORATION RATES OF NON-STRUCTURED AND STRUCTURED LIQUID MIXTURES

CHAPTER 5 EVAPORATION RATES OF IMMISCIBLE LAYERED LIQUID MIXTURES AND EMULSIONS

CONTENTS

CHAPTER 6 CONCLUSIONS AND SUGGESTIONS FOR FURTHER WORK

CHAPTER 1

INTRODUCTION

This study is concerned with the evaporation of volatile species from a variety of systems ranging from the pure liquid state to complex colloidal dispersions such as emulsions. In this introductory chapter, the motivations behind the study are outlined. A brief literature review is given for each of the areas studied in this thesis, and relevant theory is outlined.

1.1 Motivation for this study

The overall aim of the study was to gain a fundamental understanding of the relationship between the rate of release by evaporation of volatile species and the colloidal microstructure of the formulation. Such an understanding has obvious relevance to many practical applications including the assessment of hazards arising from volatile chemical spills[1-3], the release of volatile active components from commercial products[4], the control of evaporation by absorbed monolayers[5] and entrapment of the liquid within a colloidal microstructure[6]. Previous work in this field has been limited by a lack of quantitative results. The experimental technique described here allows direct quantitative measurement of evaporation rates, thereby enabling a more complete theoretical analysis.

1.2 Previous work on evaporation rates

1.2.1 Evaporation rates of pure liquids

The first theoretical model for the isothermal evaporation rate of pure water was developed by Dalton in 1834[7]. Dalton predicted that the driving force for the evaporation process was the difference between the equilibrium saturated vapour pressure of the water and its partial pressure in the environment. The relationship is given by

$$J = C(P - P_a) \qquad [1.1]$$

where J is the evaporation flux, C is the evaporation rate coefficient, P is the water vapour pressure and P_a is the partial pressure of the water vapour in air.

In the 1920's, J. N. Hinchley and G. W. Himus carried out a series of experiments to evaluate the evaporation coefficient in still air[8] and in turbulent currents of air[9] using evaporating pans contained within a duct. The evaporation rate was found to show a complex and irreproducible dependency on the gas flow rate and the streamwise length of the evaporating pan. It was suggested that this irreproducibility might be the result of edge effects in which the horizontal flowing stream of gas caught on the edge of the pan, giving complex flow patterns above the liquid and disturbing the surface.

This was supported by the fact that the ripples on the liquid surface which were always seen at higher flow rates corresponded with an increased evaporation rate. In 1943 Pasquill investigated the influence of the nature of the gas flow on evaporation rates[10] and found that rates were more predictable under laminar flows, where no surface agitation occurred. The evaporation rates of a range of volatile organic liquids have also been studied using the evaporating pan technique[11-15]and the results have been fitted to Equation [1.1] in an empirical way. Although evaporation rates from other geometries such as wetted wall columns[16] and liquid droplets[17] have been reported in the literature, the method of Hinchley and Himus remains the most consistently used method for determining evaporation rates of pure liquids.

The work of Prata and Sparrow on the evaporation of volatile liquids from an open-topped, partially filled container into a horizontal air stream[18] is of particular relevance to this study, owing to the similarity with the geometry used in this thesis (outlined in Chapter 2). In this study, the evaporation rates of cumene and toluene were measured, and a complex dependency was seen both on the nature of the gas flow and the distance between the liquid surface and the top of the container. This study is discussed further in Chapter 3.

The main advantage of using the experimental equipment outlined in Chapter 2 for the measurement of pure liquid evaporation rates is that the design minimises the edge effects seen in previous experiments by using a vertically flowing gas stream.

1.2.2 Evaporation rates from porous solids

Evaporation rates from liquids entrapped in a porous solid are of interest from a number of viewpoints including the assessment of hazards arising from the spillage of volatile liquids when soaked up by an absorbent solid[19], drying processes[20], the release of agrochemicals from soils[21] and the controlled release of volatile components from commercial products by entrapment within porous ceramic materials[4].

Several methods have been developed to investigate evaporation from porous solids. In their paper of 1998, Goia *et al*[22] used a technique in which a packed porous solid column of known dimensions was suspended above a pan of the evaporating liquid. The system was supported upon a balance and enclosed so that any mass loss could be attributed to the volatile liquid passing through the porous solid and escaping into the atmosphere. The mass loss of the system with time was recorded directly. The work of Laurindo and Prat[23] was based on a completely saturated two-dimensional transparent etched network consisting of approximately 39,000 ducts with seven classes of width ranging from 0.1 to 0.6 mm distributed at random.

The liquid evaporated through an upper diffusive layer in which the dominant transfer mechanism was vapour diffusion in the gas phase. The variation of the network weight with time was recorded directly. Simple pan methods, similar to those used for the evaporation of pure liquids have also been used. Kondo and Saiguso[24] describe results from an experiment in which water was evaporated from a pan of soil of depth 0.1 m and diameter 0.3 m under laboratory conditions.

Although Laurindo and Prat[23] and Ho and Webb[25] have investigated the existence of enhanced vapour diffusion for systems containing liquid islands, no particular consideration has been given to vapour pressure lowering due to the Kelvin effect within pores. In most cases, heat and mass transfer effects have been too large to detect the smaller Kelvin effects. In addition, the porous materials considered in these experiments have contained a wide range of pore diameters, and in many cases, the pore diameters have been too large to show any significant Kelvin effects. The experiments described in Chapter 3 are designed to study these phenomena.

1.2.3 Evaporation rates from unstructured liquid mixtures

A comprehensive literature search has revealed no previous studies on the free evaporation of mixtures of volatile liquids. However, Goia *et al*[22] have investigated the evaporation rates of ideal and non-ideal mixtures of hydrocarbons from a porous network.

For the case of the ideal mixture of n- hexane, n-heptane, n-nonane and n-decane, the rate of evaporation was well predicted by taking into account the molar concentrations of the liquids within the mixture throughout the experiment. For the non-ideal mixture of acetone and hexane, the evaporation rate was found to be highly dependent on both the activity coefficients and mole fractions of the liquids within the mixture.

1.2.4 Evaporation rates from structured liquid mixtures

Evaporation through surfactant monolayers

The first noted scientific study on the effect of surfactant monolayers on the evaporation rate of water was that of Hedenstrand in 1924[26]. Although Hedenstrand's initial study showed that the presence of a fatty acid monolayer on the water surface made no difference to the evaporation rate of water, interest in the subject remained and just one year later, Rideal showed qualitatively that the presence of a fatty acid monolayer at a water/ air interface decreased the evaporation rate of water[27]. It was not until 1943 that quantitative measurements were finally achieved by Langmuir and Schaefer[28]. They were able to show that Hedenstrand's experiments failed due to the presence of a stagnant layer above the surface of the liquid. Diffusion through this vapour layer had a greater inhibiting effect than the presence of a monolayer, and the thickness of the vapour layer varied between experiments, masking any monolayer effects.

Langmuir and Schaefer developed a simple apparatus consisting of a dessicant held above a surface balance trough filled with water. The change in weight of the dessicant over a specified time was measured for water with and without the monolayer and the total evaporation resistance, R_t was calculated from

$$R_t = a(w_w - w_d)\left(\frac{t}{m_f} - \frac{t}{m_w}\right) \qquad [1.2]$$

where a is the surface area of the water beneath the dessicant, w_w and w_d are the concentrations of water vapour in equilibrium with the water and dessicant respectively and t/m is the reciprocal evaporation rate. The subscripts f and w refer to the surface with and without the monolayer respectively.

In 1940, Sebba and Briscoe found that the evaporation resistance of the surfactant monolayer showed a large dependence on the monolayer surface pressure[29] and this was supported by the work of Langmuir and Schaefer. However, in 1954, Archer and La Mer published results which indicated that these variations were due to contamination of the surface[30] and that evaporation resistance showed no dependence on surface pressure. Archer and La Mer postulated that the resistance to evaporation was the result of an energy barrier to water droplets entering the surface. The energy barrier theory was supported by the fact that evaporation retardation has only been observed for monolayers of long hydrocarbon chain, water insoluble species at very high surface concentrations[31] and their mixtures[32, 33].

The energy barrier theory is now widely accepted and has been used by Barnes and Quickenden to develop a theoretical model which explains the observed exponential dependence of the evaporation resistance on the surfactant chain length[34]. Other theories such as the density fluctuation theory[35, 36] and the accessible area theory[37] have been postulated, but the energy barrier theory remains the most widely supported.

The use of monolayers to reduce evaporation from stored water supplies in warm countries has been well researched. In the early 1950s, W. W. Mansfield attempted to scale up the laboratory experiments of Languir and Schaefer by spreading a water insoluble monolayer over the surface of a reservoir[38] This experiment met with limited success for three reasons. Firstly, monolayers are easily destroyed by wind and waves. Secondly, the surfactant monolayer also increases the water surface temperature[39]. Finally, at higher temperatures, condensed monolayers begin to expand and become more permeable to water[40].

Research has been carried out into retarding the evaporation of volatile organic compounds by monolayers[41]. Some long-chain fluorocarbon surfactants will form condensed insoluble monolayers on hydrocarbon surfaces, and have been shown to slightly retard the evaporation of the hydrocarbon. However, the expense of fluorocarbon surfactants, coupled with the slight effects seen means that this research has not been followed up.

Evaporation from emulsions and other microstructured liquids

Friberg and co-workers have studied evaporation from emulsions extensively, and have recently turned their interests to evaporation from other microstructured liquid mixtures. This work has been covered in depth in several reviews[42, 43] and findings will be discussed briefly here.

The experimental apparatus used by Friberg consists of a watch-glass spread with a thin layer of emulsion or surfactant solution. The watch-glass is placed on a balance under a constant horizontal air flow and the weight loss is measured as a function of time. The area of the emulsion layer is measured several times within the experiment and a calibration curve is constructed. The slope of the weight loss versus time plot is then divided by the corresponding area to give the loss rate per unit area. The evaporation measurements take place at ambient temperature. This experimental apparatus is very different to that outlined in this study. Firstly, in the experimental system described in Chapter 2, emulsions are evaporated from a significant depth. Secondly, the area of the evaporating sample remains constant throughout the course of the experiments. Finally, in the experiments shown here, the temperature and gas flow rate are tightly controlled. Whilst Friberg's group have investigated the bulk evaporation rate of the whole emulsion, this study has developed a technique in which the evaporation rate of the continuous phase and dispersed phase can be measured separately. This allows quantitative determination of the energy barrier to evaporation of oil droplets from emulsions.

Friberg has investigated the evaporation of three types of oil-in-water emulsion[44]. The first emulsion contained an oil which was more volatile than water (cyclohexane), the second an oil of comparable volatility to water (decane) and the third an oil of lower volatility than that of water (hexadecane). For the emulsion containing the more volatile oil, it was found that the evaporation rate was highly dependent on the composition of the emulsion, and was intermediate between that of the oil and water. For the emulsion containing an oil of similar vapour pressure to that of water, the evaporation rate was found to be almost independent of oil vapour pressure. For the emulsion where the vapour pressure of the oil was lower than water, the evaporation rate was found to be approximately equal to that of bulk water. In this case, as evaporation proceeded, phase inversion occurred to give a water-in-oil emulsion and the evaporation rate slowed significantly.

Comparison of oil-in –water emulsion evaporation rates with system phase diagrams has indicated that the evaporation of the emulsion is significantly slowed by the presence of a lamellar liquid crystal structure[45]. This finding supports earlier work by Eccleston[46] in which the evaporation of water from a ternary CTAB/ water system was correlated with changes in the low angle x-ray diffraction pattern of the system. It was found that the evaporation proceeded rapidly initially, with little change in the interlamellar distance, and slowed as the interlamellar distances shortened.

Studies of more complicated ternary and quaternary emulsion systems[47-50] have also been carried out by Friberg's group. In these cases, the evaporation characteristics of the emulsion have been compared with the vapour pressure of the volatile evaporating species. The vapour pressures were measured using headspace chromatography. For ternary systems and quaternary systems where there are no strong interactions between evaporating species, vapour pressures have been found to remain approximately constant during the evaporation process[42, 47]. However, for systems where there are strong interactions between two evaporating components, there may be significant fluctuations in vapour pressure during the evaporation process[43].

A legal restriction on the use of volatile organic compounds in perfumes has led to a good deal of interest in the evaporation of fragrance compounds from aqueous solubilised systems. Studies into the vapour pressure of solubilised species have been carried out for micellar solutions[51], microemulsions[52-54], liposome solutions[55] and lyotropic liquid crystals[48].

For micellar solutions, the vapour pressures of hydrocarbons solubilised in aqueous micelles were higher when solubilised in anionic or cationic surfactants than when solubilised in non-ionic surfactants[51]. The vapour pressure also increased with decreasing surfactant chain length. These variations were attributed to the position of the solubilised compound within the micelle. Evaporation rates of water from micellar solutions have not previously been studied.

Vapour pressure studies in microemulsions have mainly been concerned with water vapour pressures in water – in – oil microemulsions[56]. Recent work by Clint, Fletcher and Todorov has determined the water evaporation rate from water-in-dodecane microemulsions stabilised with AOT using experimental apparatus based on that described in this study[57]. The water evaporation rate is described well by a mechanism in which diffusion of water droplets through the microemulsion is the rate determining process.

1.3 Theoretical considerations relevant to evaporation rates

1.3.1 The maximum theoretical rate of evaporation

For a pure liquid where there are no external resistances or barriers to evaporation, the maximum rate of evaporation can be calculated using the kinetic theory of gases[58]. For a liquid in equilibrium with its vapour, the number of molecules striking and condensing with the surface from the vapour must be equal to the number evaporating. Figure 1.1 shows a surface of area A perpendicular to the x-axis which is exposed to a gas. All gas molecules travelling towards the surface within the volume $A v_x \Delta t$, where v_x is a positive velocity in the x direction and Δt is a time interval, will strike the surface within Δt.

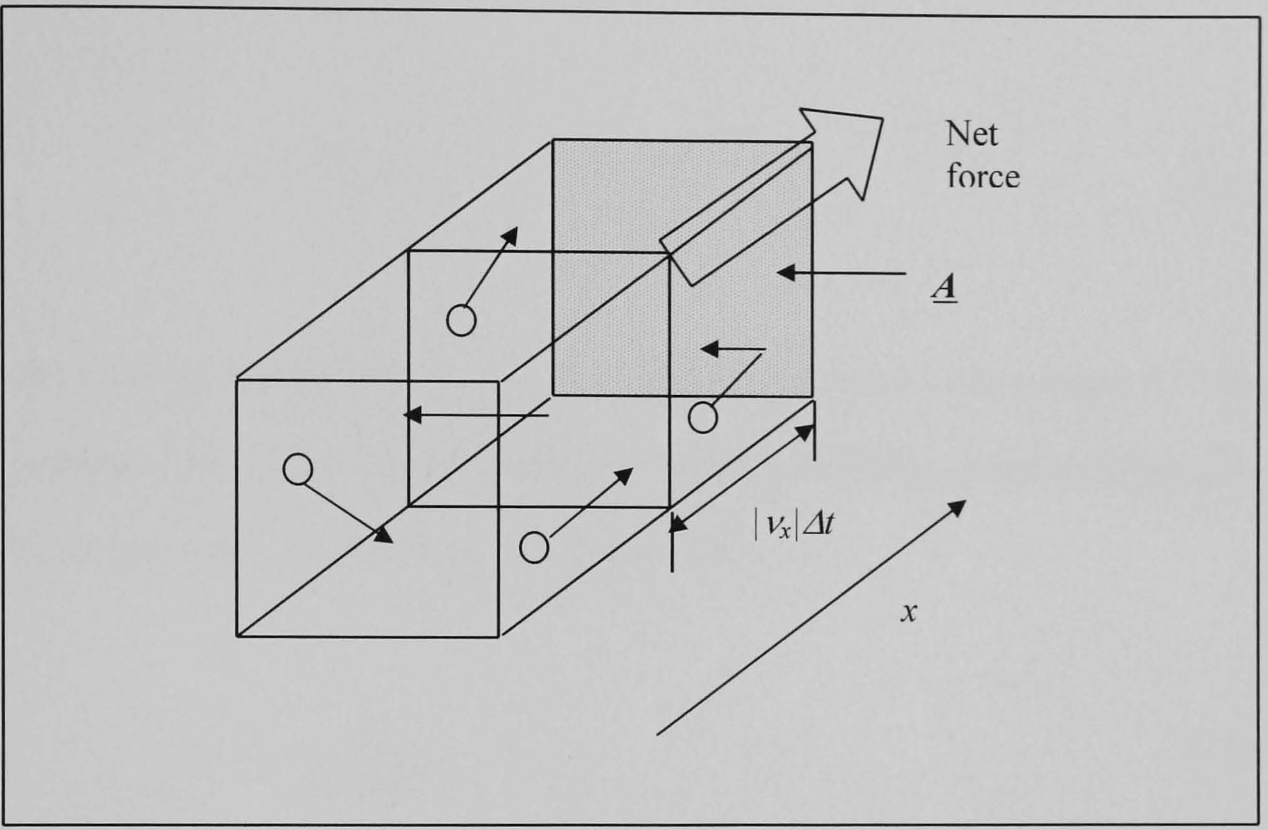

Figure 1.1 Pictorial representation of the kinetic theory of gases

The total number of collisions per unit time per unit area, Z, is given by

$$Z = NA\Delta t \int_0^\infty v_x f(v_x) dv_x \qquad [1.3]$$

where N is the number density of the molecules.

The integral can be evaluated using the Maxwell distribution to give

$$\int_0^\infty v_x f(v_x) dv_x = \left(\frac{kT}{2\pi m}\right)^{\frac{1}{2}} \qquad [1.4]$$

where k is the Boltzmann constant and m is the mass of a molecule.

Using the relationship

$$N = \frac{nN_A}{V} = \frac{P}{kT} \qquad [1.5]$$

where n is the number of moles, N_A is Avogadros constant, V is the volume, P is the pressure of the gas and T is the absolute temperature, a final expression relating Z to the pressure and temperature of the gas becomes

$$Z = \frac{P}{\sqrt{2\pi mkT}} \qquad [1.6]$$

For the evaporation process, it is assumed that a fraction σ of the molecules striking the surface condenses with it. For evaporation into a perfect vacuum, σ is assumed to be 1 and the maximum possible evaporation flux $J_{\max}$ (in mol s^{-1} m^{-2}) is given by

$$J_{\max} = \frac{P}{\sqrt{2\pi MRT}} \qquad [1.7]$$

where P is the vapour pressure at the liquid surface (assumed to be the equilibrium vapour pressure), M is the molecular weight, R is the gas constant and T is the absolute temperature.

For pure water at 20 °C, P is 2326 Pa[59] and M is 0.018 kg mol^{-1}. J_{max} is therefore 140 mol s^{-1} m^{-2}, which corresponds to a rate of loss of water depth from a surface of unit area by evaporation of approximately 2.5 mm s^{-1}.

1.3.2 Fick's Laws of diffusion

In practice, the evaporation rate of a liquid is lower (by many orders of magnitude) than this theoretical upper limit due to various resistances or barriers to the evaporation process. Commonly, the major resistance arises from the presence of a "stagnant" gaseous layer close to the surface across which the vapour must diffuse. If only flux in the x direction (i.e. perpendicular to the liquid surface) needs to be considered, the instantaneous flux at any point in the vapour layer is given by Fick's first law of diffusion.

$$J = -D\frac{\partial c}{\partial x} \qquad [1.8]$$

where D is the diffusion coefficient of the vapour through the stagnant layer gas and c is the concentration of the diffusing vapour at position x.

Fick's second law of diffusion describes the time dependence.

$$\frac{\partial c}{\partial t} = D\frac{\partial^2 c}{\partial x^2} \qquad [1.9]$$

Diffusion coefficients for specific systems can be determined using the Stefan cell[60].

1.3.3 Deviations from Fick's Laws

Under certain experimental conditions, significant deviations from Fick's laws are seen. Of particular interest in this study are deviations due to high evaporation rates and deviations due to the fluid flow conditions over the surface of the liquid.

Deviations due to high evaporation rates

At high evaporation rates, deviations from Fick's Laws are seen, since evaporation leads to a cooling of the liquid surface and a consequent reduction of the vapour pressure. Under these circumstances, the evaporation rate is linked to the rate of heat transfer in the surface region. These factors have been considered in detail in the chemical engineering literature[60, 61].

Deviations due to fluid flow conditions

Briefly, fluid flow can be classified in a number of ways, but for the evaporation process, the most important distinction is that between laminar and turbulent flow. In laminar flow, adjacent layers of gas molecules "slide" over one another and there is no interaction between individual molecules. Under laminar flow conditions, evaporation occurs through molecular mass transfer. This is the result of the thermal motion of the molecules and is well defined by Fick's laws of diffusion.

In turbulent flow, adjacent layers of molecules move with differing velocities and interaction occurs between molecules. Under turbulent flow conditions, evaporation occurs through convective mass transfer and is dependent on the properties of the fluid stream, the dynamic characteristics of the fluid flow and the geometry of the system. The nature of the fluid flow can be determined from the Reynolds number for the system. The Reynolds number is a ratio of the inertial forces and viscous forces within a fluid given by

$$N_R = \frac{\rho L v}{\eta} \qquad [1.10]$$

where ρ is the density of the fluid, v is the flow velocity, L is a characteristic length descriptive of the flow field and η is the dynamic viscosity of the fluid. The transition from laminar to turbulent flow occurs at the critical Reynolds number, which is dependent on the geometry of the system.

An approximation of the critical Reynolds number can be made using equations developed for standard geometrical models[61].

1.4 Theory of evaporation rates of more complex liquid systems

In general, evaporation is limited by one of three processes. Firstly, vapour diffusion across the stagnant layer above the liquid surface may be rate-determining. In this case, the evaporation rate is expected to be accurately predicted by the application of Fick's Laws. Secondly, there may be a significant energy barrier to the process of evaporating molecules leaving or entering the liquid surface. Thirdly, the evaporation of a volatile species from a multi-component liquid mixture may generate concentration gradients within the liquid and therefore mass transfer within the liquid may be rate determining. In this section, the complex systems investigated in the study are outlined. Vapour pressure considerations for the systems are given for all systems. Other factors which may influence the evaporation rates are also discussed.

1.4.1 Liquids contained within porous solids

Vapour pressure considerations

In the case of a pure liquid contained within a porous solid, evaporation cannot induce concentration gradients within the liquid. Assuming that diffusion through the stagnant vapour layer at the liquid surface is the rate-determining process, from Fick's Laws it can be seen that the evaporative flux is dependent on the concentration of the vapour at the liquid surface.

Since, assuming ideality, $c_s = P/RT$ the evaporative flux is dependent on the vapour pressure of the evaporating species. A liquid contained within the narrow pores of a solid will have a curved surface with a curvature dependent on the pore radius, r and the contact angle, θ, as shown in Figure 1.2.

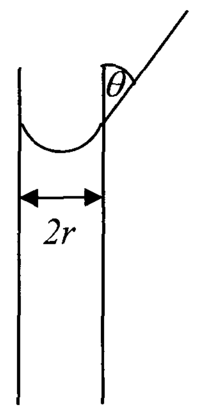

Figure 1.2 ***The curvature of the surface of a liquid with contact angle θ contained in a pore of radius r***

The pressure difference across a curved surface can be predicted by the Young-Laplace Equation.

Derivation of the Young-Laplace Equation[62]

The Young-Laplace Equation can be derived by considering a spherical bubble of radius r, as shown in Figure 1.3. The pressure outside the bubble is P' whilst that inside the bubble is P''.

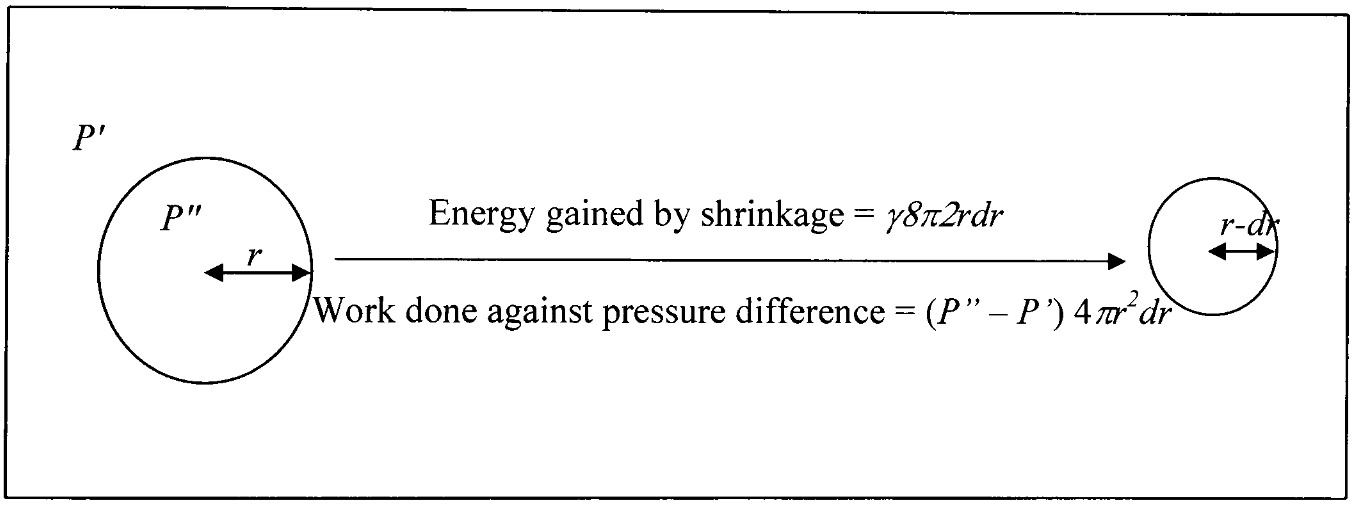

Figure 1.3 Work done in compressing a bubble of radius r

If this bubble is shrunk, the energy gained by shrinking the size of the bubble must be equal to the work done in compressing the air inside in order to maintain equilibrium. The energy gained by shrinkage is given by γdA where γ is the surface tension and A is the area of both the inside and the outside of the bubble film ($=2 \times 4\pi r^2$).

The work done against the pressure difference is $(P''-P')$ x A x the distance through which the bubble shrinks. Therefore, at equilibrium

$$\gamma da = \gamma 8\pi 2r dr = (P''-P')4\pi r^2 dr \qquad [1.11$$

which simplifies to

$$P''-P' = \frac{4\pi}{r} \qquad [1.12]$$

for a bubble.

The corresponding formula for a drop of liquid, which has only one surface, is the Young-Laplace equation.

$$P''-P' = \frac{2\gamma}{r} \qquad [1.13]$$

This form of the Young-Laplace equation applies only to spherical surfaces. When the liquid surface is curved but not spherical, it is necessary to specify the curvature in terms of two radii r_1 and r_2, measured as shown in Figure 1.4. The triangle *CXD* is at right angles to the curve *AXB*. The sum of the inverse radii $1/r_1$ and $1/r_2$ gives the mean curvature of the surface, *J'*.

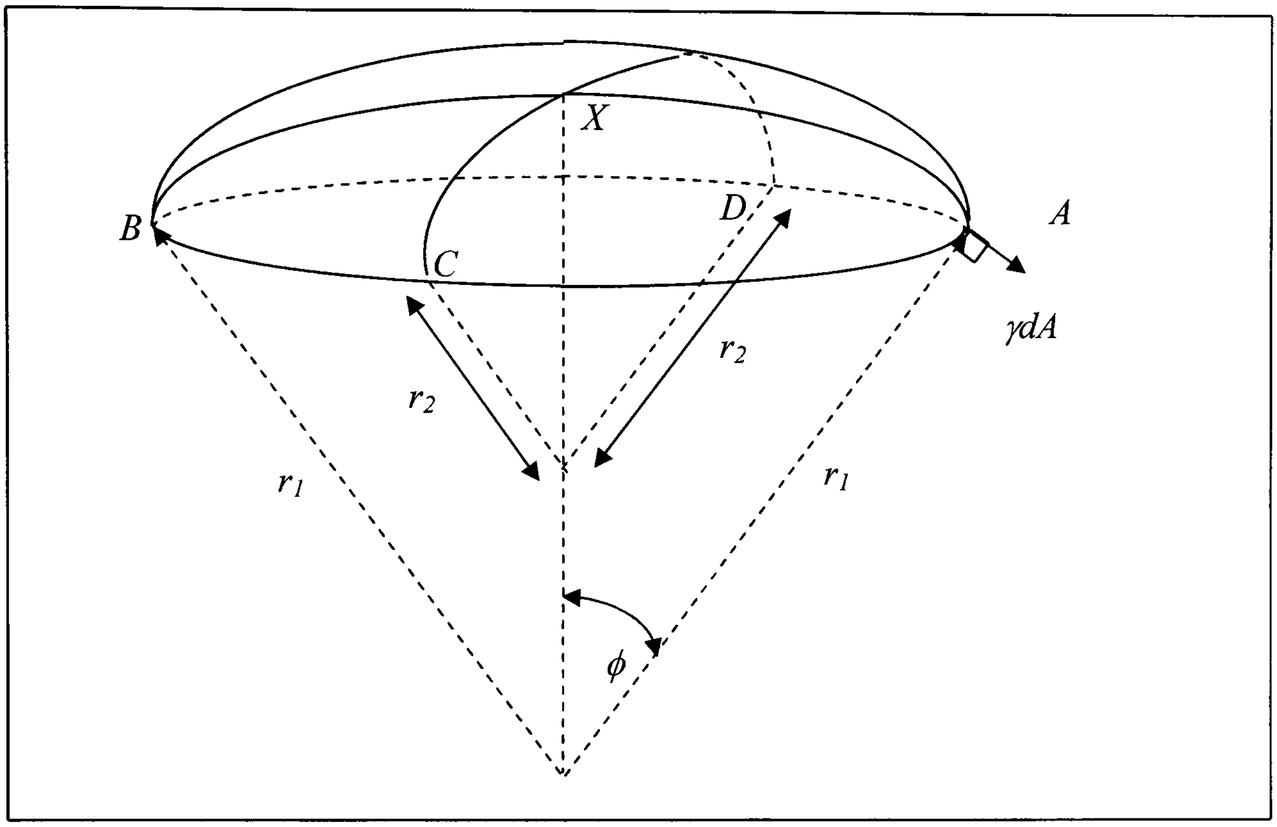

Figure 1.4 Defining the curvature of a surface at point X

As the orientation of the curve *AXB* changes, the value of r_1 also changes until at one particular orientation it reaches a maximum value of R_1. The value of r_2 at this point is a minimum, R_2, and

$$\frac{1}{r_1}+\frac{1}{r_2}=J'=\frac{1}{R_1}+\frac{1}{R_2} \qquad [1.14]$$

where R_1 and R_2 are the principal radii of curvature of the surface.

Therefore, the form of the Young-Laplace equation applied to curved surfaces becomes

$$P''-P'=\gamma\left(\frac{1}{R_1}+\frac{1}{R_2}\right) \qquad [1.15]$$

The Young-Laplace Equation predicts that the pressure on the concave side of a curved surface is always greater than that on the convex side. For a wetting liquid contained in the narrow pores of a solid, the pressure under the meniscus is therefore predicted to be less than that below a flat surface. The consequence of this decreased pressure is a reduction of the vapour pressure of the liquid. The difference in vapour pressure across a curved surface is given by the Kelvin Equation

Derivation of the Kelvin Equation[63]

For a liquid in equilibrium with its vapour, the chemical potentials of the liquid and the vapour are the same. For any change in which the equilibrium is preserved, the change in the chemical potential of one species is equal to the change in the other. When the pressure on the liquid is increased by $dP(l)$ its chemical potential changes by $V_m dP$, where V_m is the molar volume of the liquid. The accompanying change in the pressure of the vapour, $dP(g)$ corresponds to a change in the chemical potential of $V_m(g)dP(g)$ where $V_m(g)$ is the molar volume of the gas. At constant temperature, therefore,

$$V_m(g)dP(g) = V_m dP(l) \qquad [1.16]$$

Assuming the vapour behaves as a perfect gas, $V_m(g) = RT/P(g)$ and Equation [1.16] becomes

$$\frac{dP(g)}{P(g)} = \frac{V_m dP(l)}{RT} \qquad [1.17]$$

When no additional pressure acts on the liquid, its pressure and that of the vapour are both equal to the equilibrium vapour pressure, P. When an additional pressure is applied to the liquid so that $P(l) = P+\Delta P$, the vapour pressure changes from P to P'. If the molar volume of the liquid is assumed to remain constant over a small pressure range, Equation [1.17] can be integrated between these limits to give

$$\ln\frac{P'}{P} = \left\{\frac{V_m}{RT}\right\}\{P + \Delta P\} - P = \frac{V_m \Delta P}{RT} \qquad [1.18]$$

Therefore,

$$P' = Pe^{\left\{\frac{V_m \Delta P}{RT}\right\}} \qquad [1.19]$$

Equation [1.19] predicts that the vapour pressure of the liquid increases when the pressure acting on the liquid increases.

The Young-Laplace Equation states that the pressure difference across a spherically curved surface is given by $\gamma(1/R_1 + 1/R_2)$. Substituting this value for ΔP in Equation [1.19] gives the Kelvin Equation for the vapour pressure of a liquid when it is dispersed as droplets of radius r.

$$P' = Pe^{\frac{\gamma V_m}{RT}\left(\frac{1}{R_1}+\frac{1}{R_2}\right)} \qquad [1.20]$$

For a liquid below a concave meniscus, the pressure of the liquid is less than that below a flat surface and hence the sign of the exponent changes.

$$P' = Pe^{\frac{-\gamma V_m}{RT}\left(\frac{1}{R_1}+\frac{1}{R_2}\right)} \qquad [1.21]$$

For a liquid contained within a circular pore of a solid, the principal radii of curvature can be estimated to be

$$R_1 = R_2 = \frac{r}{\cos\theta} \qquad [1.22]$$

where r is the radius of the pore and θ is the contact angle made by the liquid on the porous solid material.

Therefore, the appropriate form of the Kelvin Equation is

$$P' = Pe^{-\frac{2\gamma V_m}{RT(r/\cos\theta)}} \equiv \ln\left(\frac{P'}{P}\right) = -\frac{2\gamma v_m}{RT(r\cos\theta)} \qquad [1.23]$$

If diffusion through the stagnant vapour layer above the liquid surface is the rate-determining step, Fick's Laws predict that the reduction in vapour pressure at the liquid surface will give a reduction in the evaporation rate of the liquid contained within the porous solid. Furthermore, from Equation [1.23], the reduction in vapour pressure increases as the radius of the pores decreases. These Kelvin effects are of particular interest when considering the use of porous solids to 'soak up' spillages of hazardous chemicals[19].

1.4.2 Unstructured liquid mixtures

Vapour pressure considerations

For a liquid in equilibrium with its vapour, the chemical potential of the liquid and the vapour must be the same.

The chemical potential of a gas at a pressure P is given by

$$\mu' = \mu^o + RT\ln\frac{P}{P^o} \qquad [1.24]$$

where μ^o is the standard chemical potential of the gas and P^o is standard pressure.

The chemical potential of pure liquid 1 in the vapour is therefore given by

$$\mu_1(l) = \mu_1^o + RT\ln\left(\frac{P_1}{P^o}\right) \qquad [1.25]$$

where P_1 is the vapour pressure of liquid 1.

If liquid 1 is in a mixture with several components, its chemical potential remains equal to that of its vapour, but its vapour pressure becomes P'_1 and therefore

$$\mu_1 = \mu_1(l) + RT\ln\left(\frac{p'_1}{P_1}\right) \qquad [1.26]$$

In an ideal solution, Raoult's Law states that the ratio of the vapour pressure of a component in the solution and the bulk vapour pressure is proportional to the mole fraction of the component in the liquid.

For component 1

$$P_1' = P_1 x_1 \qquad [1.27]$$

where x_1 is the mole fraction of liquid 1 in the mixture.

Combination of Equations [1.26] and [1.27] yields an expression for the chemical potential of liquid 1 in an ideal solution.

$$\mu_1 = \mu_1(l) + RT\ln x_1 \qquad [1.28]$$

Although mixtures of chemically similar liquids obey Raoult's Law very well, as the two components become more dissimilar, significant deviations may be seen. However, even for mixtures of two chemically dissimilar species, Raoult's Law is obeyed increasingly closely for the solvent as it approaches purity, making this a good approximation for dilute solutions.

In ideal solutions, the solute also obeys Raoult's Law. In real solutions, although the vapour pressure of the solute is found to be proportional to its mole fraction at low concentrations, the constant of proportionality is no longer equal to the vapour pressure of the pure substance. The linear dependence of the solute vapour pressure on mole fraction is given by Henry's Law.

If component 2 is taken to be the solute

$$P'_2 = K_2 x_2 \qquad [1.29]$$

where K_2 is a constant chosen so that the plot of vapour pressure of component 2 against its mole fraction is tangential to the experimental curve at $x_1 = 0$.

For a solution obeying Raoult's Law, the chemical potential of component 1 is given by Equation [1.27]. The form of this equation can be preserved for solutions deviating from Raoult's Law by introducing the activity of the species. For component 1 of the mixture

$$\mu'_1 = \mu_1(l) + RT \ln a_1 \qquad [1.30]$$

where a_1 is the activity of component 1.

A definition of the activity can be obtained by considering Equations [1.26] and [1.30]. Since Equation [1.26] applies to both ideal and real solutions,

$$a_1 = \frac{P'_1}{P_1} \qquad [1.31]$$

In the case of a solvent, the activity approaches its mole fraction as $x \rightarrow 1$. This convergence can be expressed conveniently by introducing the activity coefficient. For component 1

$$a_1 = \varphi_1 x_1 \qquad [1.32]$$

where φ_1 is the activity coefficient for species 1 and as $x_1 \rightarrow 1$, then $\varphi_1 \rightarrow 1$.

A corresponding equation can be written for the solute by taking a hypothetical state in which the solute is pure yet behaves in accord with Henry's Law. In this case

$$a_2 = \varphi_2 x_2 \qquad [1.33]$$

and as $x_2 \rightarrow 0$, then $\varphi_2 \rightarrow 1$.

Thus, final expressions for the variation of vapour pressure with composition for both solvent and solute can be written.

$$P'_1 = \varphi_1 x_1 P_1 \qquad [1.34]$$

and

$$P'_2 = \varphi_2 x_2 K_2 \qquad [1.35]$$

If the variation of φ with x is known for a given liquid mixture, then the vapour pressure of the components can be calculated at any composition. If the rate-determining step for the evaporation from an unstructured mixture is the diffusion through the stagnant vapour layer above the liquid surface, then the rate is expected to vary in a predictable way with the vapour pressure of the evaporating component. If, however, a significant concentration gradient develops within the liquid mixture, this will not be the case.

Convection within mixtures of volatile and non-volatile components

As previously mentioned in Section 1.3.3, the rapid evaporation of a highly volatile species may lead to significant cooling of the liquid surface. In a mixture of volatile and non-volatile components, evaporation will also lead to a local increase in the mole fraction of the non-volatile species at the surface.

The net effect is an increase in density in the surface region compared with that in the bulk liquid. For mixtures in which these effects operate, the resulting gravitational instability sets up arrays of small convective cells. It is likely these mixtures will remain well-mixed by convection and that no concentration gradients will develop.

1.4.3 Microstructured water – surfactant mixtures

Vapour pressure considerations

For mixtures of water and surfactant, there is a composition dependent lowering of the water vapour pressure in accordance with Equation [1.34]. In this case, the surfactant mixture is then expected to behave as the liquid mixtures outlined in Section 1.4.2.

Microstructure within the mixture

There are two other possible ways in which evaporation rate of water from water – surfactant mixtures may be affected, both related to the microstructure of the mixture. Firstly, a surfactant monolayer at the air-water interface may act as a physical barrier to evaporation. The evaporation rate may be influenced by the nature of the monolayer. Secondly, microstructuring of the surfactant by the spontaneous self-assembly of the surfactant into a variety of ordered mesophases may slow mass transfer within the liquid and suppress convection. Such microstructuring may therefore induce a switch from vapour phase diffusion control to liquid mass transfer control. In this case, the degree of structure within the mixture is likely to influence evaporation rates.

Surfactant molecules consist of a polar headgroup and non-polar (generally hydrocarbon) tail. The two parts of the molecules have very different solubility properties. As a result, molecules tend to adsorb at the interface between phases, where the polar headgroup will immerse itself in the more polar phase, and the non-polar tail will become immersed in the less polar phase. At low concentrations, however, surfactants still form true solutions. As the concentration is increased, the degree of adsorption increases.

Surfactant monolayers fall into three distinct types, which roughly correspond to the two-dimensional analogues of the three states of matter. The nature of the monolayer is generally dependent on the sizes of the tail of the surfactant molecule. Surfactants having short hydrocarbon chains (in the order of six to eight carbon atoms) form compressible gaseous monolayers in which molecules are separated by large distances and are considered to lie almost flat at the interface. Hydrocarbon chains of intermediate length (nine to fourteen carbon atoms) tend to form compressible expanded monolayers, in which molecules are separated by smaller distances. Surfactants with long hydrocarbon chains (typically twenty carbon atoms) form condensed monolayers, which consist of molecules closely packed at the interface and are relatively incompressible[64]. The three types of monolayer are represented in Figure 1.5. Clearly, these representations are very much stylised. In reality, most monolayers are highly disordered. Intuitively, one would expect the resistance of a monolayer to increase with the degree of order.

Soluble surfactants rarely (if ever) form the highly ordered condensed monolayers. As mentioned in Section 1.2.4, condensed monolayers formed by insoluble surfactants are the only monolayer type which have ever been proved to retard evaporation rates[31-33].

Micellar solutions and lyotropic liquid crystalline mesophases

In water-surfactant mixtures, the process of normal dissolution ceases at the critical micelle concentration (c.m.c.) and surfactant molecules begin to aggregate into micelles. The shape of micelles just above the c.m.c is largely dependent on the nature of the surfactant, the concentration of the solution and the temperature but is most likely to be spherical, cylindrical or discotic. At higher concentrations, the surfactants form a variety of liquid crystalline mesophases. For the purposes of this study, only the phases shown by the non-ionic surfactant n-dodecylhexaoxyethylene glycol ether $C_{12}E_6$ in water will be considered.

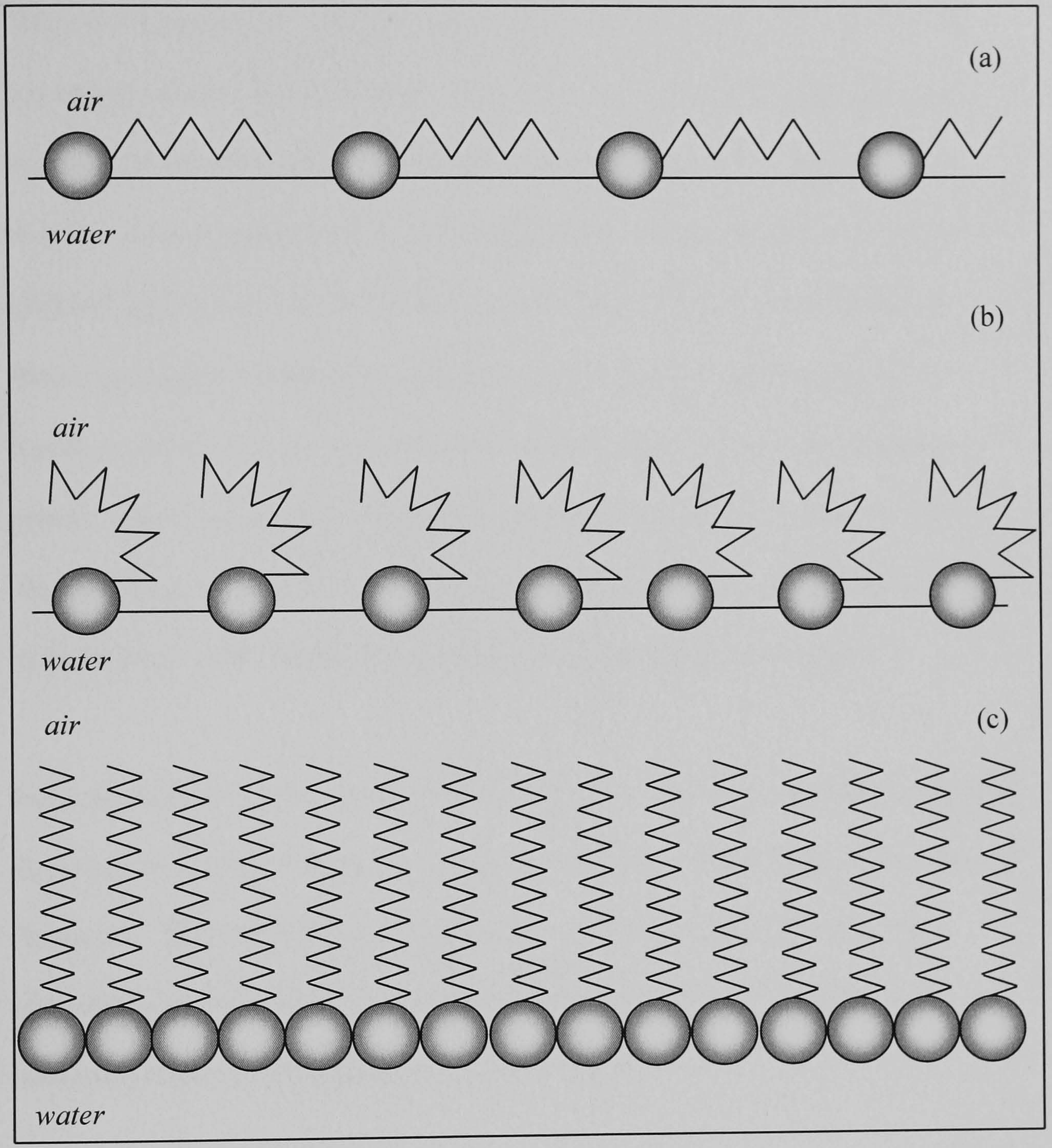

Figure 1.5 ***Schematic representation of surfactant conformation in (a) gaseous, (b) expanded and (c) condensed monolayers***

The phase diagram for $C_{12}E_6$ has been determined previously[65, 66]. Briefly, with increasing concentration, the phase sequence is isotropic micellar dispersion (L_1), normal hexagonal phase (H_1) consisting of hexagonally packed cylindrical micelles, viscous isotropic phase (V_1) consisting of a cubic arrangement of non-spherical aggregates, lamellar phase (L_α) consisting of planar bilayer surfactant sheets separated by water films and isotropic liquid phase. Each single phase region is separated by a two-phase region containing a mixture of the adjacent phases. Figure 1.6 shows the approximate structure of the L_1, H_1 and L_α phases. The most likely structure for the V_1 phase is a 'bicontinuous' network in which the surfactant tail/ water interface has both positive and negative curvature[67].

For a mechanism in which the rate-determining process is mass transfer through the liquid phase, the rate of diffusion is expected to depend on the relative viscosities of the phases. Therefore, if composition is uniform throughout the sample, the evaporation rate of water from the mesophases is likely to decrease with the increasing viscosity of the phases, $L_1 > L_\alpha > H_1 > V_\alpha$.

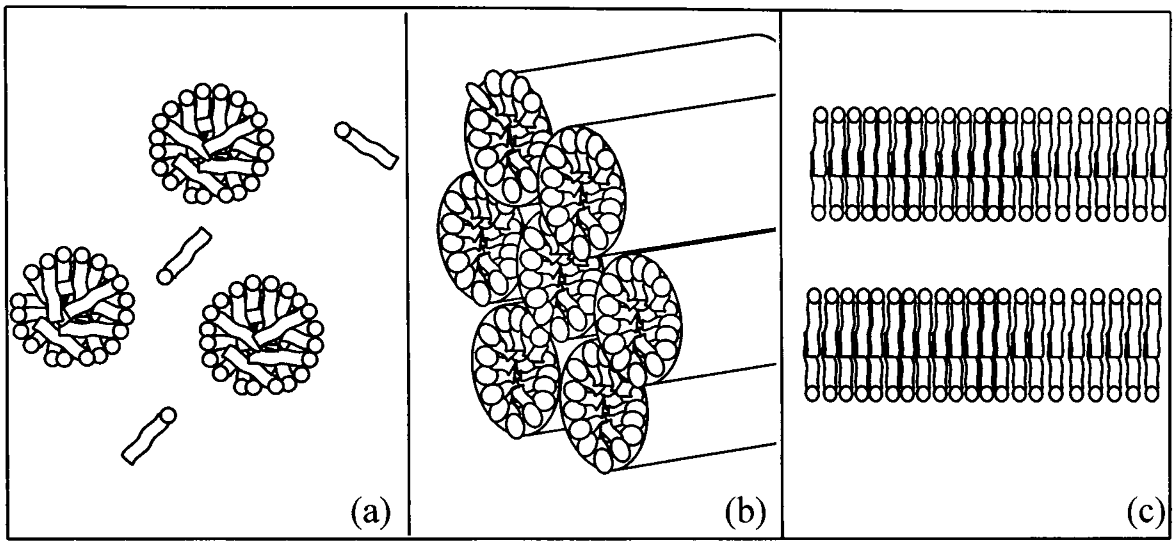

Figure 1.6 ***Simplified representation of the (a) L_1, (b) H_1 and (c) L_α mesophases***

1.4.4 Evaporation from emulsions

Vapour pressure considerations

Emulsions may be of the oil-in-water or water-in-oil types. In this study, only oil-in-water emulsions will be discussed. Oil-in-water emulsions contain a dispersion of micron sized approximately spherical oil drops within an aqueous continuous phase stabilised by the adsorbed surfactant which coats the droplets. Although thermodynamically unstable, these emulsions may be kinetically stable against the possible breakdown processes outlined below.

If the oil and water components of an emulsion are completely immiscible and the surfactant concentration is very low, the two phases within the emulsion can be considered separate and pure. Therefore, the equilibrium vapour pressures of the oil and water are expected to be virtually identical to the values of the bulk pure liquids. A slight lowering of the vapour pressure of the continuous phase is expected because of the presence of dissolved surfactant (in accordance with Equation [1.34]). Conversely, a slight increase in the vapour pressure of the oil droplets is expected to arise from the Kelvin effect (in accordance with Equation [1.23]). The equilibrium vapour pressure of the emulsion is the sum of the vapour pressures of the two components. Assuming that the surfactant is totally insoluble in the dispersed phase, the equilibrium vapour pressure of the emulsion, $P_{emulsion}$ is given by

$$P_{emulsion} = P_{oil} e^{\frac{2\gamma_{ow} V_m}{rRT}} + \varphi_{water} P_{water} x_{water} \qquad [1.36]$$

where P_{oil} and P_{water} are the vapour pressures of the pure components, γ_{ow} is the oil-water interfacial tension, V_m is the molar volume of the oil, r is the radius of the oil droplet, φ_{water} is the activity coefficient of the water in the continuous phase and x_{water} is the mole fraction of water in the continuous phase.

For a n-hexane in water emulsion stabilised with 20 mM $C_{12}E_6$ containing spherical droplets of 10 μm radius at 25°C, $P_{oil} = 20198.3$ Pa [68], $\gamma_{ow} = 0.0005$ Nm^{-1} $V_m = 1.32 \times 10^{-4}$ m^3 mol^{-1}, $\varphi_{water} = 1.0009$ [65], $P_{water} = 3167.7$ Pa[59] and $x_{water} =$ 0.9992. The value of $P_{emulsion}$ is therefore 23366 Pa. The sum of the vapour pressures of the pure oil and water components is also 23366 Pa.

In the absence of any kinetic barriers to evaporation, the emulsion evaporation rate is expected to be virtually equal to the sum of the evaporation rates of the oil and water components. Upon the depletion of one of the phases, the vapour pressure of the emulsion should revert to that of the remaining component and the evaporation rate is expected to fall correspondingly.

Emulsion instability mechanisms[69]

An oil-in-water emulsion is not thermodynamically stable. In fact, the thermodynamically stable state is that of two separated phases and all emulsions spontaneously and irreversibly move towards this.

Within an oil – in – water emulsion, the oil droplets are in continuous random motion and undergo frequent collisions. After collision, droplets in a kinetically stable emulsion will separate again. However, for kinetically unstable emulsions, the droplets may either stick to each other with a thin film between them (flocculate), or unite to form a larger droplet (coalesce). These processes are shown in Figure 1.7.

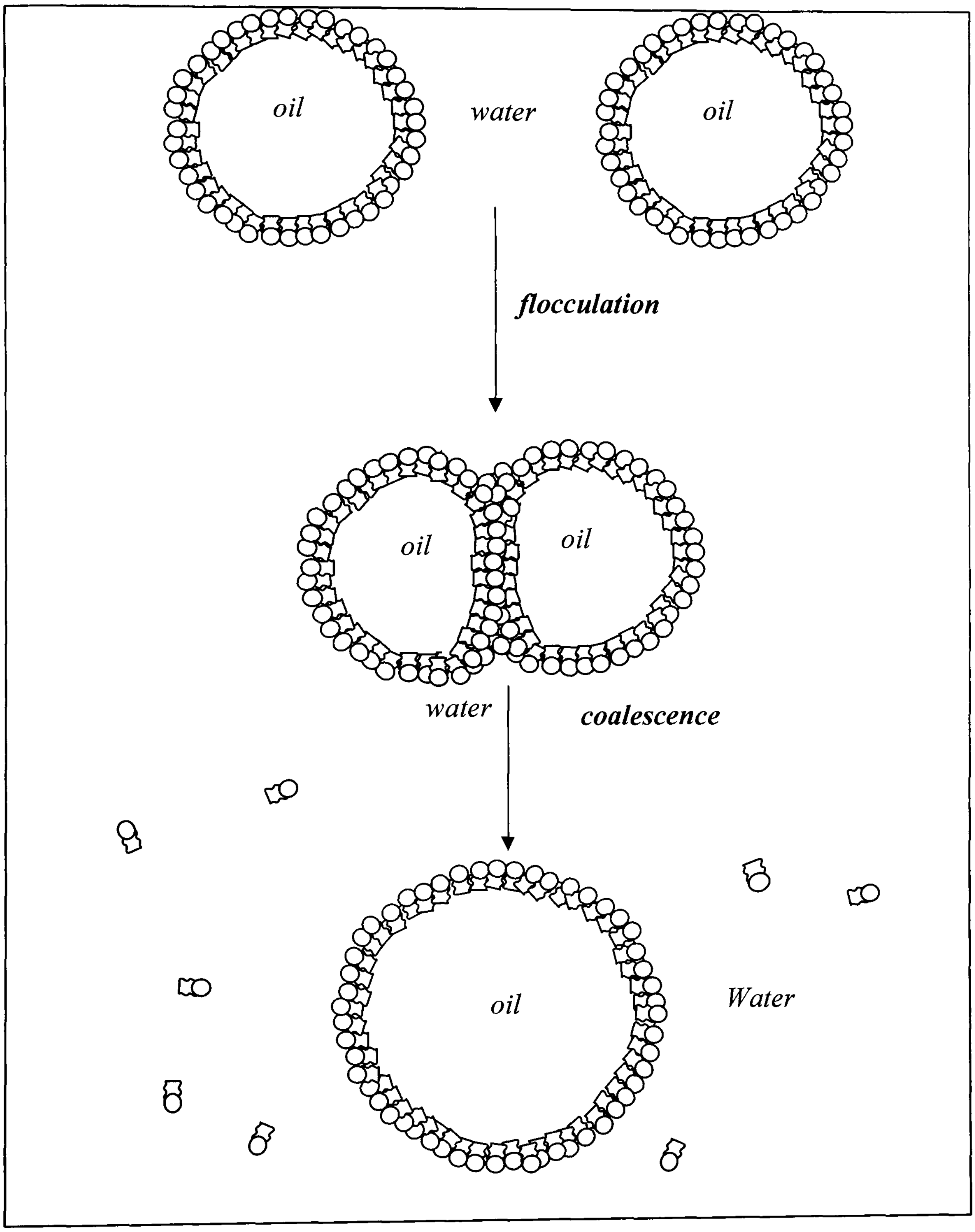

Figure 1.7 Collision between emulsion droplets leading to flocculation and coalescence

The processes of flocculation and coalescence have two implications. Firstly, the number of droplets in the emulsions is reduced. Secondly, once droplets have flocculated or coalesced, droplets may cream or sediment more rapidly.

The creaming or sedimenting processes are driven by gravity. A droplet within the emulsion moves in the gravity field. Its movement is slowed by the friction force from the continuous phase. For small droplets, the Brownian motion is also important. When the dispersed phase is less dense than the continuous phase, the droplets rise to the top of the emulsion (cream). When the dispersed phase is more dense than the continuous phase, the droplets sink to the bottom of the emulsion (sediment). The rate at which these processes occur becomes constant when the gravity force is equal to the friction force. This relationship is given by Stokes' Law.

$$v = \frac{2}{9} r^2 \frac{\Delta\rho g}{\eta} \qquad [1.37]$$

where v is the creaming or sedimenting velocity of an isolated drop, r is the radius of the droplet, g is the acceleration due to gravity, $\Delta\rho$ is the density difference between the oil and the continuous phase and η is the viscosity of the continuous phase.

It can be seen from Equation [1.37] that the rate of sedimentation is proportional to the squared radius of the droplet. Therefore, the sedimentation or creaming velocity of a droplet coalesced from two single droplets is 60 % higher than the original droplets. This leads to more rapid phase separation within the emulsion, as shown in Figure 1.8.

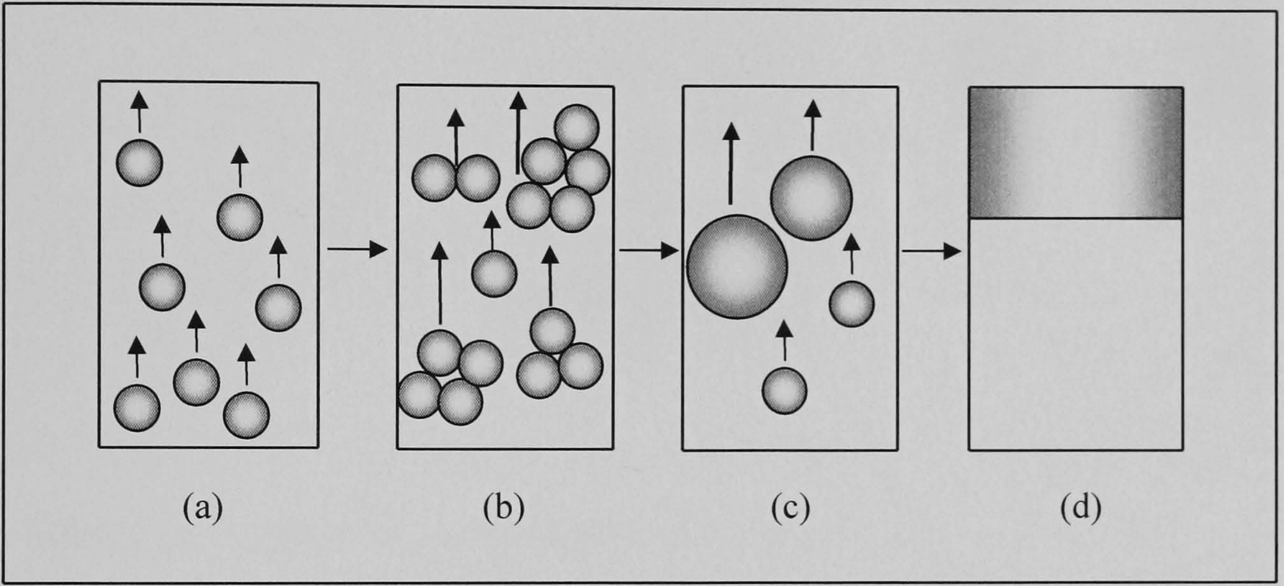

Figure 1.8 ***The processes of flocculation (a → b) and coalescence (b → c) enhance the rate of creaming and lead to complete separation***

In addition to the processes of creaming, flocculation and coalescence, emulsions may also be destabilised by Ostwald ripening[70]. Ostwald ripening is driven by the difference in solubility (and therefore chemical potential) of the large and small emulsion droplets in the continuous phase. The solubility is dependent on the radius of curvature of the droplet and increases with decreasing radius[71]. Smaller droplets may dissolve into the continuous phase and diffuse into larger droplets. Again, the outcome is a more rapid phase separation.

The process of Ostwald ripening is summarised in Figure 1.9. The rate of Ostwald ripening is directly proportional to the solubility of the oil in the continuous phase[72].

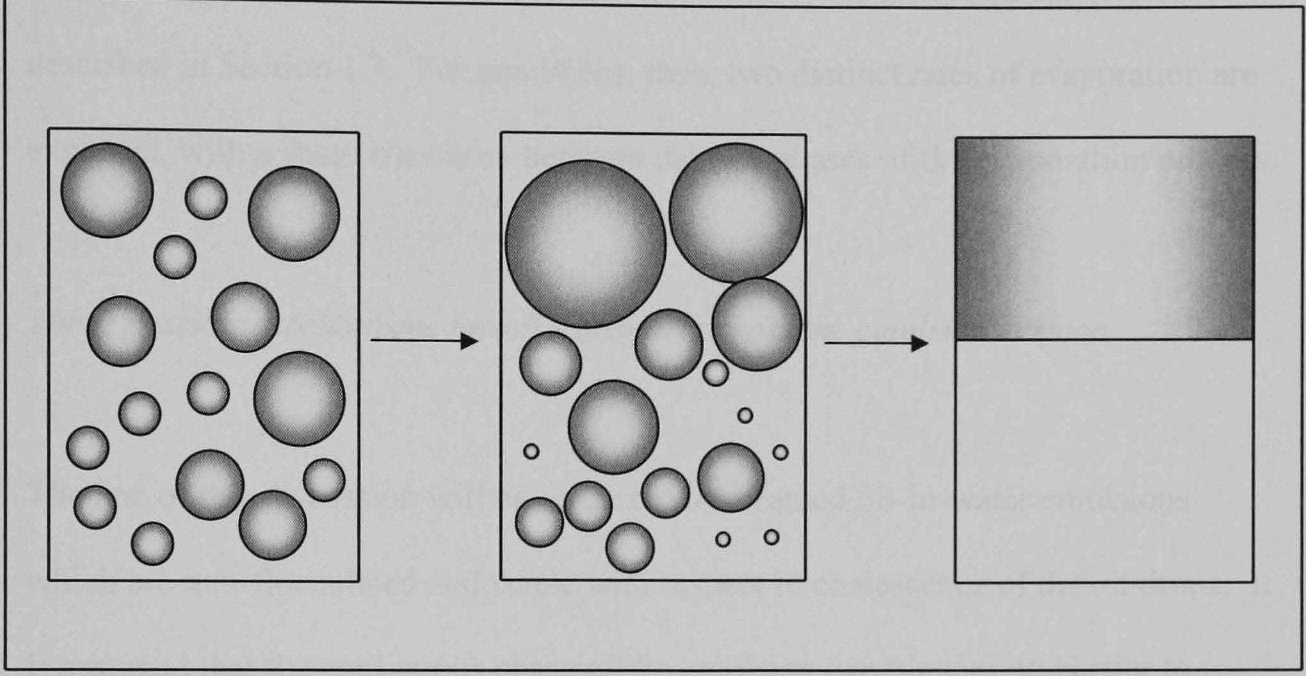

Figure 1.9 Schematic representation of emulsion destabilisation by the Ostwald ripening process

After complete phase separation, the emulsion consists of a layer of the less dense material on the surface of the more dense liquid. The two layers have virtually identical vapour pressures to those of the pure liquids. After phase separation, the evaporation rate of the upper layer is expected to be limited only by diffusion through the stagnant vapour space and to be proportional to the vapour pressure. The presence of the upper layer completely inhibits evaporation from the denser phase.

Only after the total loss of the upper layer is the surfactant solution able to evaporate. Beyond this point, the evaporation rate is dependent on the effects described in Section 1.3. For emulsions, then, two distinct rates of evaporation are expected, with a sharp transition between the two phases of the evaporation process.

Three possible mechanisms for oil transport across the emulsion surface

The rest of this discussion will be restricted to creamed oil-in-water emulsions which are non-flocculated and stable with respect to coalescence of the oil drops. It is assumed that the continuous phase of the emulsion experiences no barrier to evaporation.

The key factor determining the evaporation rate of the emulsion is therefore the mechanism of transport from the dispersed drops to the vapour phase. Three possible mechanisms of oil transport across the emulsion surface can be envisaged. As shown schematically in Figure 1.10, the emulsion surface initially contains buoyant oil drops situated below a surfactant monolayer adsorbed at the air-water surface and separated from the vapour phase by a thin water film of nanometre thickness.

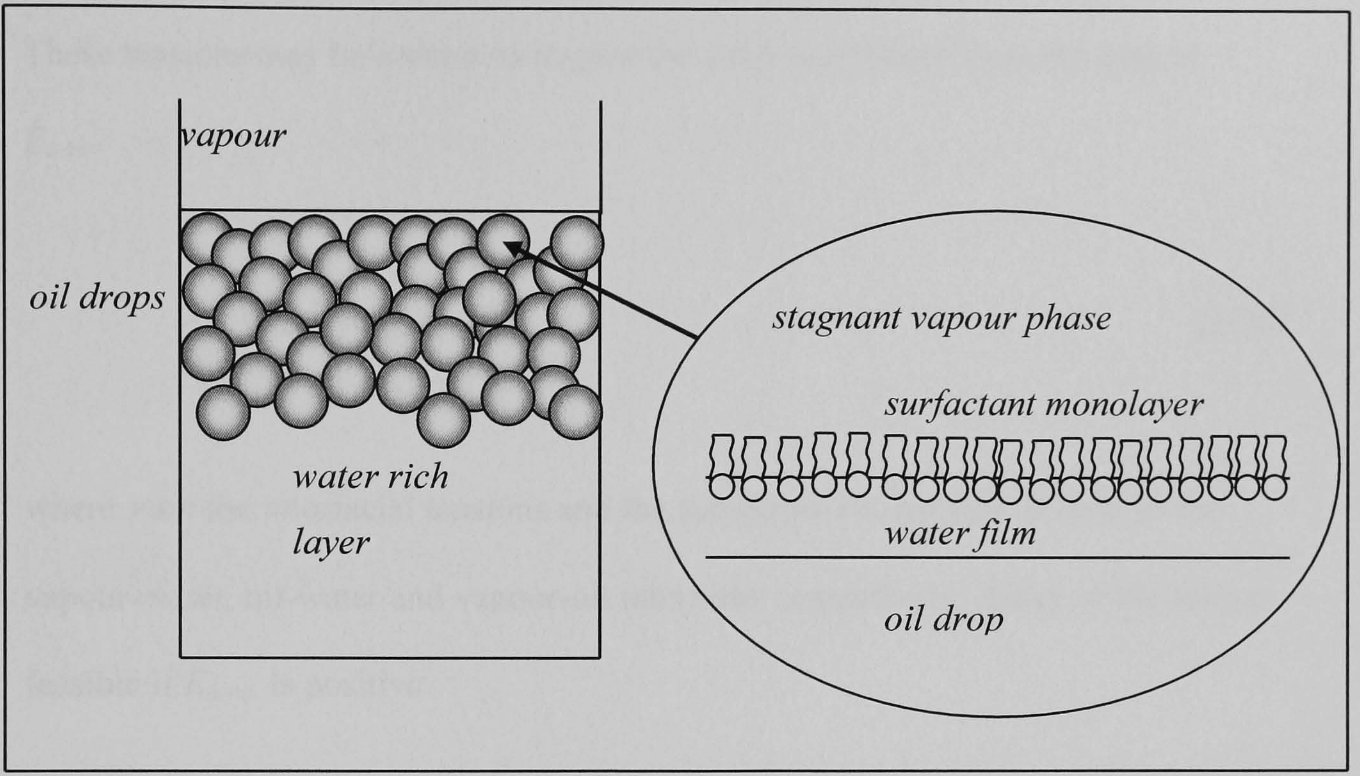

Figure 1.10 Expanded view of a creamed emulsion sample and the thin water film separating the oil drops from the vapour

Mechanism 1:

The first mechanism assumes that entry to the surface region is thermodynamically favourable. The feasibility of oil drop entry through the water film is dependent on the relative magnitudes of the oil-water, vapour-water and vapour-oil interfacial tensions[73].

These tensions may be combined to give the entry coefficient from the system, $E_{o,vw}$.

$$E_{o,vw} = \gamma_{vw} + \gamma_{ow} - \gamma_{vo} \qquad [1.38]$$

where γ are the interfacial tensions and the subscripts *vw*, *ow* and *vo* refer to the vapour-water, oil-water and vapour-oil interfaces respectively. Entry of the drop is feasible if $E_{o,vw}$ is positive.

For drops for which entry to the surface is thermodynamically favourable, surface forces may provide an energy barrier to the process of entry. Electrostatic repulsions between the drop and the surface are dependent on the surface charge on and the thickness of the diffuse double layer around the oil drop. The addition of electrolyte causes the double layer to compress, allowing the emulsion drop to approach the surface region. At close range, attractive van der Waals interactions between the surface and the oil drop overcome the electrostatic repulsions and the drop enters the surface. The size of the van der Waals interactions is also dependent on the Hamaker constant for the system.

If oil entry forms the rate limiting step to oil transport to the vapour phase, the oil evaporation rate is expected to correlate with the relative magnitudes of the oil-vapour, oil-water and water-vapour interfacial tensions and the strength of the repulsive forces across the water film. The evaporation rate would also be expected to increase with the addition of electrolyte.

Mechanism 2:

If entry does not occur, the oil droplets remain separated from the vapour phase by the thin water film at the surface. In this situation, transport may occur by molecular diffusion. If diffusion across the thin water film is the rate limiting step to oil transport to the vapour phase, the oil evaporation rate is likely to be dependent on the diffusion coefficient of the oil in water, the thickness of the oil film and the aqueous solubility of the oil.

Mechanism 3:

For non-entering drops, it may be that transport across the thin water film does not occur. In this case, oil drop evaporation can only occur when the evaporation of the upper water film "uncovers" the oil droplets. In this case, the oil evaporation rate is expected to be dependent on the thickness of the water film and relative volatilities of the oil and water.

For mechanisms 2 and 3, the thickness of the water film is predicted to influence the oil evaporation rate. Thicknesses of equilibrium water films at emulsion surfaces are known to be of the order of tens of nanometres, but are dependent on the balance between the capillary pressures and colloidal forces across them[74, 75]. Films are expected to be thicker for ionic surfactants, where electrostatic repulsions thicken the film relative to those stabilised by non-ionic surfactants. However, water film thicknesses during the dynamic evaporation process are likely to be somewhat different from the equilibrium values. It is also possible that the nature of the oil influences the film thickness. The buoyant oil drops exert a capillary pressure on the water film, which is dependent both on the oil-water and vapour-water interfacial tensions and on the oil drop sizes.

Gelled emulsions

The gelling of an emulsion prevents the sedimentation and creaming processes, giving a more uniform composition. In this study, only aqueous κ-carrageenan gels are considered. The structural unit of carrageenan is shown in Figure 1.11.

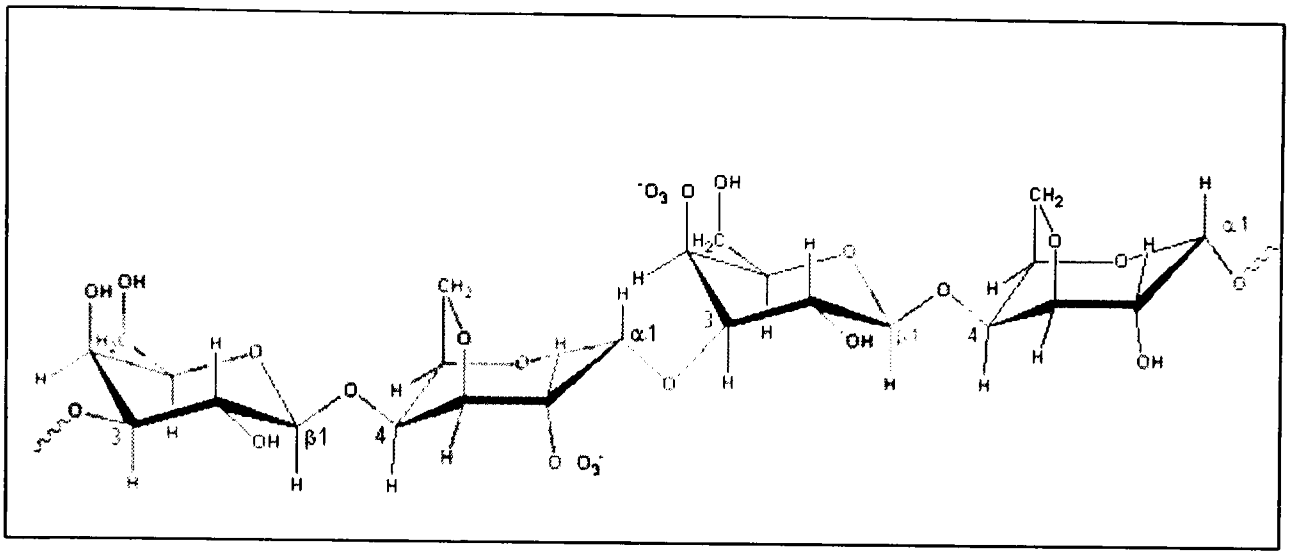

Figure 1.11 Structural unit of carrageenan

κ-carrageenan is a highly flexible polymer. At high concentrations or elevated temperatures, the molecules wind around one another to form double helical structures. For emulsions stabilised with sodium dodecyl sulphate, the sodium ions form bridges between these helices, giving a gel structure.

Gels containing emulsion droplets can be considered as a matrix in which the oil droplets are embedded. Oil transport into the vapour phase requires diffusion through the polymer network, and is expected to be correspondingly slow. In contrast to sedimented and creamed emulsions, the fact that water must diffuse from the gel network in order to evaporate means that the continuous phase may also experience a barrier to evaporation. The evaporation rate of a gelled emulsion is therefore expected to be significantly slower than the corresponding ungelled emulsion.

As evaporation proceeds, a second effect may also influence the evaporation rate of the emulsion. Loss of water from the polymer network leads to gel shrinkage[4]. As the gel shrinks, the diffusion path for the evaporating species becomes even more tortuous, until in extreme cases, diffusion is completely inhibited and the species become "trapped" in the gel network. This is of particular interest in the household goods industry, where it impacts upon the efficiency of gelled air fresheners.

1.5 Plan of this thesis

The work presented in this thesis has the following format: In Chapter Two, the apparatus and materials used in the study are detailed. In Chapter Three. the results obtained for the evaporation rates of pure liquids are discussed. A simple model is described in which the thickness of the stagnant vapour layer above the surface of the liquid determines the evaporation rate. In Chapter Three, the evaporation rates of water from porous silica particles are also discussed in light of the proposed model. Chapter Four discusses the results obtained for miscible liquid mixtures and surfactant solutions. In Chapter Five, the evaporation rates of immiscible liquid mixtures and emulsions are addressed and a preliminary model for these complex systems is described. Chapter Six highlights the conclusions reached in the study.

1.5 References

1. P. I. Kawamura and D. Mackay, *J. Hazardous Mat.,* 1987, **15**, 343.
2. P. Leonelli, C. Stramigioli and G. Spadoni, *J. Loss Prev. Ind.,* 1994, 7, 6.
3. J. Piexoto and M. Mota, *Biotechnology Techniques*, 1997, **11**, 1.
4. K. G. Das (Ed.), *"Controlled Release Technology"*, John Wiley and Sons Inc., New York, 1983.
5. G. T. Barnes, *J. Colloid Interface Sci.*, 1986, **25**, 2.
6. S. E. Friberg, *Adv. Coll. Int. Sci.*, 1998, **75**, 181.
7. D. S. L. Cardwell (Ed.), *"John Dalton and the Progress of Science"*, Manchester University Press, Manchester, 1968.
8. J. W. Hinchley, *J Chem. Soc.*, 1922, **51**, 242.
9. J. W. Hinchley and G. W. Himus, *Trans. Inst. Chem. Engrs.*, 1942, **2**, 57.
10. F. Pasquill, *Proc. Royal Soc. Lond.*, 1943, **A182**, 75.
11. T. B. Hine *Phys. Rev.*, 1924, **24**, 79.
12. R. W. Powell and E. Griffiths, *Trans. Inst. Chem Engrs.*, 1935, **18**, 175.
13. M Lurie and N. Michailoff, *Ind. Eng. Chem.*, 1936, **28**, 345.
14. S. H. Wade, *Trans. Inst. Chem Engrs.*, 1942, **20**, 1.
15. L. J. O'Brien and L. F. Stuntzman, *Ind. Eng. Chem.*, 1950, **42**, 1181.
16. T. Yoshida and T. Hyodo, *Ind. Eng. Chem. Process Des. Dev.* 1970, **9**.
17. G. O. Rubel, *J. Colloid Interface Sci.*, 1981, **81**, 188.
18. A. T. Prata and E. M. Sparrow, *Can J.Chem. Eng.*, 1986, **64**, 511.

19. R. R. DuPont, *Environ. Progr.*, 1986, **5**, 197.

20. J. B. Laurindo and M. Prat, *Chem. Engng Sci.*, 1996, **51**, 5171.

21. J. Kondo and N. Saigusa, *J. Meteorol. Soc. Jpn.*, 1994, **72**, 413.

22. F. Goia, F. Murena and A. Santoro, *J. Hazardous Mat.*, 1998, **59**, 131.

23. J. B. Laurindo and M. Prat, *Chem. Engng Sci.*, 1998, **53**, 2257.

24. J. Kondo and N. Saigusa, *J. Appl. Meteor.*, 1992, **31**, 304.

25. C. K. Ho and S. W. Webb, *J. Porous Media*, 1998, **1**, 71.

26. G. Hedenstrand, *J. Phys. Chem.*, 1924, **28**, 1244.

27. E. K. Rideal, *J. Phys. Chem.*, 1925, **29**, 1585.

28. I. Langmuir and V. J. Schaefer, *J. Franklin Inst.*, 1943, **235**, 119.

29. F. Sebba and H. V. A. Briscoe, *J. Chem. Soc. Lond.*, 1940, 106.

30. R. Archer and V. K. La Mer, *J. Phys. Chem.*, 1955, **59**, 200.

31. F. MacRitchie, *"Chemistry at Interfaces"*, Academic Press, San Diego, 1990.

32. S. S. Katto, M. V. Natekar and S. D. Sansare, *Indian J. Technology*, 1968, **6**, 10.

33. G. T. Barnes, *Colloids Surfaces A: Physicochem Eng. Aspects* 1997, **126**, 149.

34. T. L. Quickenden and G. T. Barnes, *J. Colloid Interface Sci.*, 1978, **67**, 415.

35. M. Blank, *J. Phys. Chem.*, 1964, **68**, 2793.

36. M. Blank and J. S. Britten, *J. Colloid Sci.*, 1965, **20**, 789.

37. G. T. Barnes, T. L. Quickenden and J. E. Saylor, *J. Colloid Interface Sci.*, 1970, **33**, 236.

38. W. W. Mansfield, *Nature*, 1955, **175**, 247.

39. G. T. Barnes and A. I. Feher, *J. Colloid Interface Sci.*, 1980, **75**, 584.

40. G. T. Barnes and D. S. Hunter, *J. Colloid Interface Sci.*, 1990, **136**, 198.

41. M. K. Bernett, L. A. Halper, N. L. Jarvis and T. M. Thomas, *Ind. Eng. Chem. Fundam.*, 1970, **8**, 140.

42. S. E. Friberg, Q. Yin and P. A. Aikens, *Colloids and Surfaces A: Physicochem. Eng. Aspects*, 1999, **159**, 17.

43. S. E. Friberg, *Adv. Colloid Interface Sci.* 1998, **75**, 181.

44. S.E. Friberg and B. R. C Langlois, *J. Dispersion. Sci. Technol.*, 1992, **13**, 223.

45. B. R. C. Langlois and S. E. Friberg, *J. Soc. Cosmet. Chem.*, 1993, **44**, 23.

46. G. M. Eccleston, *J. Soc. Cosmet. Chem.*, 1990, **41**, 1.

47. T. Moaddel and S. E. Friberg, *J. Dispersion Sci. Technol.*, 1995, **16**, 69.

48. S. E. Friberg, *Int. J. Cosmet. Sci.*, 1997, **19**, 75.

49. S. E. Friberg, T. Huang, L. Fei, S. A. Vona and P. A. Aikens, *Prog. Colloid Polymer Sci.*, 1996, **101**, 18.

50. S. E. Friberg, L. Fei and P. A. Aikens, *J. Molecular Liquids*, 1997, **72**, 31.

51. E. E. Tucker in *"Solubilization is Surfactant Aggregates"*, S. D. Christian and J. F. Scamelhorn (Eds.), Marcel Dekker, New York, 1995.

52. J. Biasis, L. Odberg and P. Stenius, *J. Colloid Interface Sci.*, 1982, **86**, 350.

53. E. Sjoblom, B. Johnsson, A. Johnsson, P. Stenius, P. Saris and L. Odberg, *J. Phys. Chem.*, 1986, **90**, 119.

54. I. Damaszewski and R. A. Mackay, *J. Colloid Interface Sci.*, 1984, **97**, 166.

55. M. Juszynski, R. Azoury and R. Rafaeloff, *SOFW*, 1992, **118**, 811.

56. S.E. Friberg, *Int. J. Cosmetic Sci.,* 1997, **19**, 75.

57. J. H. Clint, P. D. I. Fletcher and I. T. Todorov, *Phys. Chem. Chem. Phys.,* 1999, **1**, 5005-5009,

58. N. K. Adam, *"The Physics and Chemistry of Surfaces"*, Oxford Clarendon Press, 2nd Edn., 1938.

59. *"CRC Handbook of Chemistry and Physics"*, CRC Press Inc., Boca Raton, 62nd Edn, 1981.

60. T. K. Sherwood, R. L. Pigford and C. R. Wilke, *"Mass Transfer"*, McGraw-Hill Inc., New York, 1975.

61. J. R. Welty, C. E. Wicks and R. E. Wilson, *"Fundamentals of Momentum, Heat and Mass Transfer"*, John Wiley and Sons Inc., New York, 3rd Edn., 1984.

62. R. J. Hunter, *"Introduction to Modern Colloid Science"*, Oxford University Press, 1996.

63. P. W. Atkins, *"Physical Chemistry"*, Oxford University Press, 3rd Edn., 1986.

64. F. MacRitchie, "*Chemistry at Interfaces*", Academic Press. San Diego. 1990.

65. J. S. Clunie, J. F. Goodman and P. C. Symons, *Trans. Faraday Soc.*, 1969, **65**, 287.

66. D. J. Mitchell, G. J. T. Tiddy, L. Waring, T. Bostock and M. P. McDonald, *J. Chem. Soc., Faraday Trans. 1*, 1983, **79**, 975.

67. G. J. T. Tiddy, *Phys. Rep.*, 1980, **57**, 1.

68. "*Selected Values of Properties of Hydrocarbons and Related Compounds*", Thermodynamics Research Center, AP144, Texas A&M University, 1978.

69. S. E. Friberg, R. F. Goubran and I. H. Kayali, in "*Food Emulsions*", Eds K. Larsson and S.E. Friberg , Dekker, New York 2nd Edn, 1990.

70. P. Taylor, *Adv. Colloid Interface Sci*, 1998, **75**, 107.

71. A. S. Kabal'nov, A. V. Pertzov and E. D. Shchukin, *Colloids Surf.*, 1987, **24**, 19.

72. S. S. Davis and A. Smith, *J. Pharm. Pharmacol.*, 1972, **25**, 117.

73. R. Aveyard, B. P. Binks, P. D. I. Fletcher , T.G. Peck and C. E. Rutherford, *Adv. Colloid Interface Sci.*, 1994, **48**, 93.

74. L. Lobu and D. T. Wasan, *Langmuir*, 1993, **9** 1668.

75. V. Bergeron, M.E. Fagan and C. J. Radke, *Langmuir*, 1993, **9**, 1704.

CHAPTER 2

EXPERIMENTAL MATERIALS AND METHODS

2.1 Materials

2.1.1 Water

All water used in the following experiments was purified by reverse osmosis and passed through a Milli-Q reagent water system. Surface tension measurements showed typically a value of 71.9 mN m^{-1} at 25°C, which is in good agreement with literature values[1].

2.1.2 Organic liquids

The organic liquids used in this study are summarised in Table 2.1, together with their source and purity. All were columned twice over alumina in order to remove polar impurities.

Table 2.1: ***Summary of organic liquids used, source and purity***

Material	Source	Purity
n-pentane	Aldrich	98%
n-hexane	Beecroft and Partners	99%
n-heptane	Rathburn	98%
n-octane	Lancaster	99%
n-decane	Avocado	99%
Squalane	Aldrich	99%
Benzene	Fisons	99.8%
Cyclohexane	Rectapur	99%
Ethanol	Fisons	unknown
1-bromobutane	Avocado	98%
1-bromohexane	Lancaster	98%

2.1.3 Silica powders

The silica powders used in the study of evaporation from porous solids are listed in Table 2.2 with source and other physical characteristics, as quoted by the supplier. The powders were dried by storage in a vacuum desiccator.

Table 2.2: ***Summary of silica powders used, pore diameter and volume and source.***

Silica	Mean pore diameter/ nm	Pore volume/ $cm^3\ g^{-1}$	Supplier
Davisil™ silica gel	14.2	1.10	Supelco
Davisil™ silica gel	6.0	0.75	Supelco
Silica gel, grade 923	3.0	0.43	Aldrich

The silica particles used in the preparation of pure hexane gels were amorphous fumed silica H30, supplied by Wacker-Chemie. The surfaces were treated with dichlorodimethyl silane to render the particles hydrophobic. The primary particle diameter for the sample was 12 nm and the percentage of unreacted SiOH groups on the surface was 50%.

2.1.4 Surfactants

Table 2.3 lists the surfactants used in the study with their sources, critical micelle concentrations[2] and purities. The method of assay is also given where known. The purity was assumed to be that quoted by the manufacturer and no further purification was carried out.

Table 2.3: ***Summary of surfactants used, c.m.c., source and purity***

Surfactant	Formula	c.m.c at 25°C/ mM	Supplier	Purity	Assay method
Sodium dodecyl sulphate (SDS)	$C_{12}H_{25}O_4S^- Na^+$	8.1	BDH	98%	GLC
Sodium bis –2 – diethylhexyl sulphosuccinate (AOT)	$C_{20}H_{37}O_7S^- Na^+$	5	Sigma	~99%	-
n-decyl-β-D-glucopyranoside	$C_{16}H_{32}O_6$	12.5	Sigma	98%	GLC
Hexaethylene glycol monododecyl ether ($C_{12}E_6$)	$C_{24}H_{50}O_7$	0.08	Fluka/ Nikkol	>98%	TLC
Cetyltrimethylammonium bromide (CTAB)	$C_{19}H_{42}N^+ Br^-$	1	BDH	98%	-

2.1.5 Carrageenans

The carrageenans used in this study were Commercial Grades I and II supplied by Sigma.

2.2 Experimental Methods

All glassware was cleaned thoroughly before use with ethanolic potassium hydroxide (29 g KOH per litre of ethanol) and rinsed with copious amounts of Milli-Q grade water. The glassware was then dried in a clean oven at approximately 45°C.

2.2.1 Preparation of samples for evaporation rate measurement

Pure liquids

A known volume of pure liquid was pipetted directly into a cylindrical glass sample tube and then mounted in the evaporation rate apparatus (see Section 2.2.2). Several tubes were used during the course of the experiments and the exact dimensions for each tube were known. The sample tube was weighed before and after liquid addition so the mass of liquid was accurately known.

Porous silica and water mixtures

A known mass of silica was placed into the sample tube, so that the distance between the flattened surface and the top of the tube was approximately 22 mm.

The volume of water required to fill the pores to a given volume percentage was added and those samples requiring homogeneity were mixed thoroughly, sealed and left to equilibrate for a minimum of five hours before being placed in the evaporation rate apparatus. All mixtures with less than 80% of the total pore volume filled with water felt dry to the touch.

Miscible liquid mixtures

All mixture samples were prepared by direct weighing into the sample tube used for evaporation measurements. Viscous mixtures were mixed with heating in order to ensure homogeneity, sealed and cooled to the temperature at which they were required and reweighed prior to the evaporation measurement. Any mass loss was assumed to be due to the more volatile component.

Hexane gels

Hexane gels were prepared using H30 partially hydrophobic silica particles. A known mass of silica was added to a known mass of pure n-hexane in the evaporation sample tube. The silica was dispersed throughout the hexane using a high-intensity ultrasonic vibracell processor (supplied by Sonics and Materials with a tip diameter of 3 mm) operated at 20 kHz and up to 10 W for two minutes. The sample tube was held in an ice-bath during dispersion, and afterwards sealed and warmed to experimental temperature.

The sample was allowed to evaporate to dryness. The sample tube was weighed before and after measurement to determine the mass of silica lost during sample preparation. Any other mass loss was assumed to be due to hexane.

Immiscible liquid mixtures

Immiscible liquid mixtures were prepared by placing known volumes of the two liquids directly into the evaporation sample tube and leaving them to separate. The liquids were weighed upon addition and the mass of the remaining less volatile liquid was obtained upon removal of the sample tube from the evaporation rate apparatus.

Emulsions

Emulsions were prepared in the evaporation sample tube. A known volume of a 20 mM aqueous surfactant solution was pipetted into the sample tube and accurately weighed. A known volume of oil was added to the surfactant solution. The overall mass of the mixture was determined. The mixture was homogenised for two minutes using a Janke and Kunkel Ultra Turrax T25 homogeniser and 8 mm (outside diameter) shaft operating at 8000 rpm. Any resulting foam was allowed to break down and the overall mass determined again prior to evaporation. The mass of any emulsion remaining after evaporation was determined by weighing.

Gelled emulsions

Preparation of the gelled emulsion systems was as described above with the exception that before homogenisation a known mass of carrageenan was added to the mixture.

2.2.2 Evaporation rate measurement

Figure 2.1 is a schematic diagram of the apparatus used for the measurement of evaporation rates. The sample to be evaporated was contained in a glass sample tube suspended from a Precisa 125A balance. The dimensions of the sample tubes used in the study are given in Table 2.4. The sample tubes were simple open-topped soda glass tubes. Dry nitrogen gas was passed through a column of activated charcoal (a Puritube, supplied by Phase Sep.) to remove any impurities and a calibrated flow meter in order to record the gas volume flow rate. The purified nitrogen stream flowed through a thermostatting coil and entered the measurement vessel through an annular opening of approximately 1mm gap.

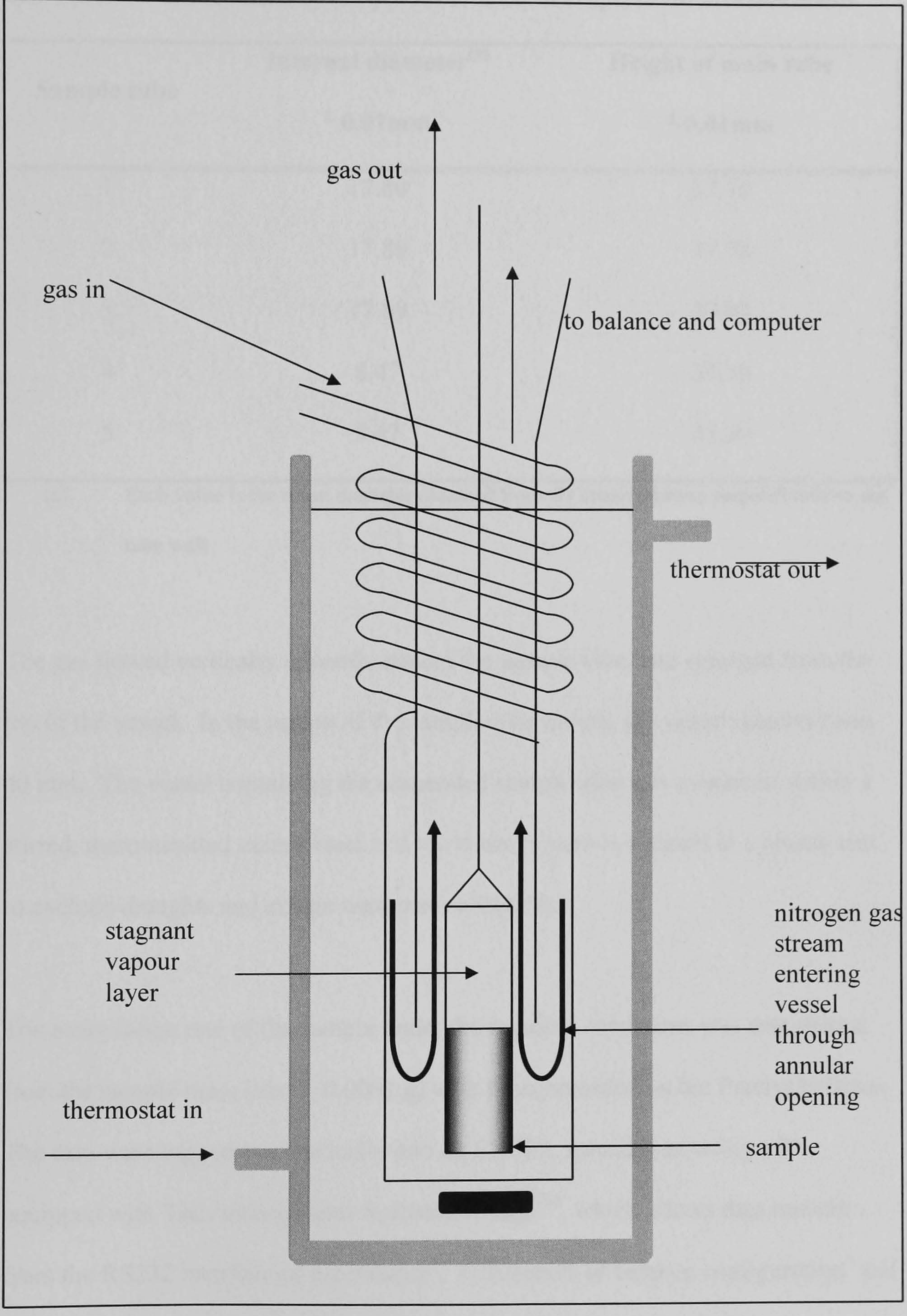

Figure 2.1: Evaporation rate measurement apparatus

Table 2.4: Dimensions of sample tubes used in evaporation measurements

Sample tube	**Internal diameter[(a)]** ± **0.01mm**	**Height of main tube** ± **0.01mm**
1	17.80	37.70
2	17.89	37.78
3	17.89	39.97
4	8.47	37.30
5	8.47	37.30

(a) Each value is the mean diameter obtained from six measurements perpendicular to the tube wall

The gas flowed vertically upwards around the sample tube, and emerged from the top of the vessel. In the region of the sample tube mouth, the vessel diameter was 40 mm. The vessel containing the suspended sample tube was contained within a stirred, theromstatted outer vessel and the entire system is encased in a plastic tent to exclude draughts and ensure temperature stability.

The evaporation rate of the sample under the required conditions was determined from the sample mass loss (± 0.0001 g) with time, recorded on the Precisa balance. The data were logged automatically into an EXCEL spreadsheet using a PC equipped with TAL technologies SoftwareWedge^{TM}, which allows data transfer from the RS232 interface of the balance[3]. Full details of balance configuration[4] and the VBA computer program module required can be found in Appendix 1.

Data recording commenced immediately after the sample was loaded into the evaporation rate measurement apparatus. Commonly, some disturbance was seen over the initial period of between 15 and 60 minutes. This data was rejected.

A typical mass loss versus time curve for pure n-hexane is shown in Figure 2.2. Plots for other systems will be found in the relevant chapters.

The experimental uncertainty in the measurements depends on the accuracy of control of the sample vapour pressure and the gas flow rate since, depending on the experimental conditions, the measured rate is proportional to the vapour pressure of the sample and either proportional to the gas flow rate or independent of the gas flow rate (see Chapter 3). The uncertainty in the sample temperature was ± 0.1 °C, which translates to an uncertainty in the vapour pressure of approximately 1% for the samples used in the study. The uncertainty in the gas flow rate was typically 3% for the flow rates and flow meter used in this work. The uncertainty in the diameter and height of the vessel was ± 0.01 mm which translates to an uncertainty of 0.1% in the area of the vessel and of 0.05% in the stagnant layer thickness. Hence the uncertainty in the measured evaporation rates is expected to vary from approximately 4% (when the rate is proportional to gas flow rate) to 1% (when the rate is independent of flow rate). In practice, repeated measurements showed the reproducibility in most cases to be between 2 – 5%.

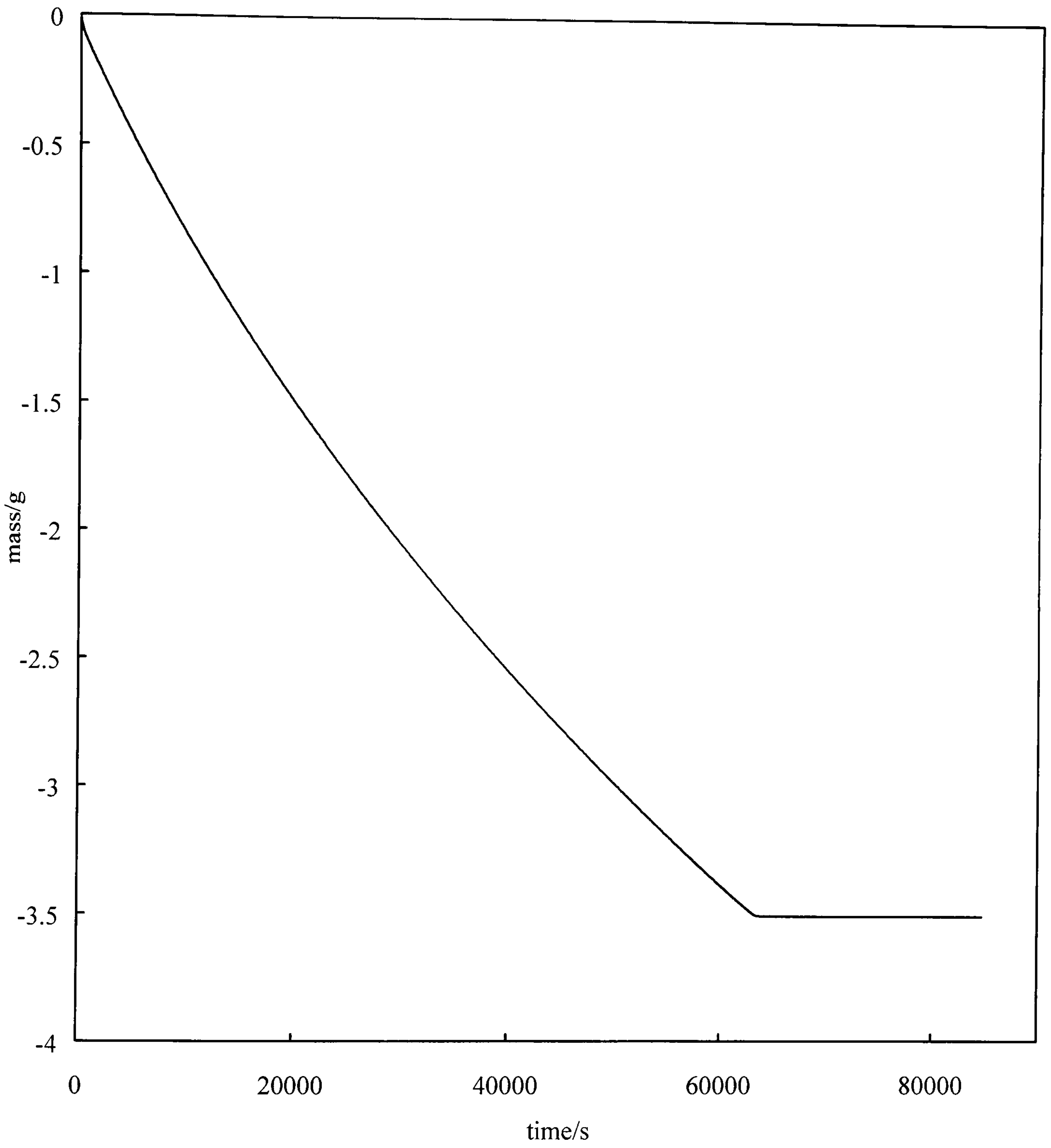

Figure 2.2: ***A mass loss versus time curve for 3.5088 g of pure n-hexane at 25°C and 1920 ml min^{-1} nitrogen gas flow rate. The horizontal part of the graph is comprised of data points collected after the hexane has fully evaporated***

2.2.3 Surface tension measurements

The du Nouy ring method

Air-water and oil-water surface tensions were measured via the du Nouy ring method using a Kruss K10 tensiometer. This consists of a platinum/iridium alloy ring and glass sample dish held within a thermostatted vessel. The ring is lowered into the liquid being measured and is first manually then automatically withdrawn from the sample. As the liquid is pulled from the solution, the force acting upon it increases until a maximum is reached, where the force is acting in a vertical direction. As the ring continues to rise, the force acting on the ring decreases and the lamella finally breaks. The Kruss K10 tensiometer uses a servo control motor to hold the ring stationary at the point where the maximum force is operating. The tension is calculated from the measured static maximum force.

Harkins and Jordan[5] have shown that the force acting on the ring at maximum pull is related to the surface tension, γ, of the liquid by equation 2.1

$$\gamma = \frac{mgF}{4\pi r} \qquad [2.1]$$

where r is the radius from the centre of the ring to the centre of the wire, g is the acceleration due to gravity and m is the mass of the solution raised at maximum force.

The correction factor, F, is a function of r^3/V and r/r_w where V is the volume of the liquid pulled from the surface by the ring and r_w is the radius of the wire forming the planar ring. The factor F can be found from tabulated data[6], the accuracy of which is within 0.25% of values obtained using a theoretical consideration of meniscus shape. This work was further extended by Zuidema and Waters[7] in order to include tensions of below 25 mN m^{-1}, where the correction factor is given by equation 2.2.

$$F = 0.725 + \sqrt{\frac{0.01425\gamma^*}{L^2/4\,\Delta\rho} + 0.04532 - \frac{1.679}{r/r_w}} \qquad [2.2]$$

where L is the wetted perimeter of the ring, γ^* is the uncorrected tension and $\Delta\rho$ is the difference in density between the two phases in contact at the surface.

Before measurement, the du Nouy ring was cleaned by immersion in alcoholic KOH and rinsed with Milli-Q water before drying in a Bunsen flame. The tensiometer was calibrated using known masses and calibration was regularly checked throughout the experiment.

2.3 References

1. "*International Critical Tables*", McGraw-Hill, London, 1928, **4**, 447.
2. P. Mukerjee and K. J. Mysels, "*Critical Micelle Concentrations of Aqueous Surfactant Systems*", United States Department of Commerce, 1971.
3. TAL Technologies, "*SoftwareWedge^{TM} for Windows^{TM}*", 1997.
4. Precisa Balances Ltd, "*Precisa Operating Manual*", 1999.
5. W. D. Harkins and H. F. Jordan, *J. Am. Chem. Soc.*, 1930, **52**, 1751.
6. B. B. Freud and H. Z. Freud, *J. Am. Chem. Soc.*, 1930, **52**,1772.
7. H. H. Zuidema and G. W. Waters, *Ind. Eng. Chem.*, 1941, **13**, 312.

CHAPTER 3

EVAPORATION RATES OF PURE LIQUIDS

In Chapter 1, the concept of a resistance to evaporation arising from a stagnant vapour space above the surface of a liquid was introduced. This chapter uses the idea to develop and test a simple model. The model predicts the variation in evaporation rate for pure liquids with liquid height within the sample tube and gas flow rate for the experimental apparatus described in Chapter 2. The model is further extended to water held within porous solids, where the Kelvin Effect is expected to play a role in reducing evaporation rate.

3.1 Development of a model to predict the evaporation rates of pure liquids

For the experimental set-up described in Chapter 2, it is assumed that the only resistance to the evaporation of a pure liquid arises from the necessity for vapour diffusion across the gas space (assumed stagnant, i.e. convection is absent) between the liquid surface and the mouth of the sample vessel.

If only flow in the vertical (x) direction needs to be considered, Fick's first law gives the instantaneous evaporative flux J (i.e. the flow of vapour per unit area in unit time) at any point

$$J = -D\frac{\partial c}{\partial x} \qquad [3.1]$$

where D is the diffusion coefficient of the vapour through the stagnant gas layer (nitrogen in this case) and c is the concentration of diffusing vapour at position x.

Fick's second law describes the time dependence.

$$\frac{\partial c}{\partial t} = D\frac{\partial^2 c}{\partial x^2} \qquad [3.2]$$

An approximate steady state is achieved when the evaporation rate reaches a constant value. At this point, $\delta c/\delta t = 0$ at all points within the stagnant vapour space and therefore $\delta c/\delta x$ is a constant.

Assuming the system is ideal, the resulting linear concentration gradient can be expressed as

$$\frac{\partial c}{\partial x} = \frac{c_o - c_s}{h} \qquad [3.3]$$

where c_s is the concentration of the vapour just above the liquid surface, c_o is the concentration at the mouth of the open vessel and h is the thickness of the stagnant vapour space.

Equations [3.1] and [3.3] can be combined so that at the steady state

$$J = -D\frac{c_o - c_s}{h} = V_L c_o \qquad [3.4]$$

where V_L is the mean linear flow velocity of the gas stream in m s^{-1}. The second relationship in Equation [3.4] arises because the flux arriving from the liquid surface at the mouth of the sample tube must be equal to that carried away by the gas stream. V_L is related to the volume flow rate F by the equation $V_L = F/A_V$ where A_V is the cross-sectional area of the vessel in the region of the mouth of the sample tube.

Solving for c_o yields an equation for J in terms of h and V_L

$$J = \left\{ \frac{Dc_s}{h} - \frac{D^2 c_s}{h^2 V_L + hD} \right\} \qquad [3.5]$$

Equation [3.5] is an approximation, since a complication arises from the presence of a convective counter-current of the nitrogen within the stagnant layer. Because the total pressure is independent of x, equal amounts of both components must diffuse in opposite directions through the surface of reference. However, in this case, the liquid surface at the lower end of the sample tube is impermeable to nitrogen and the net result is an upward convection of the gas mixture. Stefan[1, 2, 3] has shown that for upward convection of velocity v, the change in concentration due to convection in a volume element of unit cross-sectional area, bounded by two planes at x and $x+\Delta x$, during time Δt will be

$$\Delta c = -\frac{1}{\Delta x}\left[(vc)_{x+\Delta x} - (vc)_x\right]\Delta t = -\frac{\partial}{\partial x}(vc)\Delta t + \ldots \qquad [3.6]$$

Equations [3.2] and [3.6] can be combined to give the differential equation for the rate of change of concentration due to both diffusion and convection

$$\frac{\partial c}{\partial t} = D\frac{\partial^2 c}{\partial x^2} - \frac{\partial}{\partial x}(vc) \qquad [3.7]$$

When v is a constant, Equation [3.7] reduces to

$$\frac{\partial c}{\partial t} = D\frac{\partial^2 c}{\partial x^2} - v\frac{\partial c}{\partial x} \qquad [3.8]$$

Thus, at the steady state, the following diffusion equations must apply

$$0 = \frac{\partial c}{\partial t} = D\frac{\partial^2 c}{\partial x^2} - v\frac{\partial c}{\partial x} \qquad [3.9]$$

and

$$0 = \frac{\partial C}{\partial t} = D'\frac{\partial^2 C}{\partial x^2} - v\frac{\partial C}{\partial x} \qquad [3.10]$$

where C is the concentration of the nitrogen vapour and D' is the diffusion coefficient for nitrogen through the liquid vapour.

Using the boundary conditions

at $x = 0 : c = 0, C = C_o$

and at $x = -h : C = C_o - c_s ; c = c_s ; -\frac{\partial C}{\partial x} + v(C_o - c_s) = 0$ [3.11]

where C_o is the concentration of nitrogen in the open. (The second boundary condition indicates that the liquid surface is impermeable to nitrogen).

It is also true at any point in the system that

$$c + C = C_o \qquad [3.12]$$

Transformation of Equation [3.9][4] gives

$$c = c_s \frac{1 - \exp\left(\frac{v}{D}h\right)}{1 - \exp\left(-\frac{v}{D}h\right)} \qquad [3.13]$$

and this can be combined with Equations [3.11] and [3.12] to give an equation which determines *v*.

$$-D\frac{\partial C}{\partial x} + v(C_o - c_s) = \frac{c_s v \exp\left(-\frac{v}{D}h\right)}{1 - \exp\left(-\frac{v}{D}h\right)} + v(C_o - c_s) = 0 \qquad [3.14]$$

which can be simplified to

$$\frac{v}{D}h = \ln\frac{C_o}{C_o - c_s} \qquad [3.15]$$

Also, since when $x = 0$, c = 0 and there is no convection current, the flux at this point is given by

$$J = -\left(\frac{\partial c}{\partial x}\right)_o = C_o \frac{D}{h} \ln \frac{C_o}{C_o - c_s} \qquad [3.16]$$

The condition $c_o = 0$ is achieved in this experiment when the flow rate of the nitrogen gas is sufficiently large to carry away the diffusing vapour from the mouth of the sample tube immediately. When this is the case, Equation [3.5] reduces to

$$J = D\frac{c_s}{h} \qquad [3.17]$$

which can be combined with Equation [3.16] to give an expression for the corrected value of c_s in the presence of convection.

$$c_s' = C_o \left(\ln \frac{C_o}{C_o - c_s}\right) \qquad [3.18]$$

where c_s' is the effective concentration above the liquid surface in the presence of convection.

Assuming that the vapour behaves ideally, $c_s = P/RT$, where P is the vapour pressure of the diffusing vapour. The mass evaporation rate is given by $E_o = JMA$, where M is the molar mass of the diffusing vapour and A is the internal cross-sectional area of the sample tube. When these are substituted into Equation [3.5] we obtain an expression for E_o

$$E_o = \frac{MADPz}{hRT}\left\{1 - \frac{D}{hF/A_V + D}\right\} \qquad [3.19]$$

The factor z is a correction factor allowing for the convective counter-current of nitrogen and, from Equation [3.19], is given by

$$z = \left[\frac{P_{atm}}{P}\ln\left(\frac{1}{1-(P/P_{atm})}\right)\right] \qquad [3.20]$$

where P_{atm} is the total pressure and is equal to the atmospheric pressure.

Equation [3.19] predicts firstly an increase in E_o with a decrease in h, and secondly an increase of E_o with F at low flow rates. E_o is predicted to become independent of F at high flow rates.

As h approaches zero, E_o is predicted to reach a limiting value given by

$$\lim_{h \to 0} E_o = \frac{MAPF}{RTA_v} = \frac{MAPV_L}{RT} \qquad [3.21]$$

3.2 Effect of gas flow rate on evaporation rate

Figure 3.1 shows the variation in evaporation rate of pure n-heptane with gas flow rate for three different values of stagnant layer thickness, *h*. It should be noted that there is some doubt as to whether A_v should include the area above the mouth of the sample tube. For this reason, two theoretical curves are calculated for each value of *h*, the solid line having A_v equal to the total cross-sectional area of the vessel and the dashed line having A_v equal to the cross-sectional area of the vessel minus the external cross-sectional area of the sample tube. The agreement between theory and experiment is reasonable, but the precision does not allow a clear choice to be made, concerning the value of A_v.

The shapes of the plots can be explained thus. At high flow rates (where the second term in Equation [3.19] becomes negligible), the gas stream sweeps away the liquid vapour from above the sample tube efficiently and c_o approaches zero. Therefore, E_o reaches a plateau value which is independent of flow rate and scales as $1/h$. As the flow rate is reduced, c_o increases, giving a lower concentration gradient and a reduced evaporation rate.

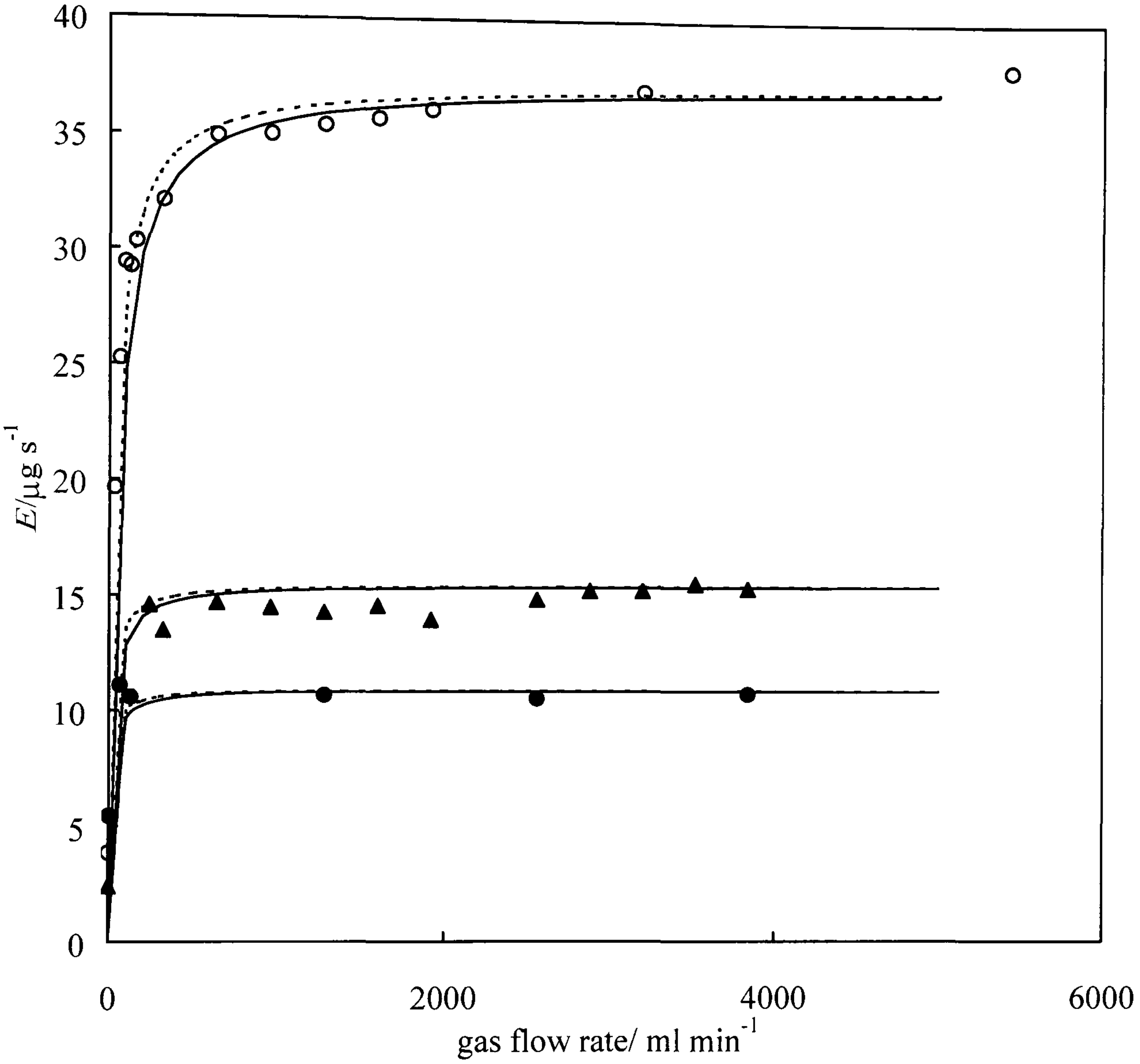

Figure 3.1 ***Variation of initial evaporation rate E_0 of n-heptane with nitrogen gas flow rate at 25°C for various fixed values of h. In ascending order, the values of h are 34 (filled circles), 24 (filled triangles) and 10 mm (open circles). Both curves are calculated using Equation [3.19] with $M = 100$ g mol^{-1}, $D = 6.1 \times 10^{-6}$ m^2 s^{-1}, $P = 6112.8$ Pa and $A = 2.49 \times 10^{-4}$ m^2. The solid curve corresponds to $A_v = 1.26 \times 10^{-3}$ m^2, whilst the dashed curve corresponds to $A_V = 0.91 \times 10^{-3}$ m^2.***

At zero flow rate, Equation [3.20] predicts zero mass evaporation rate for macroscopic values of *h*. In practice the intercepts of the curves in Figure 3.1 are small but finite. The residual mass evaporation rates are likely to arise from small natural convection currents within the vessel which cause a small concentration gradient through the stagnant layer.

3.1 Effect of stagnant layer thickness on evaporation rate

3.1.1 Experiments within which *h* remains constant

The variation in evaporation rate with stagnant layer thickness *h* is shown in Figure 3.2. The solid and dashed lines (which almost overlap) again show reasonable agreement between experiment and theory for all but very small values of *h*. When low *h* values are combined with high flow rates, there is also the possibility that the gas stream may impinge on the liquid surface and agitate it, giving a higher than expected mass evaporation rate. In summary, it can be concluded that the model accurately describes E_o for *h* greater than 10 mm and gas flow rates of 500 to 4000 ml min^{-1}.

The volumetric gas flow rate was varied from 0 to approximately 5000 ml min^{-1}, which corresponds to mean linear gas velocities of 0 to 0.09 m s^{-1} and a maximum Reynolds number of approximately 200. Because of the complex geometry of the gas flow around the sample tube, it is unclear whether the gas flow is laminar or turbulent[5].

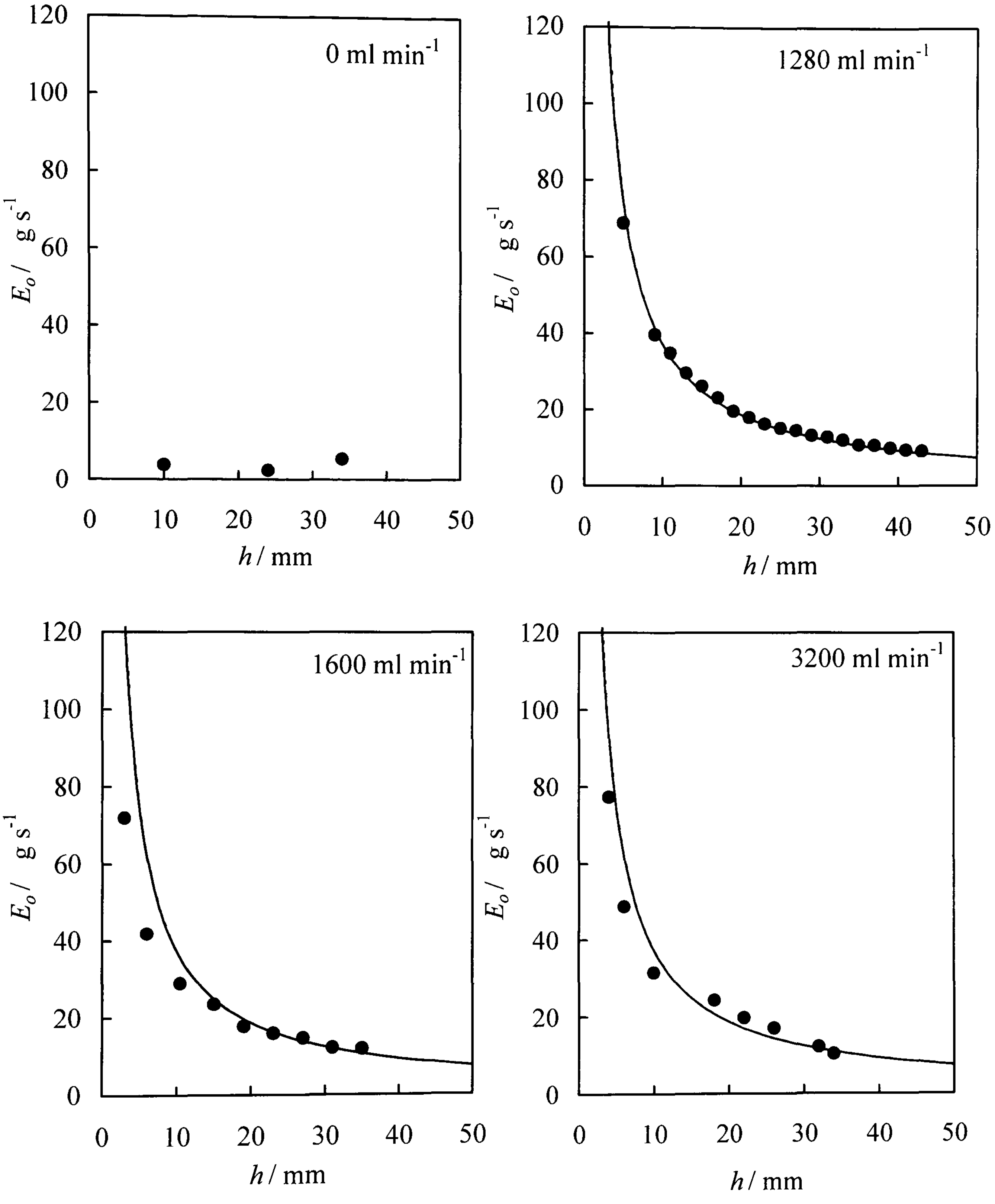

Figure 3.2 ***Variation in the initial evaporation rate E_o of n-heptane with h for the given fixed gas flow rates. The solid and dashed lines are calculated using the same parameters as in Figure 3.1.***

It is interesting to compare the evaporation rates obtained under these experimental conditions with those obtained by Prata and Sparrow[6]. They determined the evaporation rates of cumene and toluene from a partially filled container with a horizontal turbulent gas flow over the container mouth. The rates measured in this way are approximately an order of magnitude higher than those calculated using Equation [3.19]. These differences are likely to arise from deflection of the horizontal gas flow into the sample container at the downstream lip of the vessel. This would disrupt the steady-state vapour concentration gradient found under the conditions used in our study. Prata and Sparrow observed a complex dependency of evaporation rates on gas flow rates and h which is not amenable to quantitative analysis.

3.1.2 Experiments within which h varies

Under conditions of high gas flow rate it can be seen that

$$E_o = \frac{MADPz}{hRT} \qquad [3.22]$$

For a sample tube of height h_x, the volume of liquid, w, is given by

$$w = (h_x - h)A \qquad [3.23]$$

Therefore the mass of liquid remaining, *m*, is

$$m = \rho(h_x - h)A \qquad [3.24]$$

where ρ is the liquid density. Rearrangement of Equation [3.24] gives the following expression for *h*

$$h = \frac{\rho A h_x - m}{\rho A} = h_x - \frac{m}{\rho A} \qquad [3.25]$$

which can be substituted into Equation [3.22] to give

$$E_o = \frac{dm}{dt} = \frac{MADPz}{RTh_x - \frac{RTm}{\rho A}} \qquad [3.26]$$

Integration of Equation [3.26] gives a relationship between *m* and *t*

$$t = \frac{RTh_x}{MADPz}(m_o - m) - \frac{RT}{2\rho MA^2 DPz}\left(m_o^2 - m^2\right) \qquad [3.27]$$

where m_o is the initial mass of liquid at time zero.

Figure 3.3 compares measured mass loss versus time curves for n-pentane and n-hexane with those calculated using Equation [3.27]. The values of vapour pressure and diffusion coefficient used for the calculations are given in Table 3.1.

Table 3.1: Literature values of vapour pressure P and vapour diffusion coefficient in nitrogen (where available) or air at 25°C.

Liquid	**P/ Pa**	**$D^*/10^{-6}\ m^2\ s^{-1}$**
Water	3167.7[7]	24.0[9‡]
n-pentane	68367.7[8]	8.42[10]
n-hexane	20198.3[8]	8.2[9‡], 7.32[10], 8.1[11‡]
n-heptane	6112.8[8]	7.3[12‡]
n-octane	1885.2[8]	6.16[10], 6.02[13], 6.9[11‡]
n-decane	180.0[8]	5.7[11‡]
n-dodecane	18.0[8]	5.0[‡‡]
benzene	12689.6[8]	9.32[10], 9.7[14‡]
cyclohexane	13013.6[8]	7.8[9‡], 8.1[11‡], 7.95[14‡]
ethanol	7616.7[7]	11.8[10], 13.1[9‡]

[*] where multiple values of D are given, the mean value was used in Figure 3.4

[‡] Corrected to 25°C using the linear relationship quoted in Reference 11

[‡‡] Estimated by extrapolation from data for the linear chain alkanes

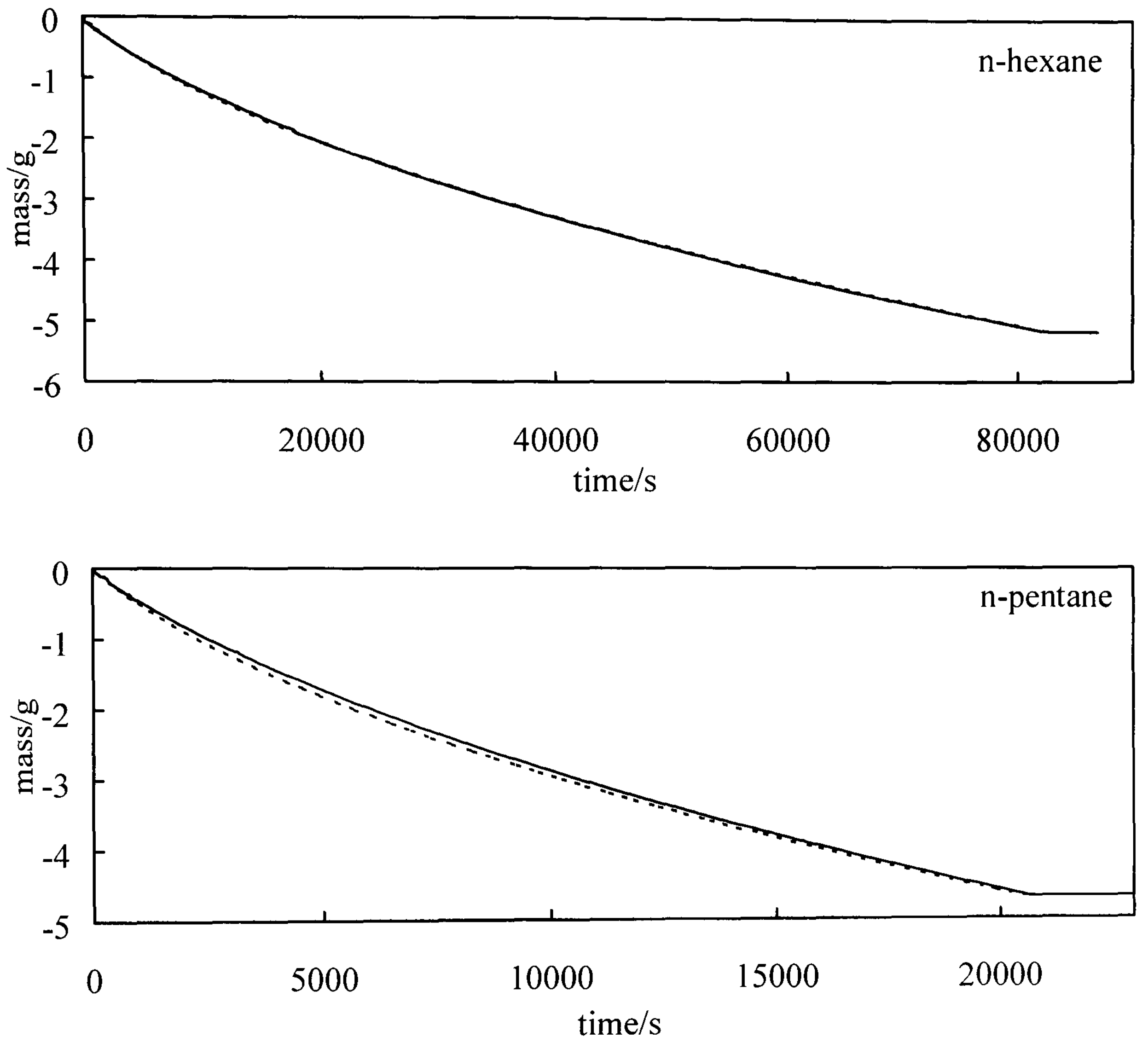

Figure 3.3 ***Mass loss versus time curves for pure n-hexane and n-pentane evaporated at 25.0°C and 1920 ml min^{-1} nitrogen gas flow rate. The solid lines are the experimental data and the dashed lines are the theoretical fits obtained using Equation [3.27] with $h_x = 40$ mm. All other apparatus constants are as in Figure 3.1. For hexane, $D = 7.90 \times 10^{-6}$ m^2 s^{-1}, $\rho = 654.7$ kg m^{-3}and $m_o = 5.116$ g. For pentane, $D = 6.85 \times 10^{-6}$ m^2 s^{-1}, $\rho = 621.2$ kg m^{-3} and $m_o = 4.689$ g. Vapour pressures are given in Table 3.1 and D values were adjusted to give the best fit for the experimental data.***

In the experimental curves, the evaporation rate decreases with increasing time (as *h* increases). The curve for n-hexane is well-described by Equation [3.27]. but there are significant deviations between theory and experiment for pentane. In particular, the initial mass evaporation rate is slower than the calculated value, and the "best-fit" value of the diffusion coefficient is anomalously low. It is likely that these deviations arise from the fact that the very high evaporation rate of pentane leads to a significant degree of cooling of the surface, which in turn gives a lower evaporation rate than predicted. For very volatile liquids, then, evaporation rate is coupled to heat conduction and cannot be considered as a simple mass transfer process.

3.4 Evaporation rates of different pure liquids

Under conditions of high gas flow rate when Equation [3.22] is valid, it becomes apparent that the factor $MDPz/RT$ is a measure of the mass "evaporatability" for a liquid of unit surface area at unit value of h. Figure 3.4 is a comparison of calculated values of the mass evaporatability (using the literature values of D and P detailed in Table 3.1) with the experimentally determined values of E_0h/A for a range of different liquids. The agreement between measured and predicted evaporatabilities is reasonably good for liquids for which the evaporation rates span over three orders of magnitude.

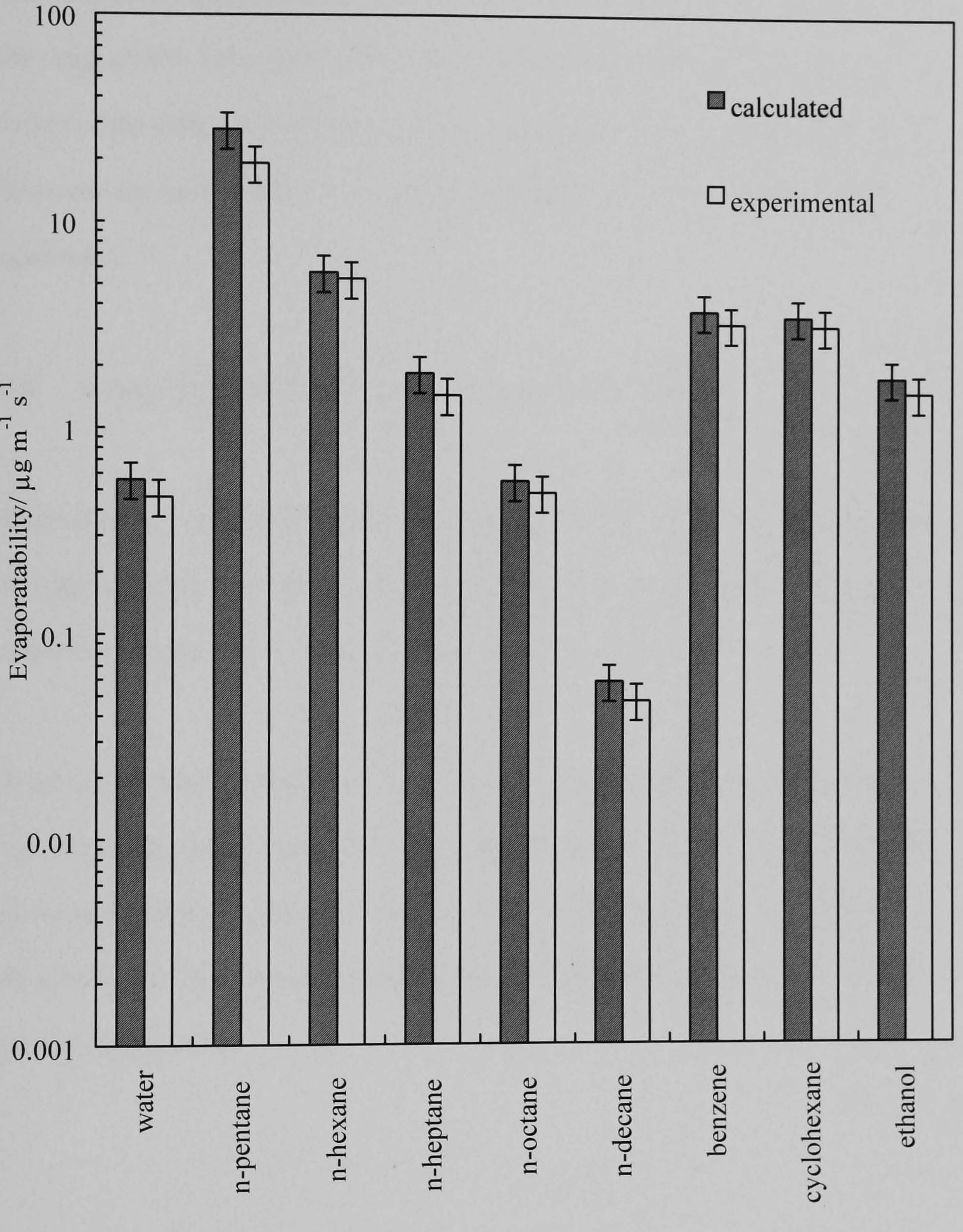

Figure 3.4 *Comparison of calculated and measured "evaporatability" values for a range of pure liquids at 25°C. The theoretical values are calculated using the diffusion coefficients and vapour pressures given in Table 3.1.*

The magnitude of discrepancies between the calculated and measured values is in the range of 10 – 20%, and is of the same order as the variation of the literature values of the diffusion coefficients given in Table 3.1. The evaporation rate of n-dodecane has been measured using the same apparatus[15] and also shows good agreement.

3.5 Evaporation rate of water from porous silica particles

When a liquid is contained within the narrow pores of a porous solid such as silica, the vapour pressure of the liquid is reduced due to the Kelvin effect. The Kelvin effect is described fully in Chapter 1, but will be discussed briefly here.

A curved surface of a liquid exerts a pressure so that the pressure on the concave side of the interface is higher that that on the convex. Thus, when a wetting liquid is contained within the pores of a porous solid, as shown in Figure 3.5, there must be a lowering of the vapour pressure within the liquid, which can be predicted by the Kelvin Equation.

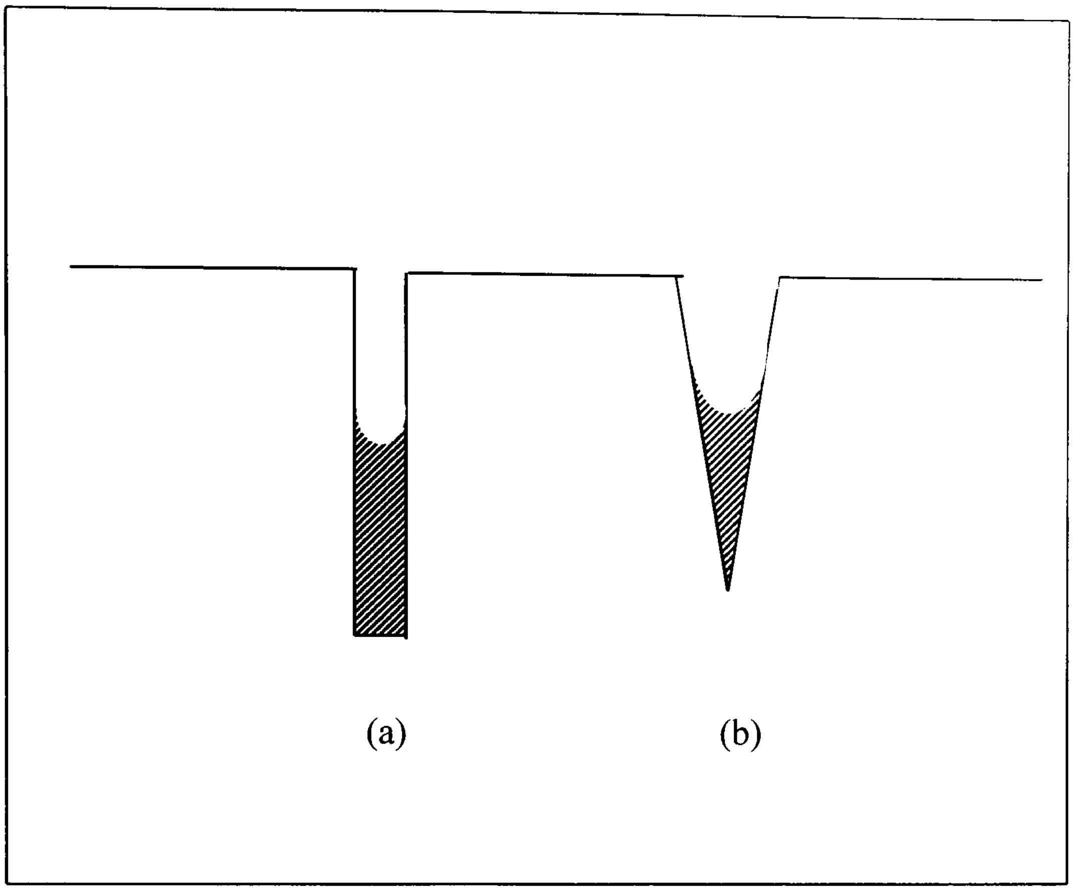

Figure 3.5: Simple schematic representation of the behaviour of a wetting liquid contained within (a) a cylindrical and (b) a conical pore of a porous solid.

The appropriate form of the Kelvin Equation in this instance is

$$\ln\left(\frac{P'}{P}\right) = -\frac{2\gamma V_m}{RT\left(r_{pore} / \cos\theta\right)} \qquad [3.28]$$

where P' is the vapour pressure of the liquid in the pores, γ is the liquid-air surface tension, V_m is the molar volume of the liquid, r_{pore} is the pore radius and θ is the contact angle made by the liquid on the porous solid material.

For liquid contained within a cylindrical pore, the vapour pressure is expected to remain constant until the pore is full, when it should reach the vapour pressure of bulk water, since *r* is the same for all parts of the pore. However, for a non-cylindrical pore, *r* varies with the fraction of the pore filled, and hence the vapour pressure is expected to change with the degree of pore filling.

By choosing to carry out experiments under conditions where Equation [3.22] is valid and ensuring that all parameters other than P' are kept constant, it is possible to equate P'/P with E/E_o where E is the mass evaporation rate for the liquid held within the pores of the solid. In order to ensure that there were no complications due to wetting, water was chosen to be the test liquid and the contact angle was assumed to be zero[16].

Figure 3.6 shows typical initial mass loss plots for pure water and water contained within silica of pore diameter 14.2, 6.0 and 3.0 nm. It can be seen that the initial mass evaporation rates of water contained within the three porous solids are reduced in comparison with that of bulk water.

Figure 3.7 compares the measured initial mass evaporation rates of water from silica particles of the three mean pore diameters with those predicted from a combination of Equation [3.22] and [3.28]. For each sample, the water content corresponds to 50% of the total pore volume as specified by the manufacturer and given in Table 2.2. Good agreement between theory and experiment is seen.

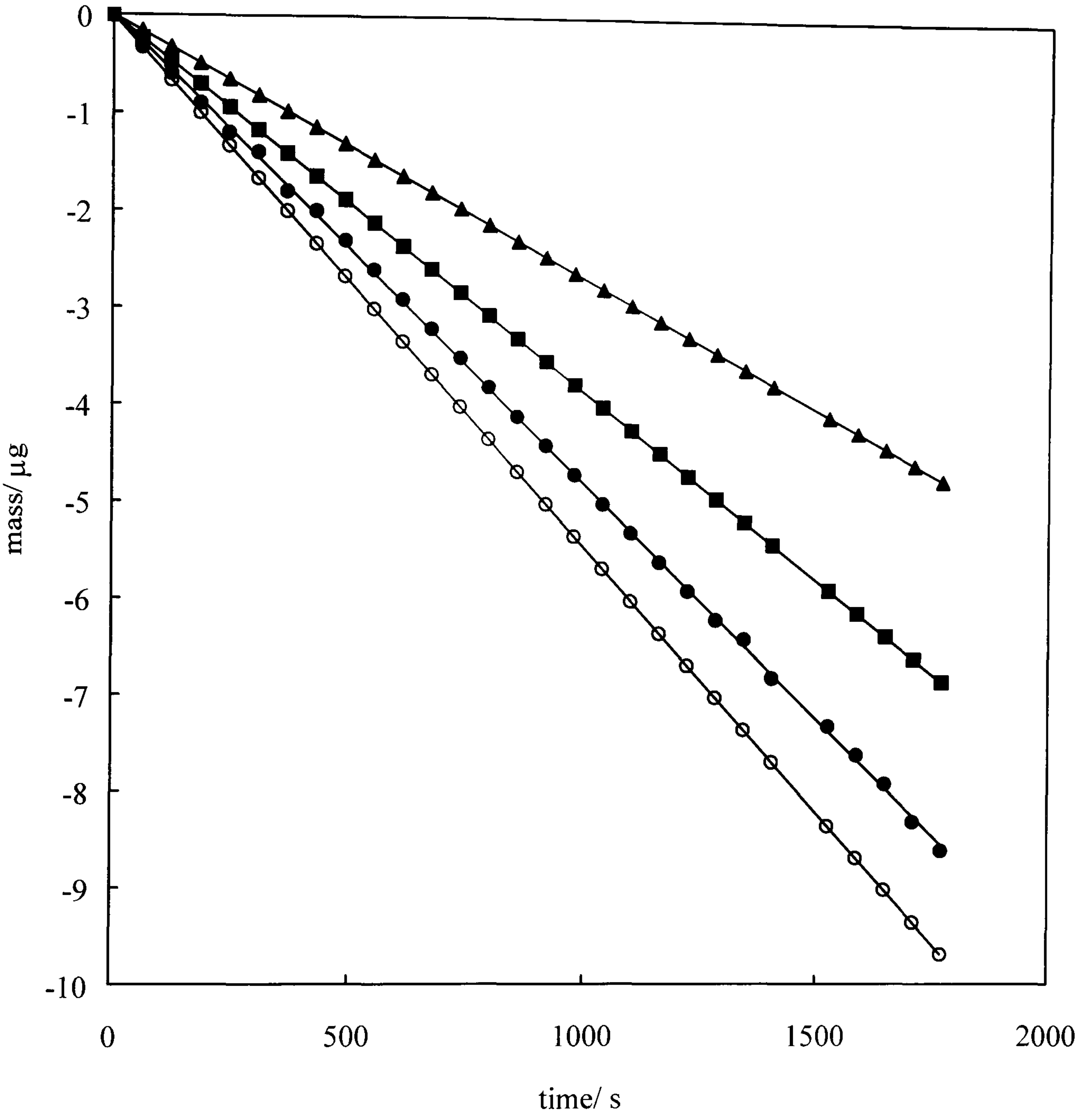

Figure 3.6 ***Mass versus time plots for pure water (open circles) and water contained in 14.2 nm diameter (filled circles), in 6.0 nm diameter (squares) and in 3.0 nm diameter (triangles) silica pores. The samples were evaporated at 25°C and 1920 ml min^{-1} nitrogen gas flow rate. In each case the pore volumes are 50% filled and the stagnant layer thickness is 21 mm. All apparatus constants are as given in Figure 3.1.***

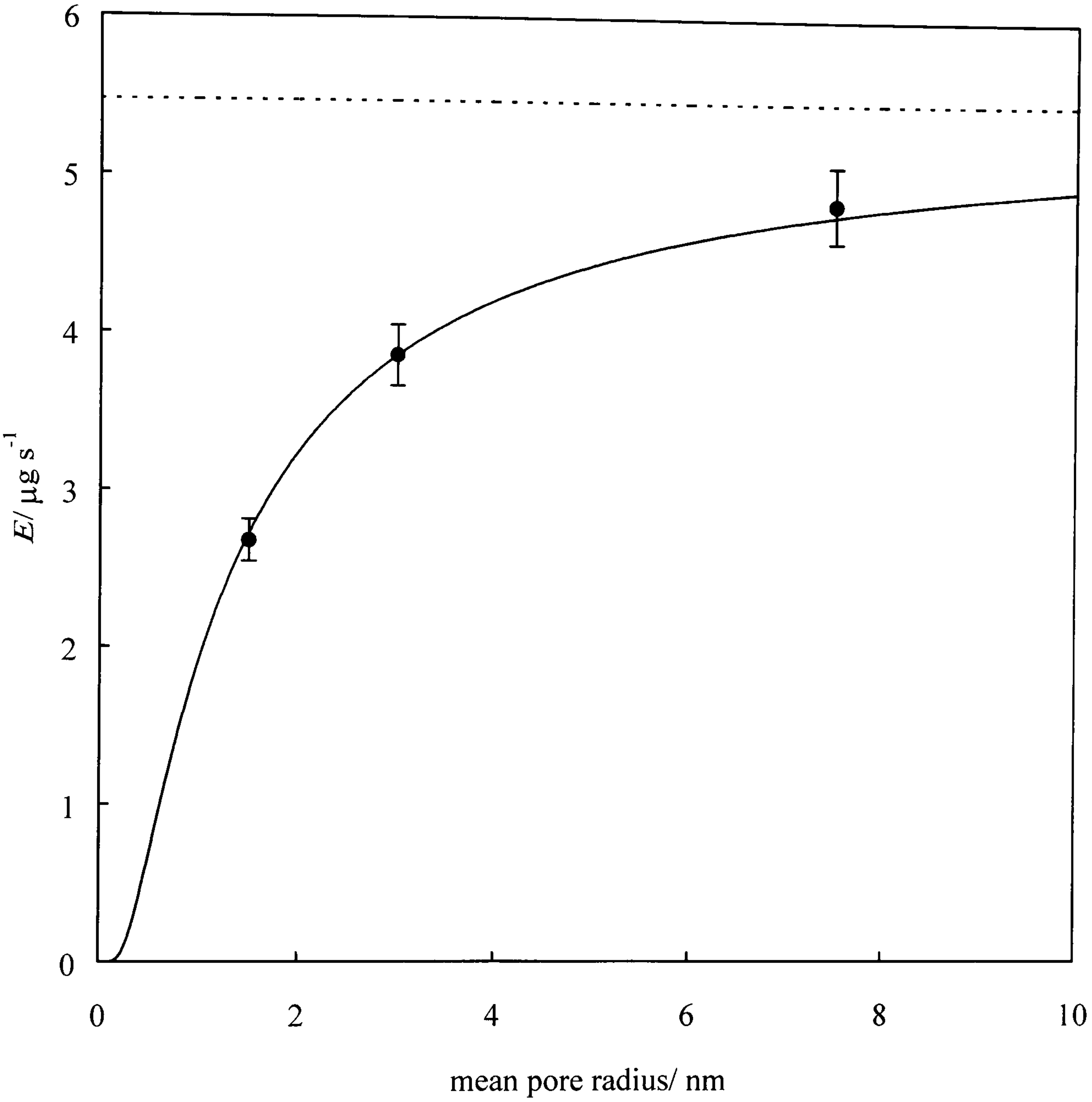

Figure 3.7 ***Variation of initial evaporation rate E_o with mean pore radius for particles with 50% filled pore volumes at 25°C and 1920 ml min^{-1} nitrogen gas flow rate. The solid line is the calculated line from Equations [3.22] and [3.28], whilst the dotted line represents the rate for pure water under the same experimental conditions. The values of γ and V_m are 0.072 N m^{-1} and 1.8 x 10^{-5} m^3 mol^{-1} respectively*** [7].

Absorbent powders are routinely used for mopping up spillages of volatile liquids, and there are important implications to be considered here. All samples used in these experiments felt dry to the touch, but it is clear that the evaporation rate of the liquid from the pores is still relatively high. In order to significantly lower the evaporation rate it is necessary for the powder to have a very small pore radius. It is also of note that a much larger vapour pressure reduction would be predicted from Equation [3.28] for liquids of higher molar volume. Volatile organic liquids have a higher molar volume than the water used in these experiments.

The variation in evaporation rates from samples which have different fractions of the total pore volume filled with water is now investigated. Figure 3.8 shows the initial mass evaporation rate as a function of the fraction of the pore volume filled.

It can be seen that the evaporation rates increase steadily with the fraction of pore volume filled. This behaviour indicates that the effective radius of the pores changes as a function of the extent of filling. Using Equation [3.28], the data from Figure 3.8 has been converted to show the variation of effective pore radius with the fraction of pore volume filled, and this is shown in Figure 3.9. Although the experimental uncertainties become large for big pore radii, it can be concluded from this figure that the silica samples contain a wide distribution of pore radii with the small radius pores being filled at low water contents.

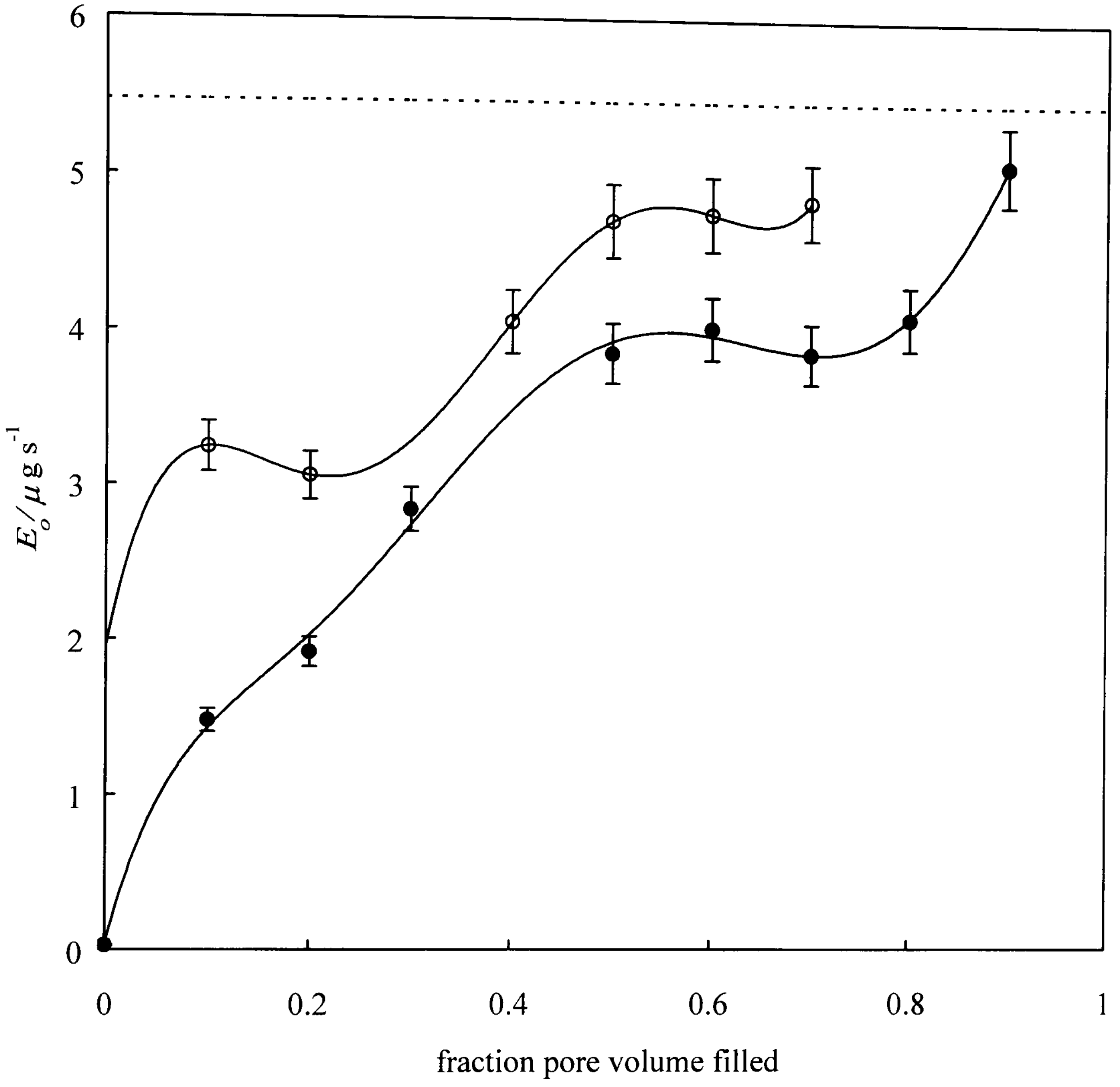

Figure 3.8 ***Variation of initial evaporation rate E_o with fraction of pore volume filled for 3.0 nm (closed circles) and 7.1 nm (open circles) pore radius silica powders. The solid lines are the line of best-fit for the data. Measurements were taken at 25°C and 1920 ml min^{-1} nitrogen gas flow rate. All apparatus constants are as given in Figure 3.1. The dashed line shows the initial evaporation rate for pure water under the same conditions.***

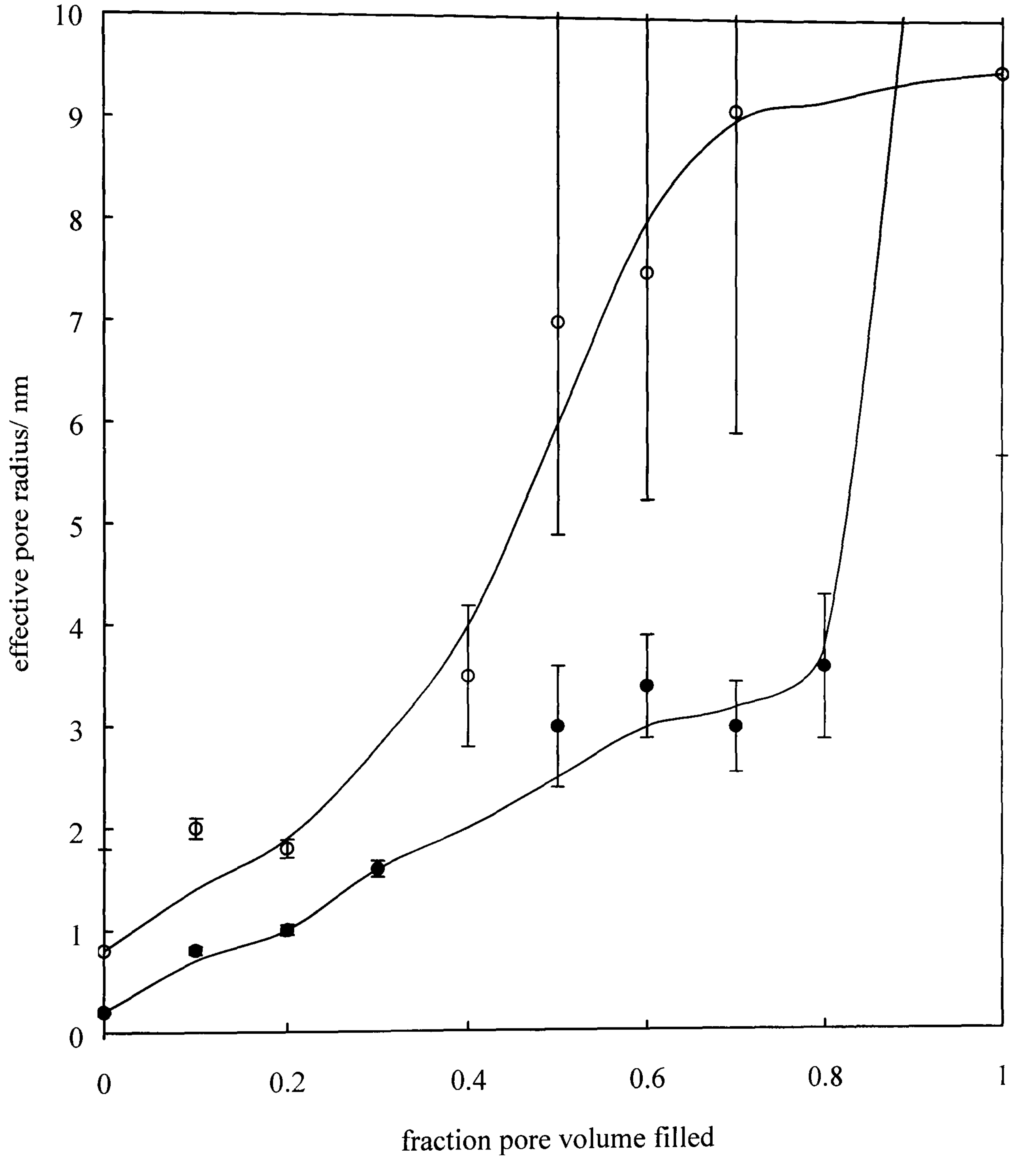

Figure 3.9 ***Effective pore radius versus fraction of pore volume filled for 3.0 nm (filled circles) and 7.1 nm (open circles) mean pore radius samples, calculated using data from Figure 3.8. The solid lines are the lines of best-fit for the data.***

A more complex system is encountered when a sample of powder which contains liquid is overlaid with dry powder. Figure 3.10 shows a sample in which the lower half of the sample contains water corresponding to 50% filling of the pore volume and the upper half of the sample is completely dry.

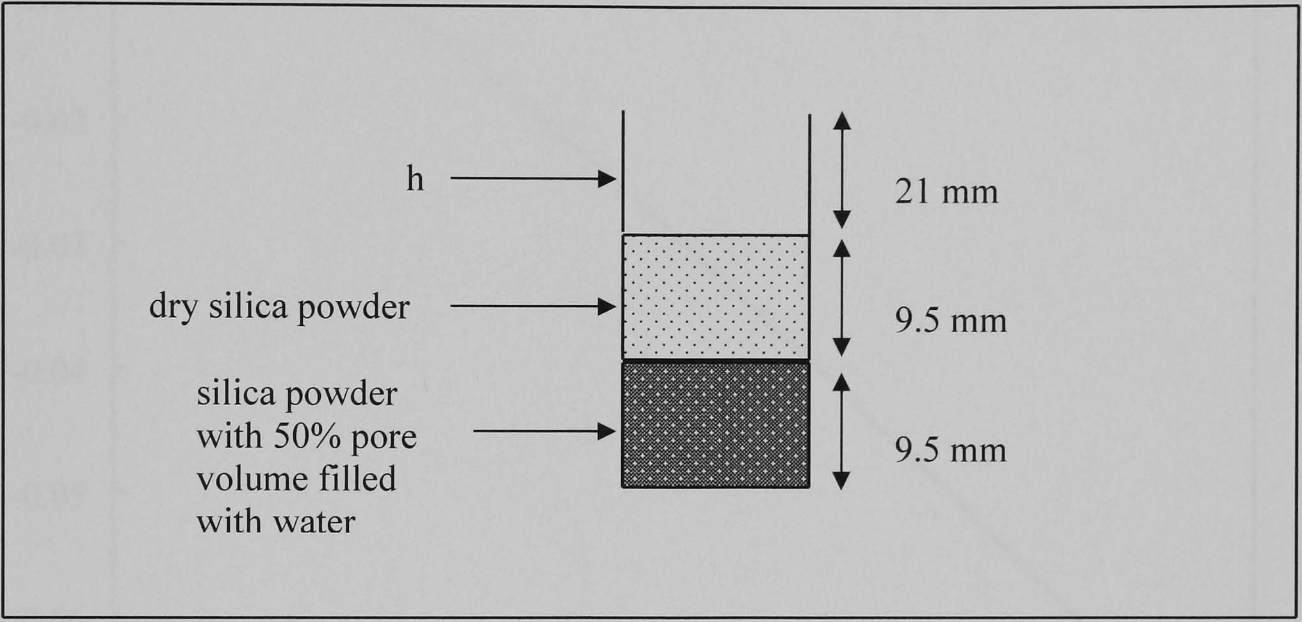

Figure 3.10 Schematic representation of a sample of silica containing liquid overlaid with dry silica powder.

Figure 3.11 shows the mass versus time curve for the sample shown in Figure 3.10. Initially, water evaporates from the 50% filled layer and equilibrates with the dry powder layer to give a sample corresponding to 25% pore volume filling. The data of Figure 3.11 were differentiated to show the mass evaporation rate versus time in Figure 3.12. The dashed line indicates the evaporation rate expected from a sample in which the pores are filled to 25% of their total volume. The rate approaches this rate at long times. The time taken to achieve homogeneous distribution of the water throughout the total powder volume is approximately five hours.

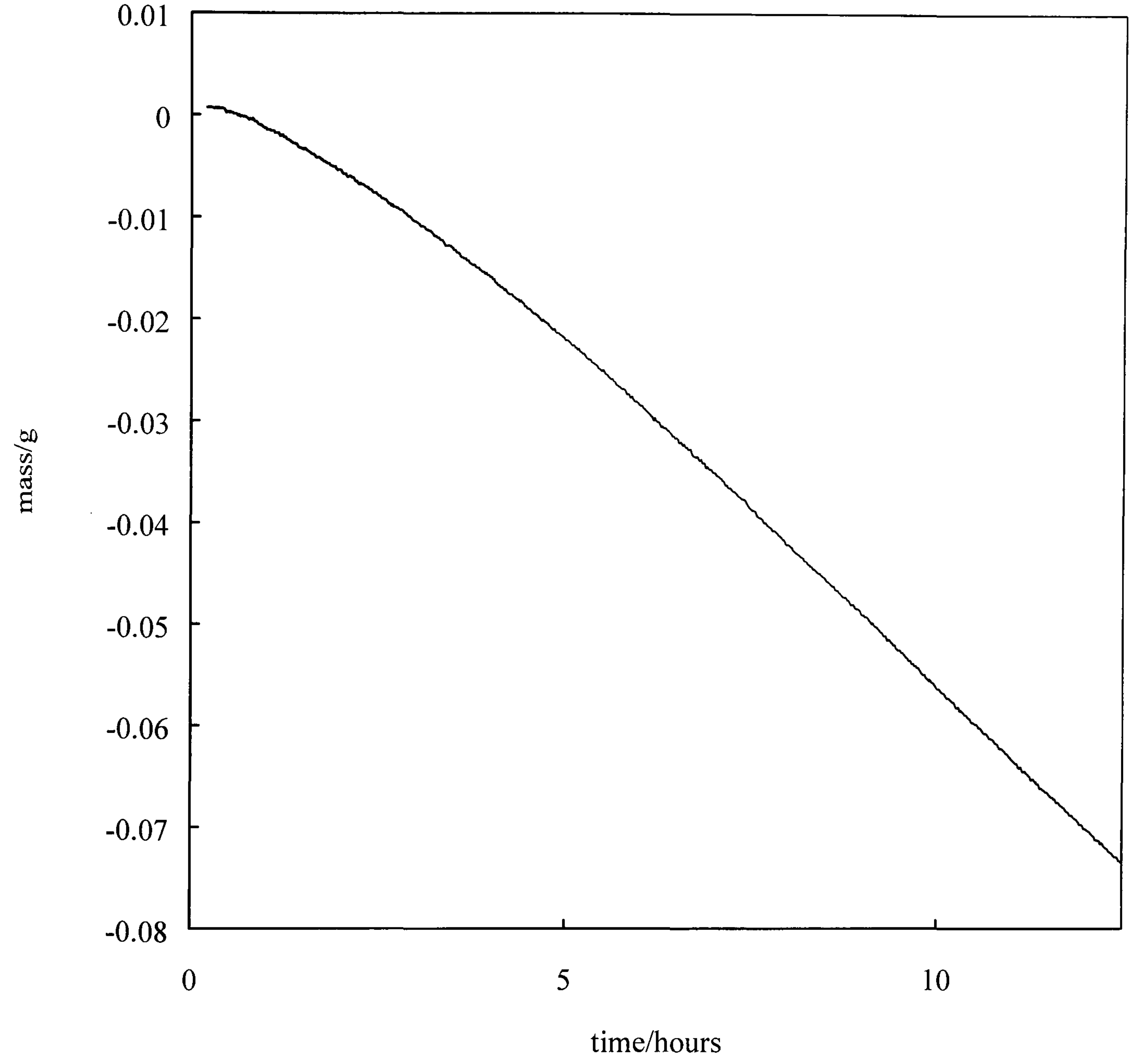

Figure 3.11 ***Mass versus time curve for water evaporating from a sample containing 1.04 g of 3.0 nm pore radius silica to which a volume of water corresponding to 50% pore volume filled has been added and overlaid with 1.04 g of dry silica of 3.0 nm pore radius. Measurements were made at 25°C and 1920 ml min^{-1} nitrogen gas flow rate. All apparatus constants are as given in Figure 3.1.***

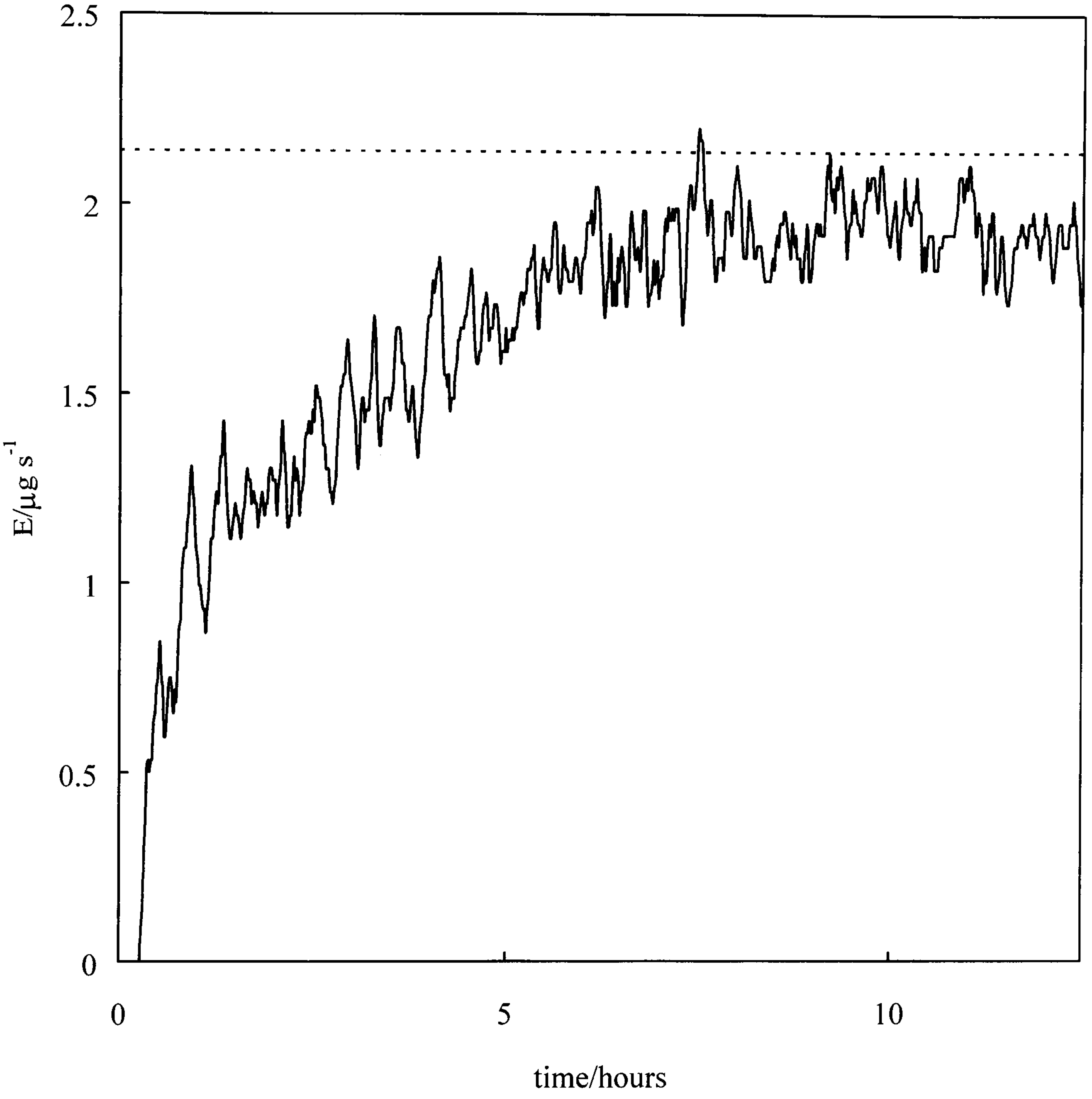

Figure 3.12 ***Evaporation rate E versus time for the sample shown in Figure 3.10 evaporated at 25°C and 1920 ml min^{-1} nitrogen gas flow rate. The dashed line shows the theoretical rate for 2.08 g of 3.0 nm silica with 25% pore volume filled with water. All apparatus constants are as given in Figure 3.1. The values of diffusion coefficient and vapour pressure used to calculate the dashed line are given in Table 3.1.***

3.6 Conclusions

In Chapter 3 it has been shown that the experimental equipment described in Chapter 2 can be used to determine absolute liquid mass evaporation rates to within a few percent. A simple model for the prediction of mass evaporation rates has been developed, tested and found to successfully account for the variation in measured mass evaporation rate with gas flow rate and stagnant vapour layer thickness *h*. A plateau region in which the mass evaporation rate is independent of gas flow rate can be predicted has been determined and the mass evaporation rates of liquids with vapour pressures ranging from 10 to 67,000 Pascals (0.1 to 500 Torr) have been measured in this region and show good agreement with predicted values.

It has also been shown that the mass evaporation rate of water contained within porous silica particles of different mean pore diameters is correctly predicted by the Kelvin Equation and varies with the extent of filling of the total pore volume for the samples investigated. Finally, it has been shown that the mass evaporation rate from a sample of silica containing water within the pores overlaid with dry powder shows an initially slow rate but reaches the rate expected for a homogeneously filled sample after several hours.

3.7 References

1. A. Stefan, *Sitzbungsber. Wiener Akad. Wissensch.* II , 1873, **68**, 385.
2. A. Stefan, *Sitzbungsber. Wiener Akad. Wissensch.* II , 1889, **98**, 1418.
3. W. Jost, *"Diffusion in Solids, Liquids and Gases"*, Academic Press Inc., New York, 1952.
4. R. Fuerth, Article Diffusion in F. Auerbach and W. Hort *"Handbuch physik techn. Mechamik"*, Vol 7. Leipzig, 1931.
5. J. R. Welty, C. E. Wicks and R. E. Wilson, *"Fundamentals of Momentum, Heat and Mass Transfer"*, 3rd edn., John Wiley and Sons Inc., New York, 1984.
6. A. T. Prata and E. M. Sparrow, *Can J. Chem. Eng.*, 1986, **64**, 511.
7. *"CRC Handbook of Chemistry and Physics"*, CRC Press Inc., Boca Raton, 62nd edn., 1981.
8. *"Selected Values of Properties of Hydrocarbons and related Compounds"*, Themodynamics Research Center, AP144, Texas A&M University, 1978.
9. R. C. Reid, J. N. Prausnitz and T. K. Sherwood, "*The Properties of Liquids and Gases*", 3rd edn., McGraw-Hill, New York, 1977.
10. G. A. Lugg, *Anal. Chem.*, 1968, **40**, 1072.
11. G. A. McD. Cummings and A. R. Ubbelohde, *J. Chem. Soc.*, 1953, 3751.
12. L. T. Carmichael, B. H. Sage and W. N. Lacey, *Am. Inst. Chem. Eng. J.*, 1955, **1**, 385.
13. E. Mack Jr., *J. Am Chem. Soc.*, 1925, **47**, 2468.

14. G. A. Hudson, J. C. McCoubrey and A. R. Ubbelohde, *Trans. Faraday Soc.*, 1960, **56**, 1144.

15. J. H. Clint, P. D. I. Fletcher and I. T. Todorov, *Phys. Chem. Chem. Phys.*, 1999, **1**, 5005.

16. A. W. Adamson and A. P. Gast, *"Physical Chemistry of Surfaces"*, John Wiley and Sons Inc., New York, 6th edn., 1997.

CHAPTER 4

EVAPORATION RATES OF NON-STRUCTURED AND STRUCTURED LIQUID MIXTURES

Chapter 3 describes a quantitative model which accurately predicts the evaporation rate of pure liquids. In this chapter, the analysis is extended to non-structured and structured liquid mixtures. The study begins by considering evaporation from unstructured mixtures of miscible liquids in which only one component is volatile. It continues to investigate the effect of structure on evaporation rate, firstly from a volatile liquid gelled with solid particles and then from a surfactant / water mixture which exhibits a variety of liquid crystal phases.

4.1 Evaporation rates of squalane/alkane mixtures

Consider a liquid mixture containing a volatile species and an involatile species. The equilibrium vapour pressure of the volatile component within the liquid mixture is given by

$$P = \varphi P_o x_1 \qquad [4.1]$$

where P_o is the vapour pressure of the pure volatile component, x_1 is the mole fraction of the volatile species and φ is the activity coefficient.

The activity scale here corresponds to $\varphi = 1$ when $x = 1$ and the vapour-gas mixtures are assumed to behave ideally.

The variation of φ with x_1 for squalane mixtures with a range of linear alkanes has been measured by Ashworth and Everett[1]. Briefly, the activity coefficient is the sum of two contributing effects

$$\ln \varphi = \ln \varphi^{ath} + \ln \varphi^{th} \qquad [4.2]$$

where φ^{ath} is an athermal term arising from statistical effects due to the difference in sizes of the molecules in the mixture and φ^{th} is a temperature dependent term associated with the interaction energies between the molecules in the mixture.

For a mixture of molecules with volume ratio r, the logarithm of φ_1^{ath} has been calculated theoretically[2] and shown to be equal to

$$\ln \gamma_1^{ath} = \ln\left(\frac{1-\phi_2}{x_1}\right) - \frac{\zeta}{2}\ln\left\{1-\left(1-\frac{1}{r}\right)\frac{2\phi_2}{\zeta}\right\} \qquad [4.3]$$

where φ_1^{ath} is the statistical term of the activity coefficient for the small molecule in the mixture, ϕ_2 is the volume fraction of the larger molecule in the mixture and ζ is the number of nearest neighbour sites to a given segment of a molecule.

The volume fraction of the larger molecule is given by

$$\phi_2 = \frac{rx_2}{x_1 + rx_2} = \frac{r(1 - x_1)}{x_1 + r(1 - x)} \qquad [4.4]$$

The Flory-Huggins theory[3] sets

$$\ln \varphi_1^{th} = \chi\phi_2^2 \qquad [4.5]$$

where χ is an interaction parameter, determined experimentally.

Combination of Equations [4.2], [4.3] and [4.5] gives a final expression relating φ to x_1.

$$\varphi = \exp\left\{ \ln\left(\frac{1-\phi_2}{x_1}\right) - \frac{\zeta}{2}\ln\left(1 - \left(1 - \frac{1}{r}\right)\frac{2\phi_2}{\zeta}\right) + \chi\phi_2^2 \right\} \qquad [4.6]$$

The parameter ζ was taken to be 6 and values of r and χ for the volatile components are given in Table 4.1. For the squalane / volatile alkane mixtures considered here, φ^{ath} is much greater than φ^{th} and χ is virtually temperature independent. Therefore, values of χ determined at 30°C in reference (1) were used in the calculation. This approximation introduces negligible error.

Table 4.1: Values of r and χ at 25°C for squalane / volatile alkane mixtures[1]

Liquid	**r**	χ
n-pentane	4.495	0.152
n-hexane	3.966	0.094

Figure 4.1 shows the variation of activity coefficients with composition for pentane and hexane in squalane at 25°C, calculated using Equation [4.6].

Figure 4.2 shows the mass versus time curves for a mixture of n-pentane and squalane and a mixture of n-hexane and squalane. The plots appear very similar to those seen for pure liquids in Chapter 3. In order to show the differences more clearly, the data from these plots were numerically differentiated and the analysis carried out on the resulting evaporation rate versus time plots.

It has already been shown that for pure liquids at high gas flow rate, the mass evaporation rate is given by

$$E = -\frac{dm}{dt} = \frac{MADPz}{hRT} \qquad [4.7]$$

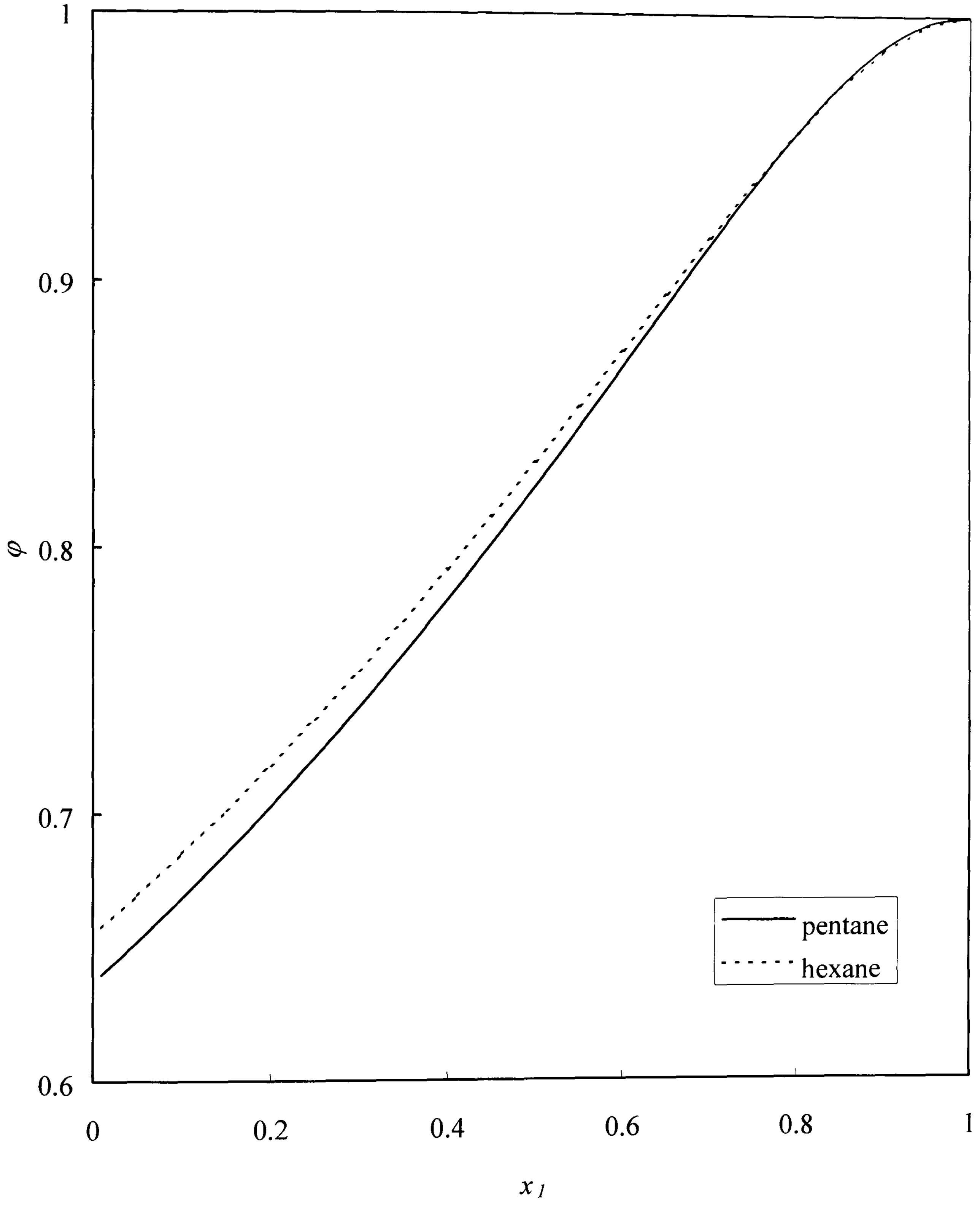

Figure 4.1 *Variation of activity coefficients with composition for n-pentane and n-hexane in mixtures with squalane at 25°C. The lines are calculated as described in the text.*

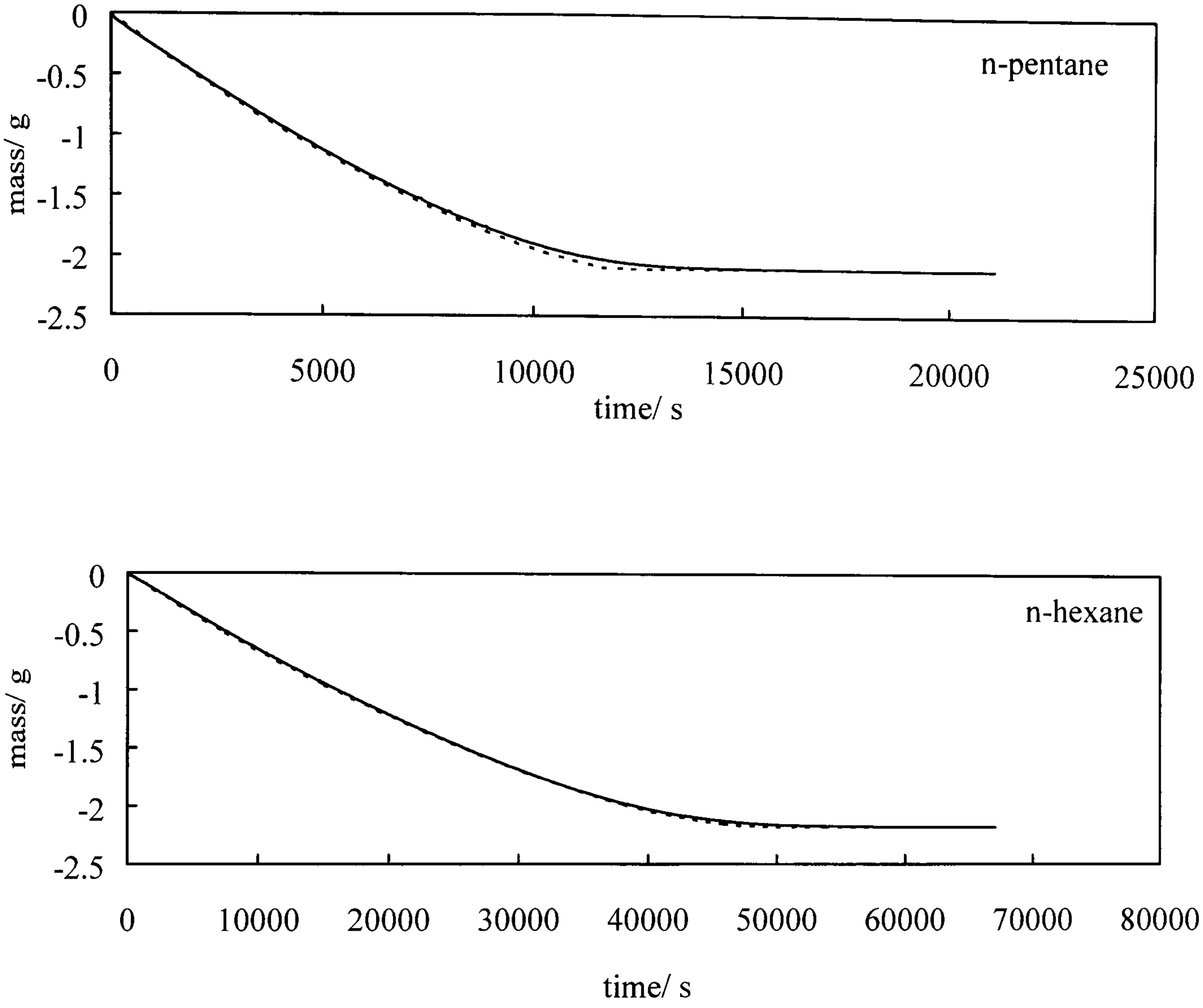

Figure 4.2 ***Comparison between calculated (dashed lines) and measured (full lines) mass versus time curves for mixtures of (a) n-pentane and squalane and (b) n-hexane and squalane at 25°C and 1920 ml min^{-1} nitrogen gas flow rate. For (a) the initial mass of n-pentane, $m_{o,1}$, was 2.106 g, the initial mass of squalane, $m_{o,2}$, was 0.415 g and $h_x = 39.97$ mm^2. For (b) the initial mass of n-hexane, $m_{o,1}$, was 2.181 g, the initial mass of squalane, $m_{o,2}$, was 0.410 g and $h_x = 35.37$ mm^2. The dotted lines were calculated using the data in Table 4.2 and Figure 4.1. For both runs, $A = 2.51 \times 10^{-4}$ m^2.***

Combination of Equations [4.1] and [4.7] give an expression which allows the prediction of the evaporation rate for any mole fraction.

$$E = \frac{MAD\varphi P_o x_1 z}{hRT} \qquad [4.8]$$

It should be noted that since z is dependent on the vapour pressure of the evaporating species (see Chapter 3), it would also change with mole fraction and this is taken into account in the following analysis.

The mole fraction of the volatile species at any point during the evaporation process is given by

$$x_1 = \frac{\left(m_{o,1} + m \big/ M_1\right)}{\left(m_{o,1} + m \big/ M_1\right) + m_{o,2} \big/ M_2} \qquad [4.9]$$

where $m_{o,1}$ and $m_{o,2}$ are the initial masses and M_1 and M_2 are the molar masses of the volatile and non-volatile components in the mixture and m is the mass change of the mixture.

h at any point is given by

$$h = h_x - \left(\frac{\left({m_{o,2}}/{\rho_2} \right) + \left({(m_{o,1} + m)}/{\rho_1} \right)}{A} \right) \qquad [4.10]$$

where ρ_1 and ρ_2 are the densities of the two components.

Combination of Equations [4.8], [4.9] and [4.10] allows the accurate calculation of evaporation rate over the whole time course. Values of molar mass, vapour diffusion coefficients, vapour pressures and liquid densities required for the rate calculations are given in Table 4.2.

Figure 4.3 compares measured and calculated evaporation rates for n-pentane-squalane and n-hexane-squalane mixtures. The agreement between calculated and experimental values is excellent. The fact that the x_1 dependent vapour pressure of the surface layer is correctly predicted from the bulk composition provides clear evidence that no significant concentration gradients are developed within the liquid mixtures as evaporation proceeds. As seen for pure liquids, there is no significant energy barrier to transport across the liquid vapour surface. It is concluded that the rate-limiting process in these unstructured liquid mixtures is diffusion of vapour across the stagnant layer gas.

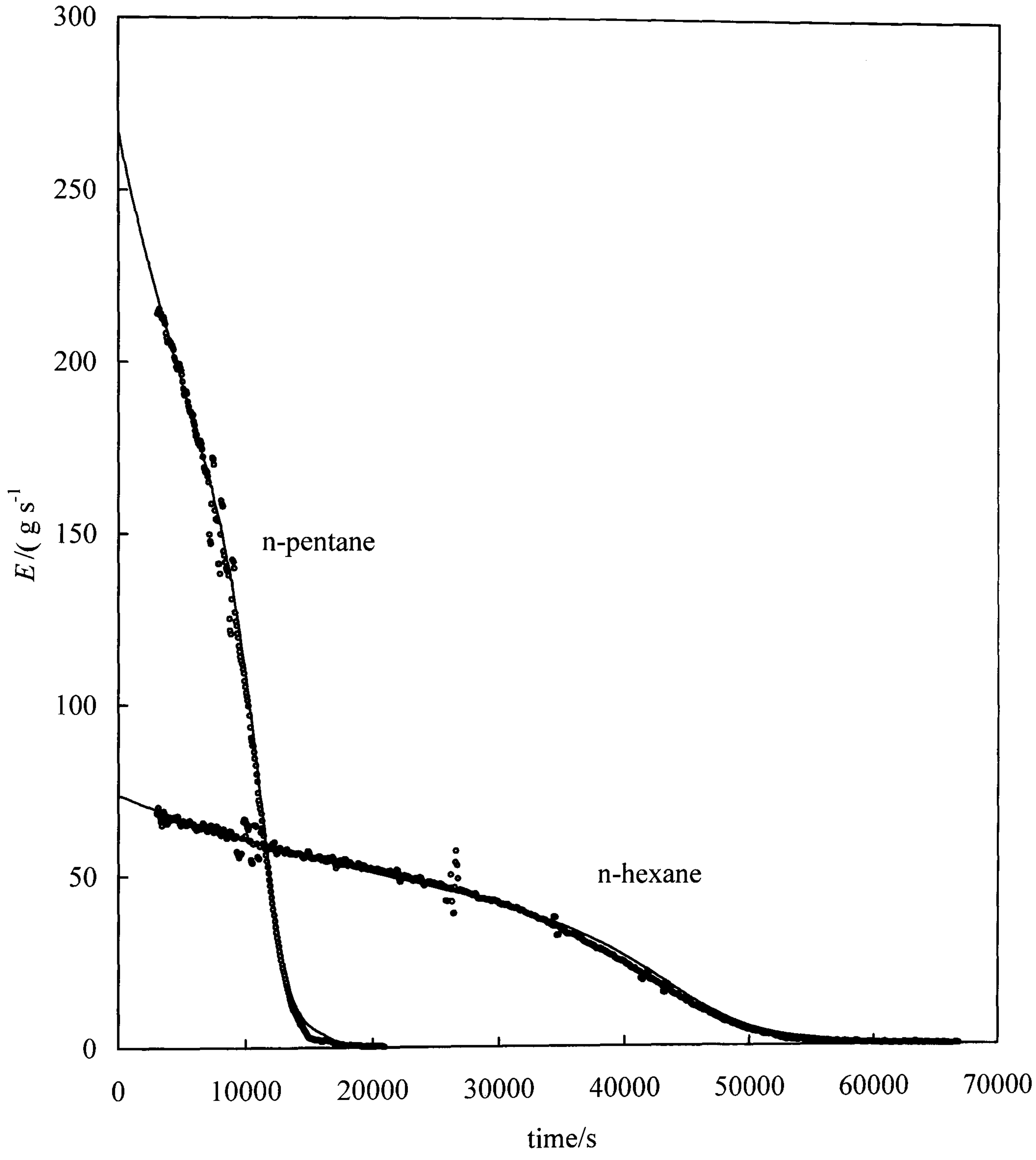

Figure 4.3 ***Measured (open circles) and calculated (solid lines) evaporation rates versus time for mixtures of n-pentane and n-hexane with squalane at 25°C and 1920 ml min^{-1} nitrogen gas flow rate. The solid lines are calculated using the data in Figure 4.1 and Table 4.2. All experimental parameters are as given in Figure 4.2.***

Table 4.2: ***Values of molar masses M, vapour pressures P_o, diffusion coefficients D and densities ρ used in the calculation of evaporation rates at 25°C.***

Component	***M*/ kg mol^{-1}**	***P_o*/ Pa**	***D*/ 10^{-6} m^2 s^{-1}**	***ρ*/ kg m^{-3}**
n-pentane	0.072	68368 [4]	8.42 [6]	621.2 [4]
n-hexane	0.086	20198 [4]	7.90 [7]	654.7 [4]
Water	0.018	3168 [5]	24.0 [8]	997.1 [5]
Squalane	0.422	-	-	804 [4]
$C_{12}E_6$	0.450	-	-	1000*

* Estimated value

The uniformity of concentration is likely to arise from convection within the liquid mixture induced by the evaporation at the liquid/vapour surface. Loss of the volatile species from the liquid surface results in (a) a slight cooling, and (b) a local increase in the mole fraction of squalane in the surface region. Both effects produce an increase in the density of the surface region compared with the density of the bulk mixture. This density difference produces a gravitational instability which sets up an array of small convective cells. The net result is good mixing of the liquid. This effect has been observed during the evaporation of water from aqueous sucrose solutions[9]. Polygonal cells measuring a few millimetres in diameter are seen within the sucrose solutions. Liquid velocities of a few μm s^{-1} (measured using latex tracer particles) are established within the mixture.

It is concluded that similar convection processes occur in the squalane/ volatile alkane mixtures studied here and cause the surface concentration to be maintained at the bulk value during the evaporation process.

4.2 Evaporation rate of n-hexane gelled with solid particles

The evaporation of n-hexane gelled by the addition of silica particles is now considered. In this system, the silica particles form a separate and immiscible phase and the vapour pressure of the hexane remains constant and equal to P_o for all compositions.

Figure 4.4 shows the mass versus time and evaporation rate versus time plots for a n-hexane gel sample. Again, the mass versus time curves appear very similar to those seen for pure liquids, and the differential plot shows the variations more clearly. The theoretical line is calculated by assuming the rate-limiting step remains diffusion through the stagnant layer. Initially, the gel appeared highly viscous and showed no flow when the sample tube was inverted. Visual observation of the evaporating samples showed that partial evaporation produced a gel layer sitting below a very loosely packed layer of silica particles. The measured rate is consistent with the predicted rate up to times of around eight hours. Figure 4.5 shows the evaporation rate data from Figure 4.4 plotted as a function of mass fraction of n-hexane in the n-hexane-silica mixture. It can be seen that the mass fraction of n-hexane in the mixture at this time is approximately 0.6.

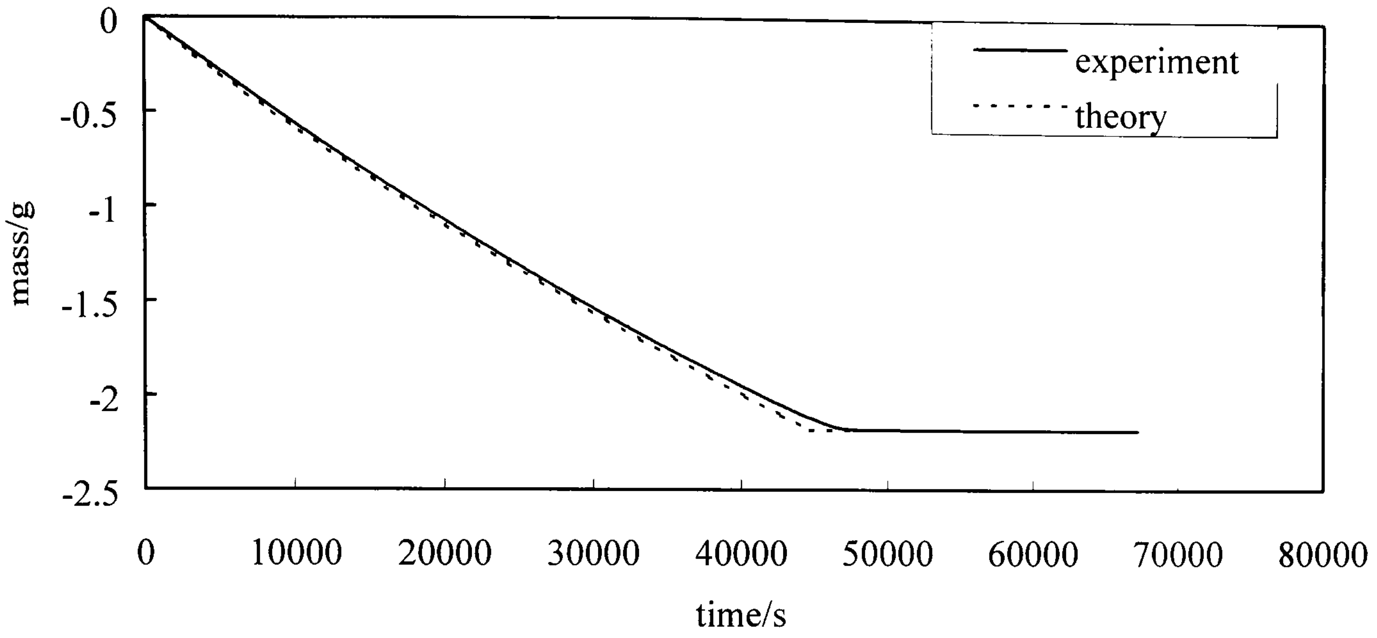

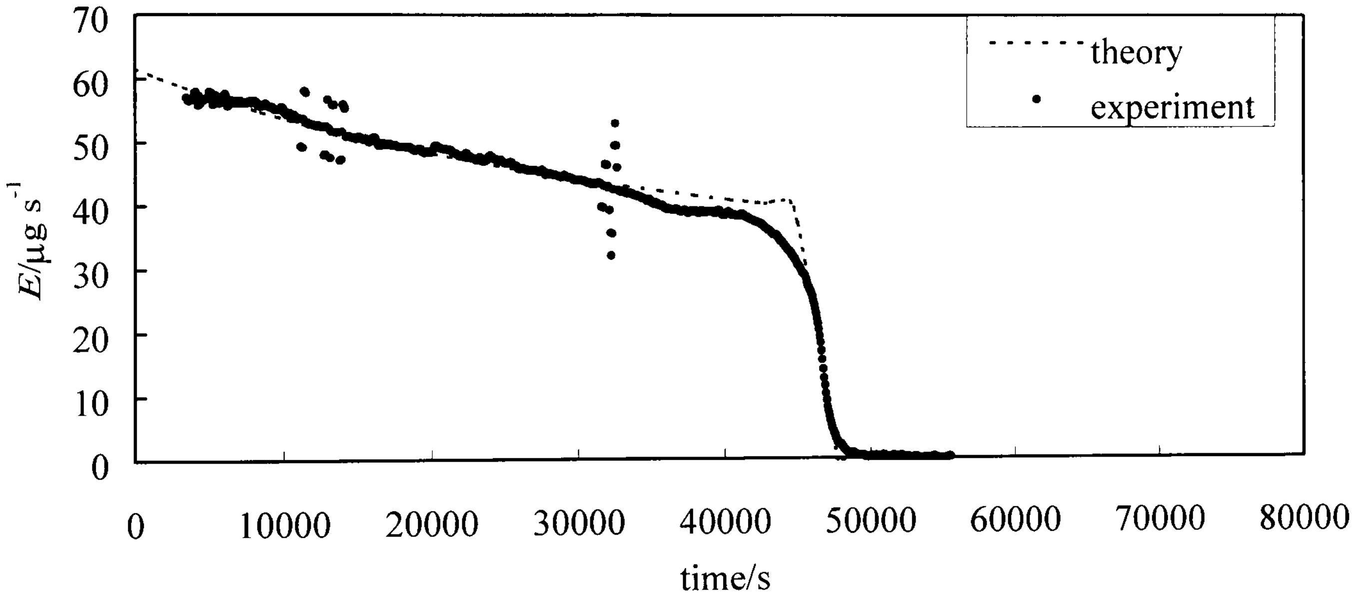

Figure 4.4 ***Mass versus time and evaporation rate E versus time plots for n-hexane gelled with silica particles at 25°C and 1920 ml min^{-1} nitrogen gas flow rate. The dotted lines are calculated on the basis that the n-hexane has an independent vapour pressure equal to that of pure n-hexane. The mixture initially contained 0.2607 g of silica and 2.1801 g of n-hexane. For this experiment h_x = 37.97 mm and all other parameters are as for Figure 4.3. Rate measurements are averaged over three values to reduce scatter.***

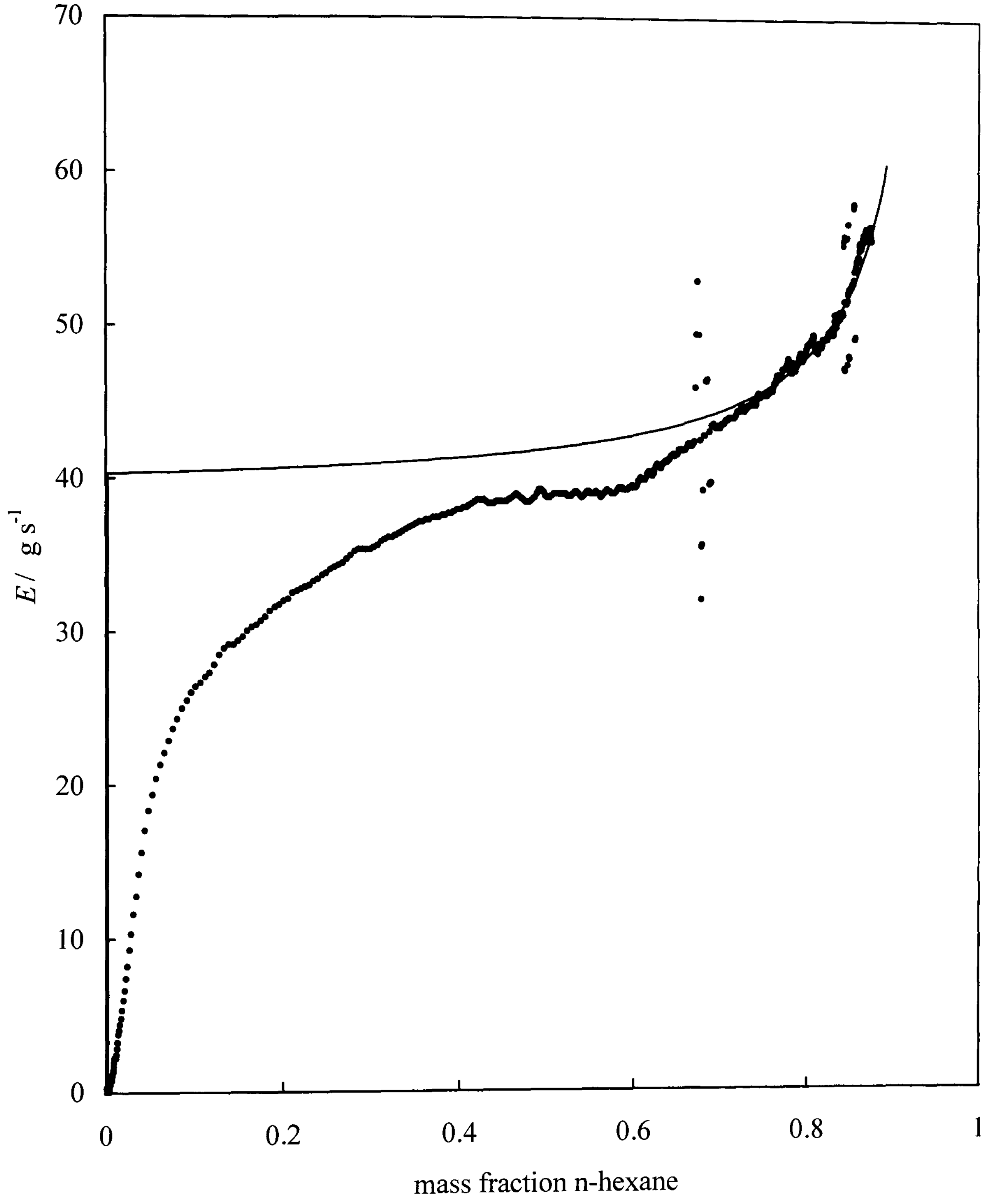

Figure 4.5 *The data of Figure 4.4 re-plotted as a function of mass fraction of n-hexane in the n-hexane –silica particle mixtures. The solid line is the calculated E value, whilst the filled circles are obtained from the measured values.*

At longer times (which correspond to lower solvent mass fractions), the measured rates fall below the calculated values, probably as a result of two main effects. Firstly, the loosely packed silica powder layer on the surface may serve to slow the vapour diffusion rate slightly by an obstruction effect. Erratic partial collapse of this layer may account for the less smooth appearance of these curves as compared with the non-gelled samples shown in Figure 4.2. Secondly, at very low n-hexane mass fractions towards the end of the evaporation process, the small amount of n-hexane remaining is expected to form small liquid bridges at the points of contact between two adjacent particles. This is shown schematically in Figure 4.6. The liquid surfaces of the n-hexane bridges are very highly curved, and the Kelvin Effect leads to a lowering of the n-hexane vapour pressure. As shown in Chapter 3, this vapour pressure lowering results in a reduced evaporation rate. Both effects are relatively minor, and it can be concluded that n-hexane gelled using silica particles shows a similar evaporation rate profile to that of pure non-gelled n-hexane with vapour diffusion across the stagnant gas layer being rate limiting.

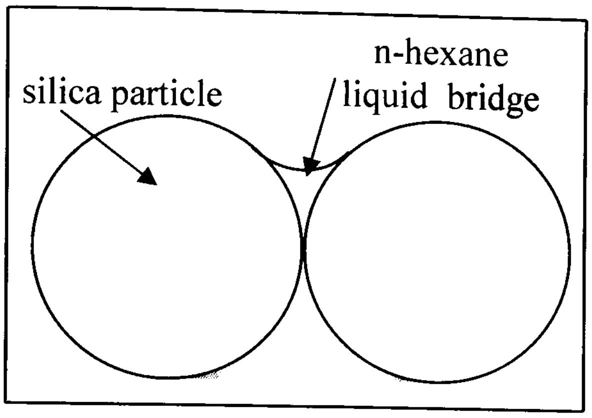

Figure 4.6 ***Diagram showing the presence of n-hexane liquid bridges between adjacent silica particles in hexane-silica gels. The liquid bridges are formed by capillary condensation. The n-hexane surface is highly curved, and this is expected to cause a decrease in n-hexane vapour pressure (as described in Chapter 3).***

4.3 Evaporation rate of water from mixtures with $C_{12}E_6$

In Section 4.1, it was concluded that convection processes within unstructured liquid mixtures maintained the surface concentration at the bulk value. The purpose of the final experiments detailed in this chapter was to determine whether these convection processes could be suppressed by structuring of the liquid mixture. Suppression would result in a reduction in the evaporation rate as the volatile component in the surface layer is depleted by evaporation.

The mixtures considered here consist of water (the volatile component) mixed with the non-ionic surfactant n-dodecylhexaoxyethylene glycol ether $C_{12}E_6$ (involatile). In these mixtures, the surfactant induces both a (composition dependent) lowering of the water vapour pressure according to Equation 4.1, and a microstructuring of the liquid by the spontaneous self-assembly of the surfactant into a variety of ordered mesophases. The variation of water activity with mole fraction $C_{12}E_6$ for water-$C_{12}E_6$ mixtures has been determined by Clunie *et al*[10] and is shown in Figure 4.7. The data have been used to calculate the variation of φ_{water} with x shown in Figure 4.8. A clear break can be seen in the data of Figure 4.7 and two polynomials were fitted to the experimental data. These are shown in Figure 4.8 (a) and (b). Figure 4.8 (c) is the combination of the polynomials fitted in (a) and (b). These relationships were combined with Equation [4.8] in order to calculate the rate expected if gas diffusion across the stagnant layer is the rate-limiting step.

In Chapter 1, the retardation of water evaporation by surfactant monolayers is discussed, and it is relevant to comment here that the presence of an adsorbed monolayer of $C_{12}E_6$ at the surface does not appreciably slow evaporation. Retardation has only been observed for monolayers of long hydrocarbon chain, water insoluble species at very high surface concentrations (typically ≥ 5 chains per nm^2)[12]. Adsorbed monolayers of soluble surfactants such as $C_{12}E_6$, with maximum surface concentration of around 2 chains per nm^2, are highly disordered and show no evaporation retardation[11].

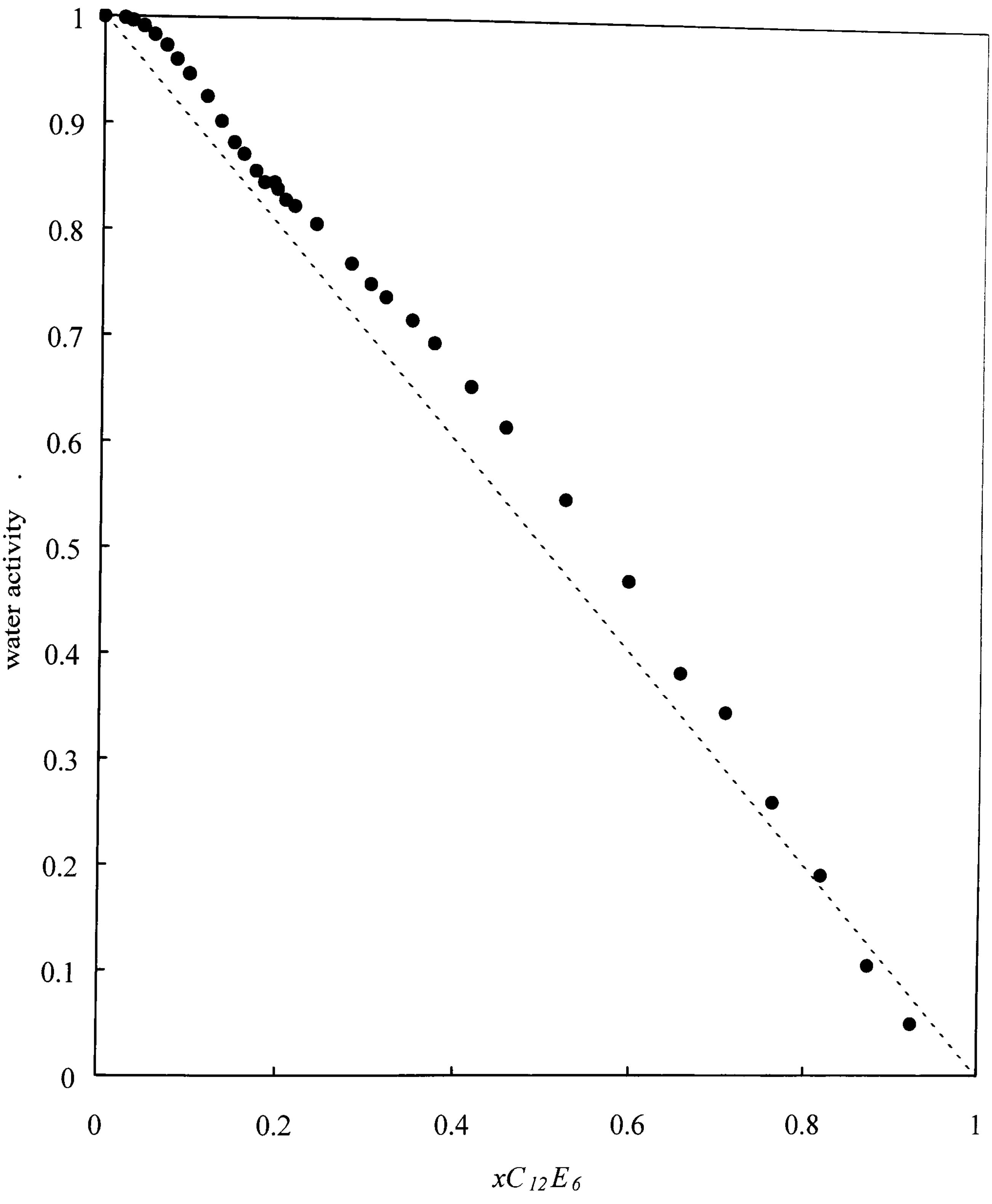

Figure 4.7 ***The variation of water activity with mole fraction of surfactant at 25°C, reproduced from reference (10). The dashed line shows Raoult's Law behaviour.***

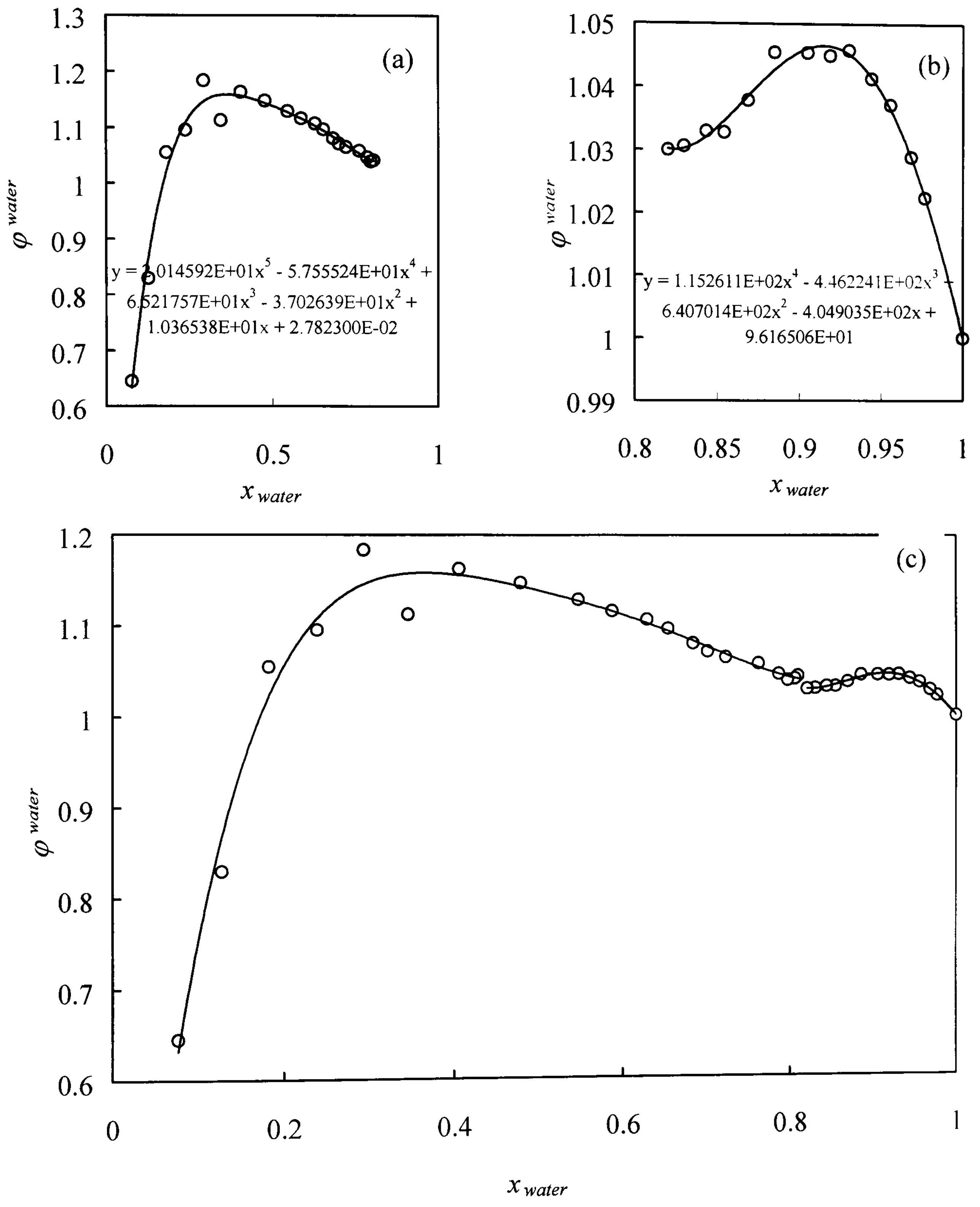

Figure 4.8 ***Variation of φ_{water} with x_{water} for mixtures of $C_{12}E_6$ at 25.0°C. The solid lines shown in (a) and (b) are the polynomials fitted to the data from Figure 4.7. These are combined to give (c).***

The phase diagram for water/ $C_{12}E_6$ has been determined by Clunie *et al*[10] and further elucidated by Mitchell *et al*[13]. The equilibrium phase boundaries at 25°C are summarised in Table 4.3.

Table 4.3: Equilibrium phase boundaries for $C_{12}E_6$ plus water mixtures at 25°C

x_{water} **range**	**Phases present**
1-0.9758	Isotropic micellar L_1
0.9578-0.9746	Isotropic micellar L_1 + normal hexagonal H_1
0.9746-0.9406	Normal hexagonal H_1
0.9406-0.9389	Normal hexagonal H_1 + viscous isotropic V_1
0.9389-0.9243	Viscous isotropic V_1
0.9243-0.9235	Viscous isotropic V_1 + lamellar L_α
0.9235-0.8201	Lamellar L_α
0.8201-0.8082	Lamellar L_α + isotropic liquid
0.8082-0	Isotropic liquid

With increasing $C_{12}E_6$ concentration, the phase sequence is isotropic micellar dispersion (L_1), normal hexagonal phase (H_1) consisting of hexagonally packed cylindrical micelles, the viscous isotropic phase (V_1) consisting of a cubic arrangement of non-spherical aggregates, a lamellar phase (L_α) consisting of planar bilayer surfactant sheets separated by water films and an isotropic liquid phase.

Each single phase region is separated by a two-phase region containing a mixture of both adjacent phases. At the experimental temperature of 25°C, pure $C_{12}E_6$ is a liquid.

Figure 4.9 shows a comparison of calculated and measured evaporation rates for seven runs with differing initial composition. The rates are plotted as the product *Eh* (in order to normalise out differences in the stagnant layer thickness) against water mole fraction. For water-rich compositions ($x_{water} > 0.85$) measured rates are only slightly lower than predicted. This indicates that the vapour pressures at the liquid surface are only slightly lower than those predicted from the overall composition, *i.e.* the mixtures have not developed large concentration gradients. No significant rate changes are observed as the phase boundaries from the L_1 to H_1, V_1 and L_α phases are crossed. At the end of the first run (at which point the average value of x_{water} has fallen to approximately 0.9), the evaporation rate is approximately 20% lower than the start of run 2 (which has an initial homogenous rate of approximately 0.9). The development of the concentration gradient in run 1 is a very slow process (the time span between start and finish is approximately eleven days). For run 2, a sharp fall in rate is observed at x_{water} of approximately 0.83 (corresponding to approximately three and a quarter days) to give a rate of only approximately 10% of that expected for the mixture in the absence of concentration gradients.

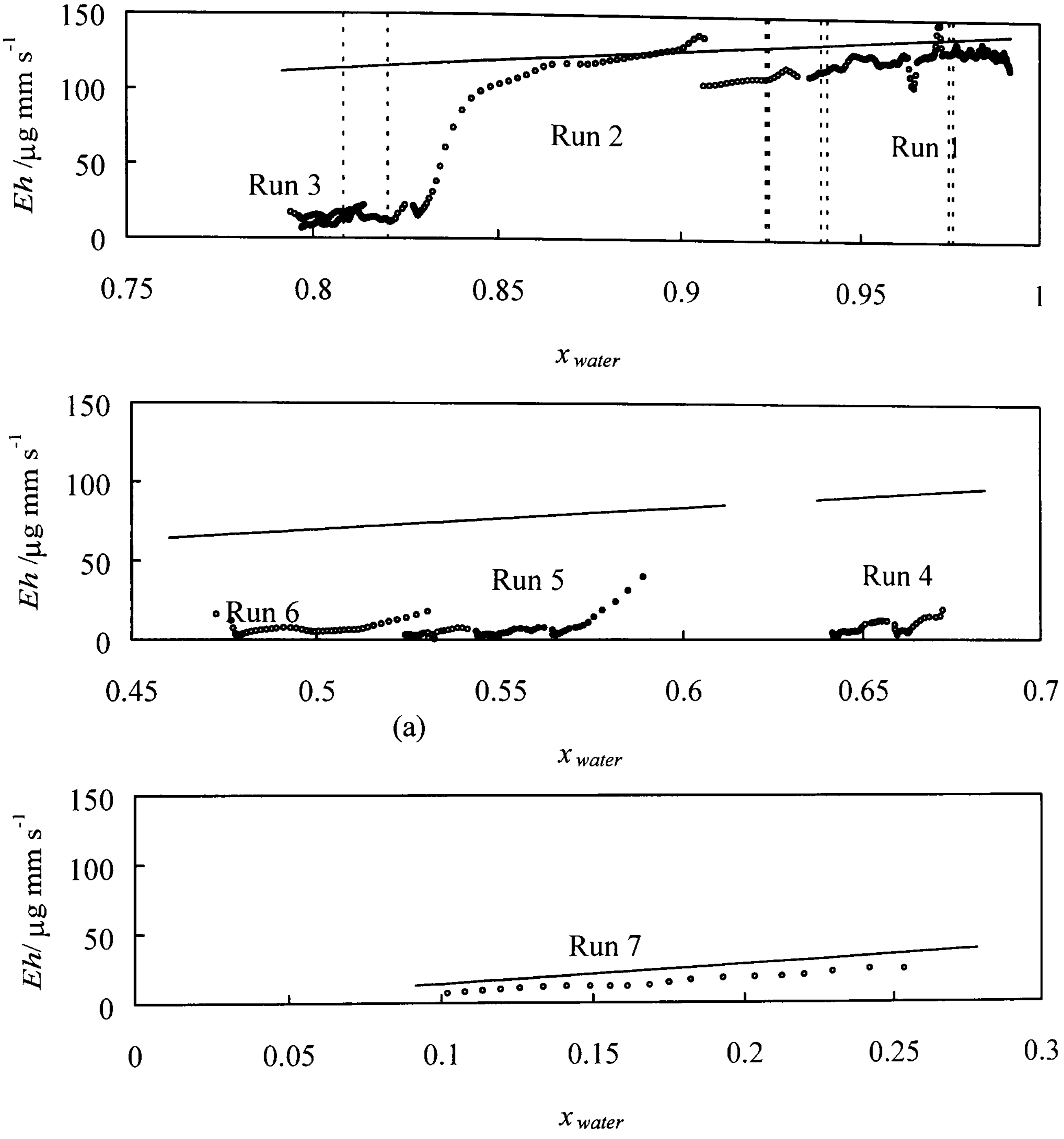

Figure 4.9 ***Comparison of measured (circles) and calculated (solid lines) variation of Eh for mixtures of water and $C_{12}E_6$ evaporated at 25.0°C and 1920 ml min^{-1} nitrogen gas flow rate. A total of seven runs with different initial compositions are shown in plots (a) –(c). The vertical dashed lines show the phase boundaries listed in Table 4.3.***

For run 3, starting at x_{water} of approximately 0.82, the initial rate is low, indicating that a large concentration gradient has developed within the time between sample preparation and the start of the measurement (approximately 15 minutes). Runs 4 – 6 are also characterised by the development of a large concentration gradient within this time. For lower water contents (x_{water} from 0.25 to 0.1) the measured rates approach the calculated values more closely. This is consistent with the fact that pure $C_{12}E_6$ is a liquid at 25°C and the concentration gradient development of the liquid is reduced in this regime.

Overall, structuring of the mixtures resulting in concentration gradient development (and consequently evaporation rate reduction) is strongest for mid-range mole fractions (x_{water} from approximately 0.83 to 0.4, corresponding to water mass fractions from 0.16 to 0.03) and shows no correlation with mesophase boundaries in the system.

A depression in evaporation rate is expected when the time required for the relaxation of the concentration gradients in the liquid phase is slow relative to the time required for vapour diffusion across the stagnant gas layer. To model the rate reduction in detail would involve the estimation of mass transfer by diffusion and convection within the microstructured (and commonly multi-phase and anisotropic) liquid mixtures. This is beyond the scope of this work and has not been attempted.

The method and analysis shown here allows only the estimation of the surface concentration of the evaporating species during the evaporative process by comparison of the measured rate with the overall composition expected to give the same rate. It does not yield information on the full composition profile of the liquid.

4.4 Conclusions

The evaporation rates of pentane and hexane from mixtures with squalane are limited by vapour diffusion rates across the stagnant gas layer. Mixing within the liquid phases (probably by convection) is rapid relative to this process.

Evaporation rates of hexane gelled with silica particles are similar to those of pure un-gelled liquid because the hexane vapour pressure is unaffected by the addition of the silica particles. Some minor deviations between the measured and calculated rates are seen which are likely to result from (a) obstruction to the diffusive pathway by loose silica powder on the liquid surface and (b) a lowering of the vapour pressure for hexane contained in liquid bridges between silica particles.

Water evaporation rates from mixtures with the non-ionic surfactant $C_{12}E_6$ are reduced to approximately 10% of the rate predicted, owing to the development of concentration gradients within the mixtures. This effect is strongest for water mole fractions from 0.4 to 0.83 and shows no correlation with the mesophase boundaries.

4.5 References

1. A. J. Ashworth and D. H. Everett, *Trans. Faraday Soc.*, 1960, **56**, 1609.
2. E. A. Guggenheim, *"Mixtures"*, Oxford Press, Oxford, 1952.
3. T. Tompa, *"Polymer Solutions"*, Butterworth Press, Woburn, 1959.
4. *"Selected Values of Properties of Hydrocarbons and Related Compounds"*, Thermodynamics Research Centre, AP144, Texas A&M University, 1978.
5. *"CRC Handbook of Chemistry and Physics"*, CRC Press Inc., Boca Raton, 62nd edn., 1981.
6. G. A. Lugg, *Anal. Chem.*, 1968, **40**, 1072.
7. G. A. D. McD. Cummings and A. R. Ubbelohde, *J. Chem. Soc.*, 1953, 3751.
8. R.C. Reid, J. N. Prautsnitz and T. K. Sherwood, *"The Properties of Liquids and Gases"*, 3rd edn., McGraw-Hill, 1977.
9. B. Simon in *"Dynamics of Multiphase Flows across Interfaces"*, ed. A. Steinchen, Springer, Berlin, 1996.
10. J. S. Clunie, J. F. Goodman and P. C. Symons, *Trans. Faraday Soc.*, 1969, **65**, 287.
11. F. MacRitchie, *"Chemistry at Interfaces"*, Academic Press, San Diego, 1990.
12. N. M. Van Os, J. R. Haak and L. A. M. Rupert, *"Physico-Chemical Properties of Selected Anionic, Cationic and Nonionic Surfactants"*, Elsevier, Amsterdam, 1993.
13. D. J. Mitchell, G. J. T. Tiddy, L. Waring, T. Bostock and M. P. McDonald, *J. Chem. Soc., Faraday Trans. 1*, 1983, **79**, 975.

CHAPTER 5

EVAPORATION RATES OF IMMISCIBLE LAYERED LIQUID MIXTURES AND EMULSIONS

In Chapter 4, it was shown that the evaporation characteristics of liquid mixtures are dependent on the degree of structure within the mixture. Chapter 5 aims to build on the conclusions of this work by considering evaporation from emulsions. Initially, layered systems of two immiscible liquids are considered. The study then moves on to oil-in-water emulsions and some preliminary results for creamed, sedimented and gelled systems are discussed.

5.1 Evaporation rates of immiscible layered systems

When two very chemically dissimilar liquids are mixed together in the absence of surfactant, the two components will phase separate, usually within seconds. The less dense liquid forms a layer on the surface of the more dense liquid. For liquid pairs with very low mutual solubility, the layers will consist of virtually pure liquid. The process of evaporation is predicted to be limited only by diffusion through the stagnant vapour space. The evaporation rate for the less dense liquid will therefore be virtually identical to the pure liquid. The evaporation of the more dense liquid is completely inhibited by the presence of the less dense liquid, and will only begin when the upper layer has all evaporated.

In Chapter 3 it was shown that the mass versus time curves for pure liquids could be predicted using Equation [3.27]. This equation can be modified to predict the evaporation rate of the upper layer taking into account the volume occupied by the lower layer. The thickness of the upper layer plus the stagnant vapour space $h_{x.u}$ is given by

$$h_{x,u} = h_x - \frac{m_{o,l}}{\rho_l A} \qquad [5.1]$$

where h_x is the height of the sample tube, $m_{o,l}$ is the initial mass of the more dense liquid and ρ_l is the density of the more dense liquid. Combination of Equations [3.27] and [5.1] yields an expression which predicts the relationship between mass and time for the upper layer.

$$t = \frac{RT\left(h_x - \left(m_{o,l}/\rho_l A\right)\right)}{M_u A D_u P_u z_u}\left(m_{o,u} - \left(m_{o,u} + dm\right)\right) - \frac{RT}{2\rho_u M_u A^2 D_u P_u z_u}\left(m_{o,u}{}^2 - \left(m_{o,u} + dm\right)^2\right) \qquad [5.2]$$

where the subscript u refers to the less dense liquid and dm is the change in mass from $t = 0$.

Equation [5.2] is valid until the upper layer has completely evaporated. The time at which this occurs t_u is given by

$$t_u = \frac{RTm_{o,u}\left(h_x - \left(m_{o,l}/\rho_l A\right)\right)}{M_u A D_u P_u z_u} - \frac{RTm_{o,u}^{\;2}}{2\rho_u M_u A^2 D_u P_u z_u} \qquad [5.3]$$

After t_u, the more dense liquid is able to evaporate. The relationship between mass and time in this region is given by

$$t = t_u + \frac{RTh_x}{M_l A D_l P_l z_l}\left(m_{o,l} - m_l\right) - \frac{RT}{2\rho_l A^2 D_l P_l z_l}\left(m_{o,l}^{\;2} - m_l^{\;2}\right) \qquad [5.4]$$

where the subscript l refers to the more dense phase. m_l is the mass of liquid remaining at time t and is given by

$$m_l = m_{o,l} + m_{o,u} + dm \qquad [5.5]$$

A Visual Basic program was written which combines Equations [5.3], [5.4] and [5.5] to predict the full mass versus time plot for layered systems. The VBa coding for this program can be found in Appendix 1.

Figure 5.1 shows the mass loss versus time and evaporation rate versus time plots for two different layered systems. Evaporation rate versus time plots were obtained by numerical differentiation of the mass versus time curves. Values of molar masses, vapour diffusion coefficients, vapour pressures and liquid densities required to calculate the theoretical fits are given in Table 5.1.

Table 5.1: ***Values of molar masses M, vapour pressures P_o, diffusion coefficients D and densities ρ at 25.0 °C used in the calculation of the theoretical fits for Figure 5.1.***

Component	M/ kg mol^{-1}	P_o/ Pa	D/ 10^{-6} m^2 s^{-1}	ρ/ kg m^{-3}
n-hexane	0.086	20198 [1]	7.90 [3]	654.7 [1]
Water	0.018	3168 [2]	24.00 [4]	997.1 [2]
1-bromobutane	0.137	5333 [2]	7.80*	1268.7 [2]

* Estimated from evaporation measurements for pure 1-bromobutane

In both cases, the evaporation proceeds at a uniform rate until the top layer is depleted, at which point a sharp break in the mass versus time curve is seen. For (a) and (b), where the more volatile component is less dense than water, the evaporation rate slows abruptly at the break point. For (c) and (d), where the more volatile component has a higher density than water, the reverse is seen.

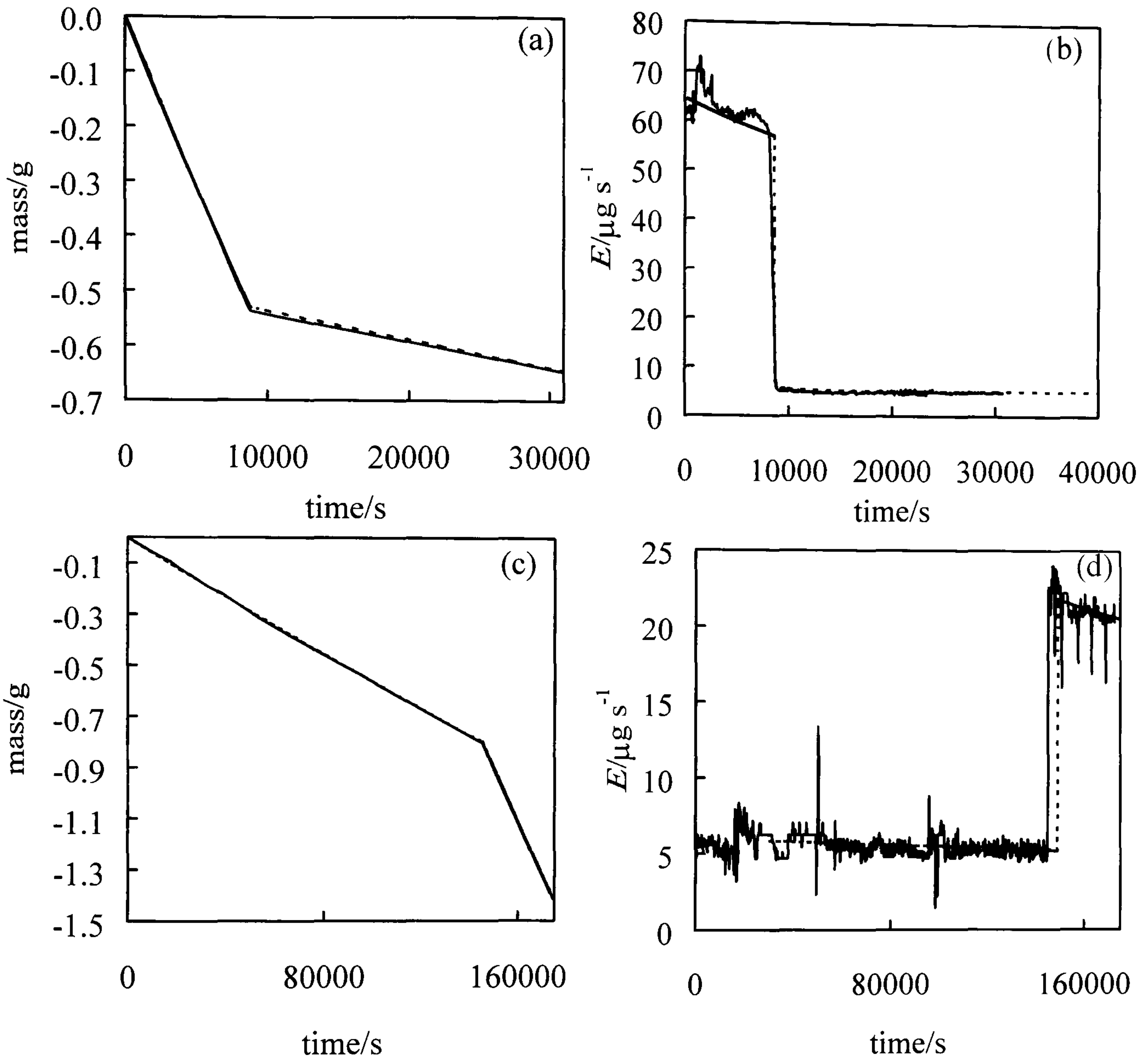

Figure 5.1 ***Mass versus time and evaporation rate versus time plots for layered systems of n-hexane and water ((a) and (b)) and 1-bromobutane and water ((c) and (d)). Measurements were made at 25^oC and 1920 ml min^{-1} nitrogen gas flow rate. For (a) and (b), the initial mass of n-hexane was 0.530 g and the initial mass of water was 3.190 g. For (c) and (d), the initial mass of 1-bromobutane was 4.054 g and the initial mass of water was 0.805 g. The solid lines are the experimental data, whilst the dotted lines are calculated using the data in Table 5.1.***

The agreement between the calculated and experimental values for both mixtures is very good. It is concluded that the rate limiting process in the evaporation of the upper liquid in these layered systems is diffusion of vapour across the stagnant layer gas.

5.2 Evaporation rates of creamed oil – in – water emulsions

The evaporation of a volatile oil from a creamed oil-in-water emulsion is now considered. As described in Chapter 1, the equilibrium vapour pressures of the oil and water within the emulsion are expected to be equivalent to those in the layered systems investigated in Section 5.1. A slight lowering of the vapour pressure may be expected for the continuous phase, arising from the presence of the dissolved surfactant. However, this effect is negligible for the low surfactant concentrations used here. Conversely, a slight increase in the oil vapour pressure due to the Kelvin Effect might also be expected. However, for the oil drop sizes and oil-water surface tensions in the emulsions considered here, this effect is also negligible. It is expected that both the continuous water and dispersed oil components of an emulsion evaporate simultaneously but at different rates[5-7]. The difference between the two systems is that the oil droplets within the emulsion may experience an energy barrier to evaporation.

Figure 5.2 is a schematic representation of the upper layer of a fully creamed oil-in-water emulsion at the beginning of the evaporation process. The buoyant oil droplets are in an approximately three-dimensional hexagonal close-packing arrangement with the continuous water phase occupying the spaces in between. There is a thin film of continuous phase at the emulsion surface, the thickness of which is expected to be in the nanometre range and is dependent on the colloidal forces.

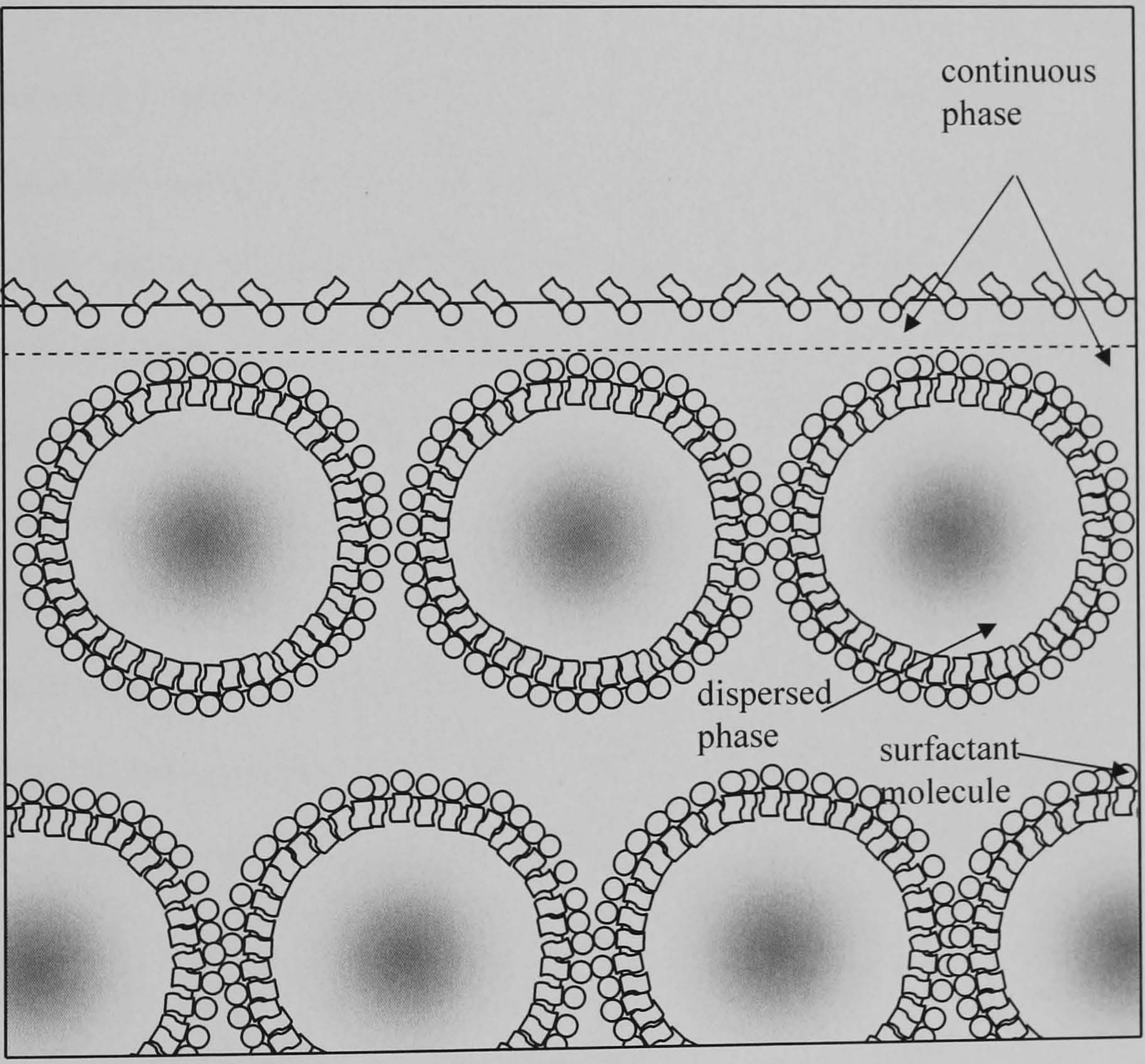

Figure 5.2 ***Schematic representation of the creamed layer of an oil – in – water emulsion.***

There are three possible fates for an oil droplet within the emulsion, which were discussed fully in Chapter 1. Briefly, depending on the relative magnitudes of the oil-water, water-vapour and oil-vapour interfacial tensions, entry of the oil drops through the water film to the emulsion surface may or may not be thermodynamically feasible[8]. Although the prediction of drop entry under dynamic evaporation conditions is uncertain, if oil drop entry forms the rate limiting step to oil transport to the vapour phase, oil evaporation rates would be expected to correlate with the relative magnitudes of the three relevant interfacial tensions and the strength of repulsive colloidal forces across the water film. If entry to the surface is unfavourable, however, the drops remain separated from the vapour phase by the thin water film. In this case there are two possible outcomes. Firstly, transport can occur by molecular diffusion and the oil evaporation rate is predicted to depend on the solubility of the oil in water, its diffusion coefficient in water and the water film thickness (and therefore the colloidal forces). These two processes are summarised in Figure 5.3. Secondly, it is possible that a non-entering drop is unable to evaporate until the layer of continuous phase above it has been completely depleted. In this case, then, the emulsion evaporation rate should depend on the relative volatilities of the oil and water. This third process is summarised in Figure 5.4.

This study aims now to further develop the model for layered systems calculated in Section 5.1 to cover emulsions, and thus quantify any possible barrier to evaporation. The effect of oil solubility and surfactant type will then be investigated in order to elucidate which of the mechanisms outlined for oil transport is most likely.

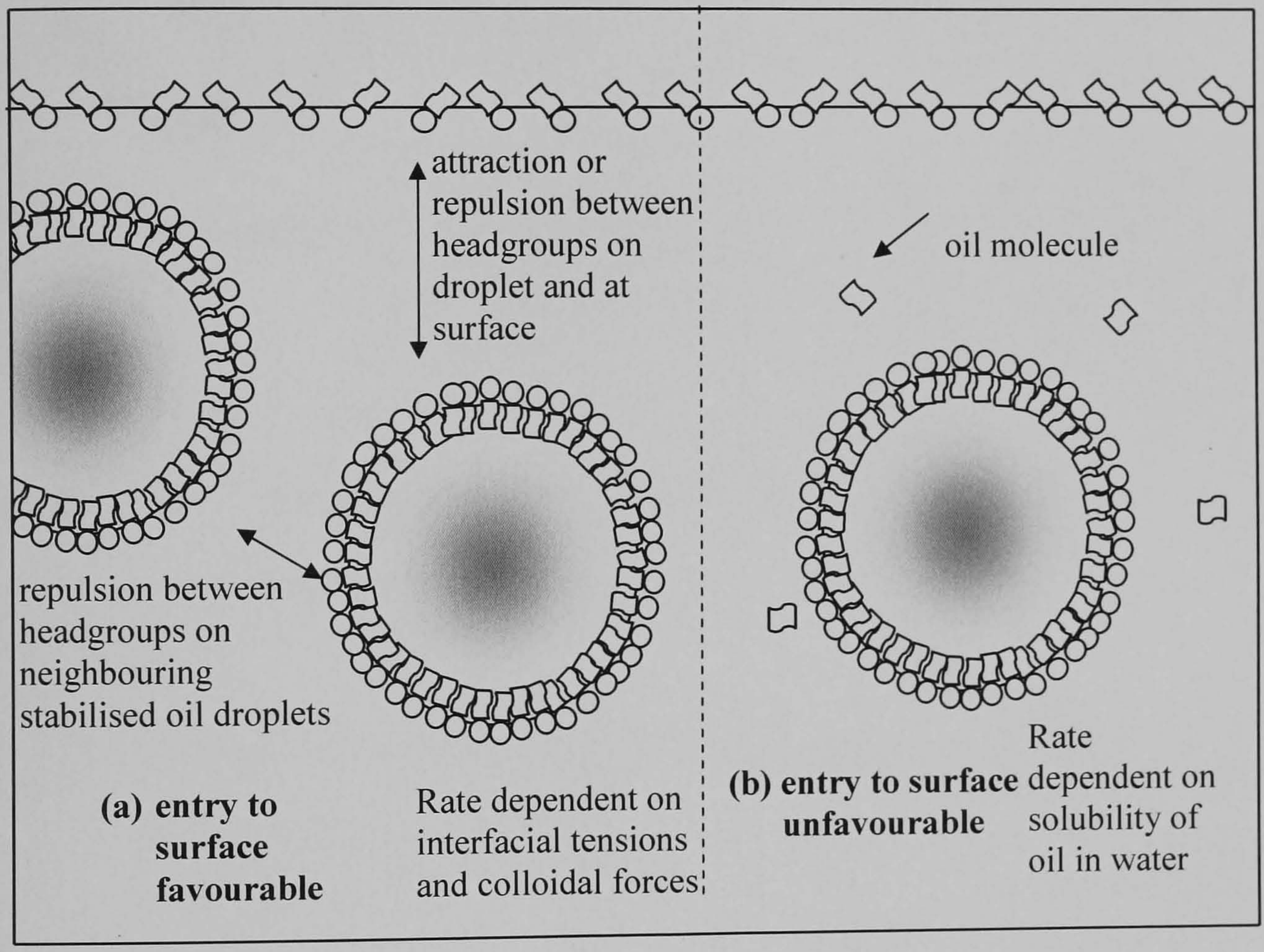

Figure 5.3 ***Schematic representation of two possible fates for oil droplets in an evaporating oil – in – water emulsion***

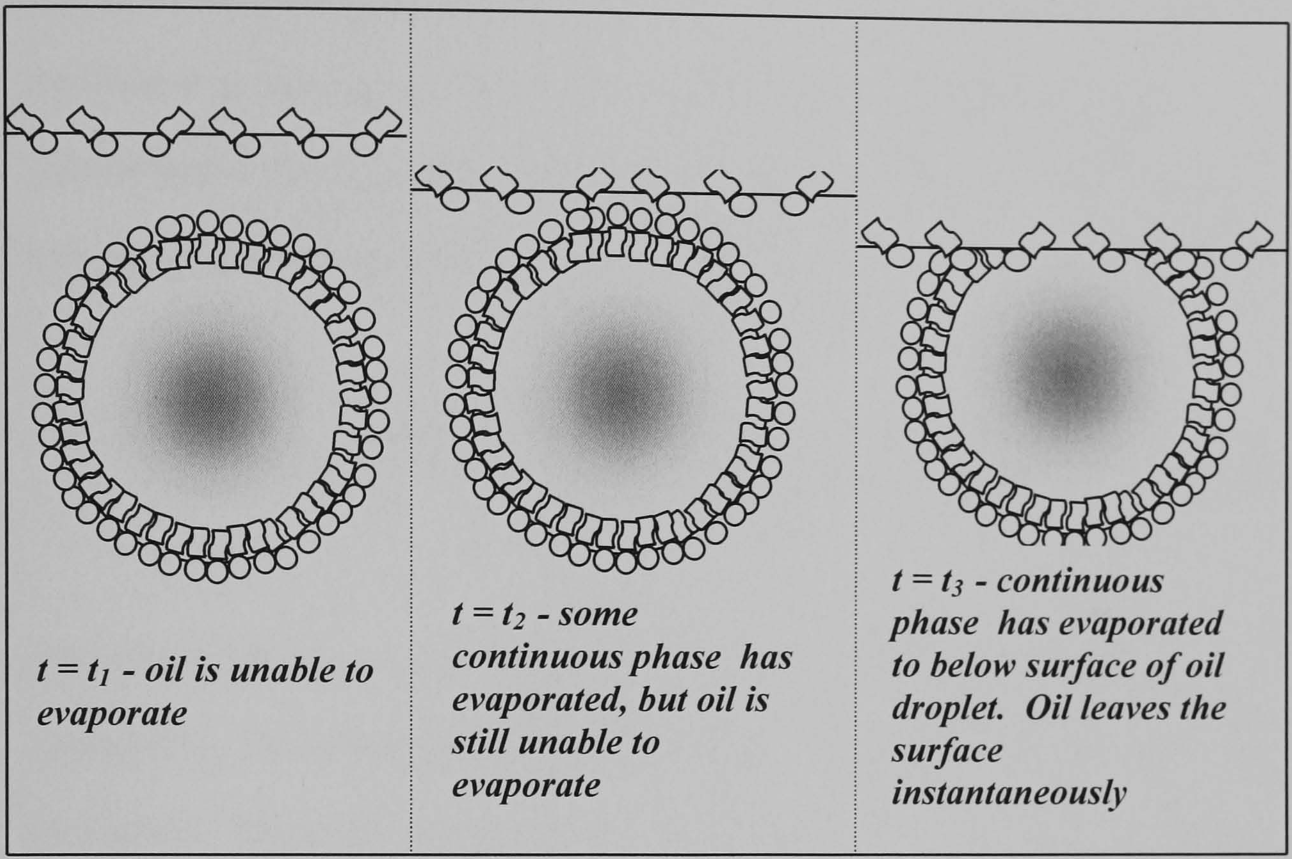

$t = t_1$ - oil is unable to evaporate

$t = t_2$ - some continuous phase has evaporated, but oil is still unable to evaporate

$t = t_3$ - continuous phase has evaporated to below surface of oil droplet. Oil leaves the surface instantaneously

***Figure 5.4** Schematic representation of the third possible fate for an oil droplet*

5.2.1 Development of a model to predict the evaporation rate of a creamed oil – in- water emulsion

The model for the evaporation of creamed oil – in- water emulsions differs from the model for layered systems, since over some time range, both continuous and dispersed phases will be evaporating simultaneously. This is true for each of the possible oil transport mechanisms outlined.

The model developed here assumes that the continuous phase evaporates from the emulsion at its bulk rate and that the dispersed oil drops evaporate with a rate reduced below that of the bulk pure liquid by a factor *f*. For a creamed emulsion, then, the emulsion evaporation rate E_{em} is given by

$$E_{em} = \frac{-dm_c}{dt} - f\frac{dm_d}{dt} = \frac{M_c A D_c P_c z_c}{hRT} + f\frac{M_d A D_d P_d z_d}{hRT} \qquad [5.6]$$

where the subscripts *c* and *d* indicate the continuous and dispersed phases respectively. *f* is the factor measuring the barrier to evaporation experienced by the oil droplets. Where the droplets experience no barrier, $f = 1$. Where there is total suppression of oil evaporation, $f = 0$.

Equation [5.6] can be written as

$$E_{em} = \frac{A}{hRT}(\alpha + \beta) \qquad [5.7]$$

where $\alpha = M_c D_c P_c z_c$ and $\beta = f M_d D_d P_d z_d$. The ratio α/β can be considered as a measure of the relative likelihood of the continuous and dispersed phases to evaporate.

The value of h at any point is given by

$$h = h_x - \left(\frac{m_d}{\rho_d A} + \frac{m_c}{\rho_c A} \right) \qquad [5.8]$$

where m_d and m_c are the masses of dispersed and continuous phase remaining.

The total mass of emulsion remaining, m_e, can be expressed as

$$m_e = m_{o,e} + m_{e,b} \qquad [5.9]$$

where $m_{o,e}$ is the initial mass of the emulsion and $m_{e,b}$ is the change in mass from time t_o. Analogous expressions can be written for the dispersed and continuous phases.

$$m_d = m_{o,d} + m_{d,b} \qquad [5.10]$$

$$m_c = m_{o,c} + dm_{c,b} \qquad [5.11]$$

It is clear that

$$m_e = m_c + m_d \tag{5.12}$$

and it follows that

$$m_{e,b} = m_{d,b} + m_{c,b} \tag{5.13}$$

Substitution of α/β in Equation [5.13], followed by rearrangement, yields an expression for $m_{d,b}$ in terms of α, β and $m_{e,b}$.

$$m_{d,b} = \frac{\beta m_{e,b}}{\alpha + \beta} \tag{5.14}$$

Thus, $m_{c,b}$ is given by

$$m_{c,b} = m_{e,b} - \frac{\beta m_{e,b}}{\alpha + \beta} \tag{5.15}$$

Substitution of Equations [5.14] and [5.15] into Equations [5.10] and [5.11] respectively, followed by substitution into Equation [5.8] gives an expression for h in terms of $m_{e,b}$.

$$h = h_x - \frac{\left(m_{o,d} + \frac{\beta m_{e,b}}{\alpha+\beta}\right)}{\rho_d A} - \frac{\left(m_{o,c} + m_{e,b} - \frac{\beta m_{e,b}}{\alpha+\beta}\right)}{\rho_c A} \qquad [5.16]$$

For a creamed emulsion in which the dispersed and continuous phases are evaporating simultaneously, the evaporation rate is given by

$$E_{em} = -\frac{dm_e}{dt} = \frac{A(\alpha+\beta)}{\left(h_x - \left(\frac{m_{o,d} + \frac{\beta m_{e,b}}{\alpha+\beta}}{\rho_d A}\right) - \left(\frac{m_{o,c} + m_{e,b} - \frac{\beta m_{e,b}}{\alpha+\beta}}{\rho_c A}\right)\right)RT} \qquad [5.17]$$

Integration of Equation [5.17] gives the relationship between $m_{e,b}$ and t.

$$t = \frac{RTm_{e,b}}{A^2(\alpha+\beta)}\left(\frac{m_{o,d}}{\rho_d} + \frac{\beta m_{e,b}}{2\rho_d(\alpha+\beta)} + \frac{m_{o,c}}{\rho_c} + \frac{m_{e,b}}{2\rho_c} - \frac{\beta m_{e,b}}{2\rho_c(\alpha+\beta)} - Ah_x\right) [5.18]$$

Equation [5.17] is only valid when both phases are evaporating from the emulsion. i.e. when $\left(m_{o,d} + \frac{\beta m_{e,b}}{\alpha + \beta}\right) \geq 0$. When this condition is not satisfied, mass loss is due to the continuous phase only and hence the rate is expected to be equal to that of the bulk continuous phase. E_{em} in this region is given by

$$E_{em} = \frac{M_c A D_c P_c z_c}{hRT} = \frac{\alpha A}{hRT} \qquad [5.19]$$

and h is given by

$$h = h_x - \left(\frac{m_{o,c} + m_{e,b} + m_{o,d}}{\rho_c A}\right) \qquad [5.20]$$

Combination of Equations [5.19] and [5.20] gives an expression for the evaporation rate of the emulsion after the completion of the evaporation of the dispersed oil phase.

$$E_{em} = \frac{-dm_e}{dt} \frac{\alpha A}{\left(h_x - \left(\frac{m_{o,c} + m_{e,b} + m_{o,d}}{\rho_c A}\right) RT\right)} \qquad [5.21]$$

When the evaporation rate switches from that predicted by Equation [5.17] to that predicted by Equation [5.21], $m_{e,b}$ is given by

$$m_{e,b} = -\frac{-m_{o,d}(\alpha+\beta)}{\beta} \qquad [5.22]$$

Substitution of Equation [5.22] into Equation [5.18] gives the critical time at which this switch in rate occurs, t_s.

$$t_s = \frac{m_{o,d}RT}{A^2\beta}\left(\frac{m_{o,d}}{\rho_d} + \frac{\beta m_{e,b}}{2\rho_d(\alpha+\beta)} + \frac{m_{o,c}}{\rho_c} - \frac{m_{o,d}(\alpha+\beta)}{2\rho_c\beta} + \frac{m_{o,d}}{2\rho_c} - Ah_x\right) \qquad [5.23]$$

Integration of Equation [5.21] between the limits $t = t_s$ and $t = t$ gives the following expression

$$t' = \frac{RT}{\alpha\rho_c A^2}\left(m_{e,b}\left(m_{o,d} + m_{o,c} + \frac{m_{e,b}}{2}\right) - \left(-m_{o,d} + \frac{\alpha m_{e,b}}{(\alpha+\beta)}\right)\left(m_{o,d} + m_{o,c} - \frac{m_{o,d}}{2} + \frac{\alpha m_{e,b}}{2(\alpha+\beta)}\right)\right)$$

[5.24]

The relationship between $m_{e,b}$ and t after the depletion of the dispersed phase is the sum of Equations [5.23] and [5.24].

$$t = t' + t_s \qquad [5.25]$$

Combination of Equations [5.17] and [5.21] allow the prediction of the full evaporation rate versus time plot for a creamed oil – in – water emulsion. The corresponding mass loss versus time curve can be obtained by combination of Equations [5.18], [5.23] and [5.24]. The Visual Basic code written to combine these equations and generate theoretical data can be found in Appendix 1. These programs were incorporated as macros in an EXCEL spreadsheet. The spreadsheet allows the fitting of the experimental data by floating the values of f, $m_{o,d}$, $m_{o,c}$ and D_d.

Figure 5.5 shows the evaporation rate versus mass loss, mass versus time and evaporation rate versus time plots for a hexane in water emulsion stabilised with 20 mM AOT, fitted using the values given in Table 5.2. The theoretical fits for (a) and (b) are obtained using the macros described earlier, with $f = 0.374$, whilst the theoretical plot for (c) is obtained from the combination of (a) and (b). The rapid initial rate corresponds to the loss of both oil and water from the oil-rich creamed layer, whilst the slower rate is that of the continuous phase alone when all the oil has evaporated. The good agreement between the theoretical and measured plots indicates that the assumption that the continuous phase evaporates at the bulk rate is correct. A barrier to evaporation for the emulsion is confirmed by comparison of plots (b) and (c) with (a) and (b) of Figure 5.1. In both cases, the oil and water components are identical, yet in the non-emulsified system the initial evaporation rate is significantly faster than that of the emulsified system.

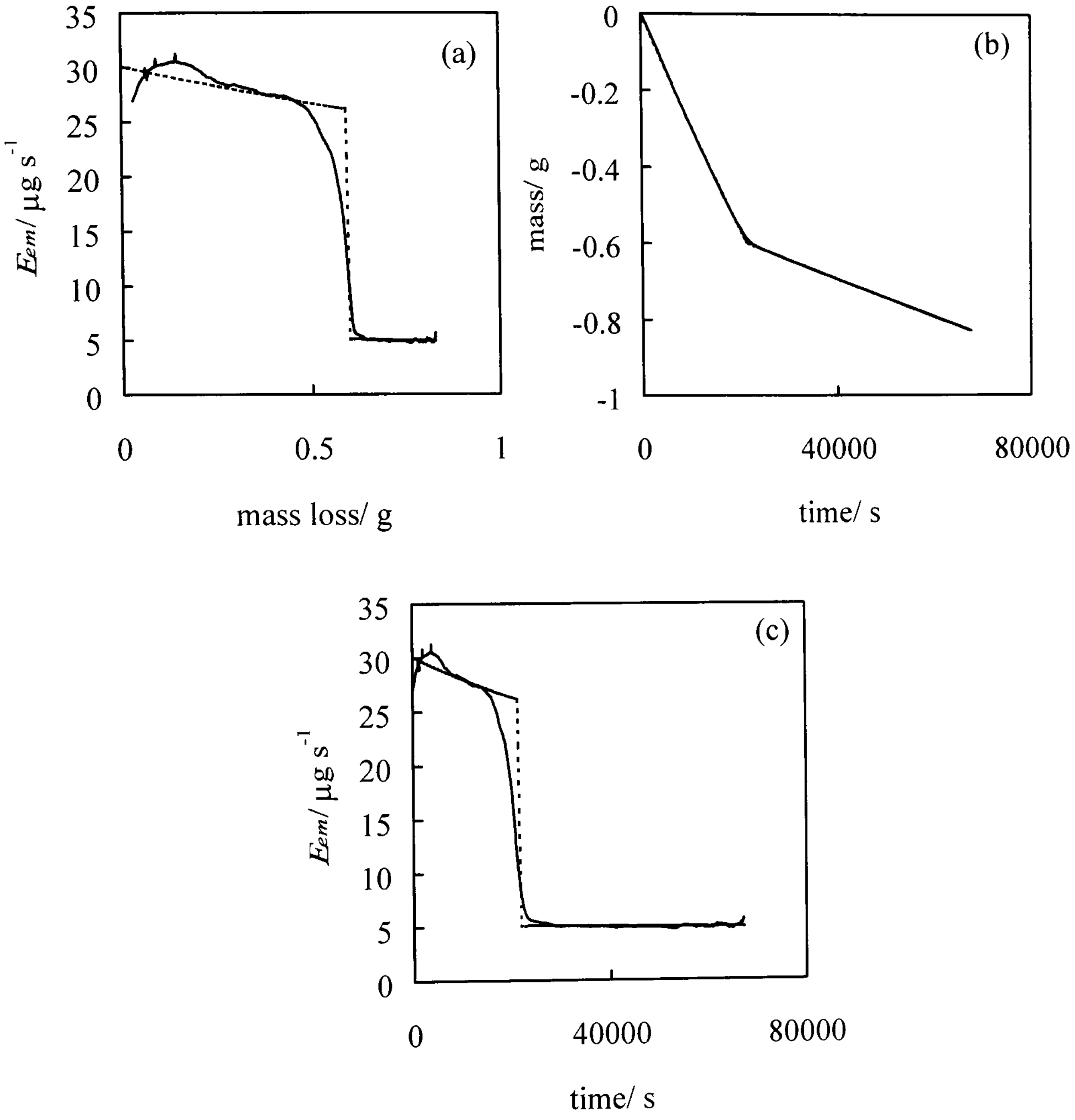

Figure 5.5 ***(a) Evaporation rate versus mass loss, (b) mass versus time and (c) evaporation rate versus time plots for a 20 vol% n-hexane in water emulsion stabilized with 20 mM AOT at 25.0°C and 1920 ml min^{-1} nitrogen gas flow rate. The solid lines are the experimental data, whilst the dotted lines are calculated as described in the text. All parameters used for fitting are given in Table 5.2. The measured rates were averaged in blocks of ten to reduce scatter. The value of f was found to be 0.374.***

Table 5.2 ***Parameters used to calculate the theoretical plots shown in Figure 5.5***

	M/ kg mol^{-1}	P_o/ Pa	D_d/ 10^6 m^2 s^{-1}	m_o/g	f	ρ / kg m^{-3}
n-hexane	0.086	20198[1]	7.30[3]	0.481	0.374	654.71[1]
water	0.018	3168[2]	22.0[4]	3.188	1.000	997.1[2]

5.2.2 Effect of oil solubility on the evaporation rates of creamed oil – in – water emulsions

Figure 5.6 shows mass versus time curves for a series of creamed oil – in – water emulsions containing different oils stabilised with 20 mM sodium dodecyl sulphate. The parameters used to fit the theoretical plots are given in Table 5.3.

Table 5.3 ***Parameters used to calculate the theoretical mass versus time plots shown in Figure 5.6.***

	M	P_o	D_d	$m_{o,d}$	$m_{o,c}$	f	ρ
	kg mol^{-1}	Pa	10^6 m^2 s^{-1}	g	g		kg m^{-3}
n-heptane	0.100	6113[1]	7.30[3]	0.3864	3.3033	0.204	679.46[1]
n-hexane	0.086	20198[1]	7.30[3]	0.3720	3.0671	0.298	654.71[1]
n-pentane	0.072	68368[1]	8.45[3]	0.0088	1.4539	0.456	612.12[1]
Toluene	0.092	3783[2]	7.53[3]	0.5184	2.9394	0.918	870.12[2]

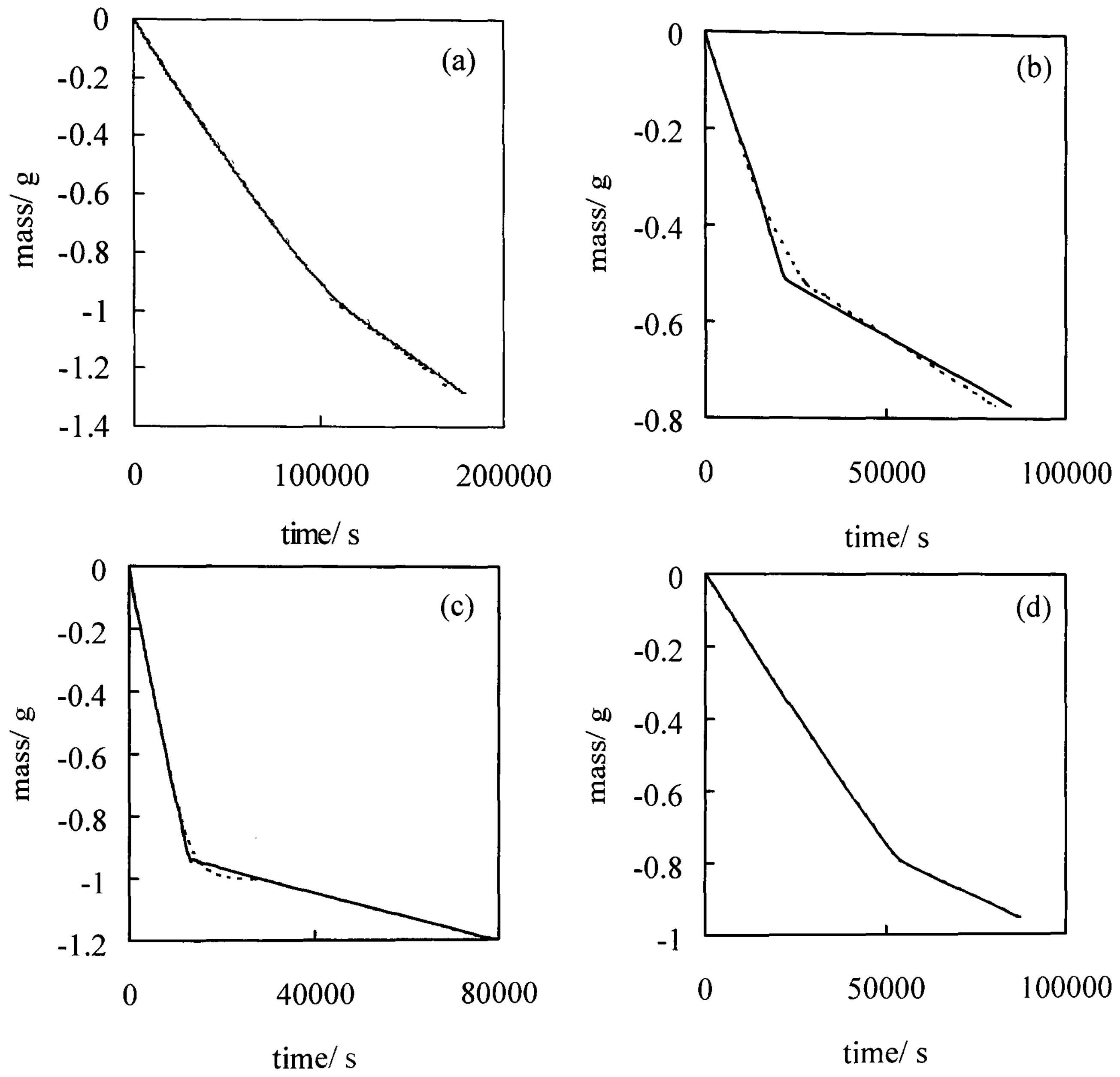

Figure 5.6 ***Mass versus time plots for approximately 20 vol% creamed oil – in – water emulsions stabilized with 20 mM sodium dodecyl sulphate, measured at 25°C and 1920 ml min^{-1} nitrogen gas flow rate. The oils used were (a) n-heptane, (b) n-hexane, (c) n-pentane and (d) toluene. The dashed lines represent the theoretical fit obtained as described in the text. The solid lines are the experimental data. All parameters to calculate the theoretical fit are given in Tables 5.1 and 5.3.***

Figure 5.7 shows the variation of f with oil solubility in water. It can be seen that f increases with increasing oil solubility. This supports the theory that oil transport in these emulsion systems occurs by molecular diffusion through the thin film of continuous phase at the surface.

5.2.3 Effect of surfactant type on the evaporation rates of creamed oil – in – water emulsions

If oil transport is governed by molecular diffusion across the thin water film at the emulsion surface, then a dependence on surfactant type is also expected, since the film thickness is dependent on colloidal forces. Figure 5.8 shows mass versus time curves for 20 vol% creamed heptane – in – water emulsions stabilised with four different surfactants. The additional parameters used to calculate the theoretical fits are given in Table 5.4.

Table 5.4 ***Parameters used to calculate the theoretical mass versus time plots shown in Figure 5.8.***

surfactant	$m_{o,d}/g$	$m_{o,c}/g$	f
CTAB	0.4315	3.1124	0.196
SDS	0.3864	3.3033	0.204
AOT	0.5381	3.3822	0.477
$C_{12}E_6$	0.5387	3.2746	0.578

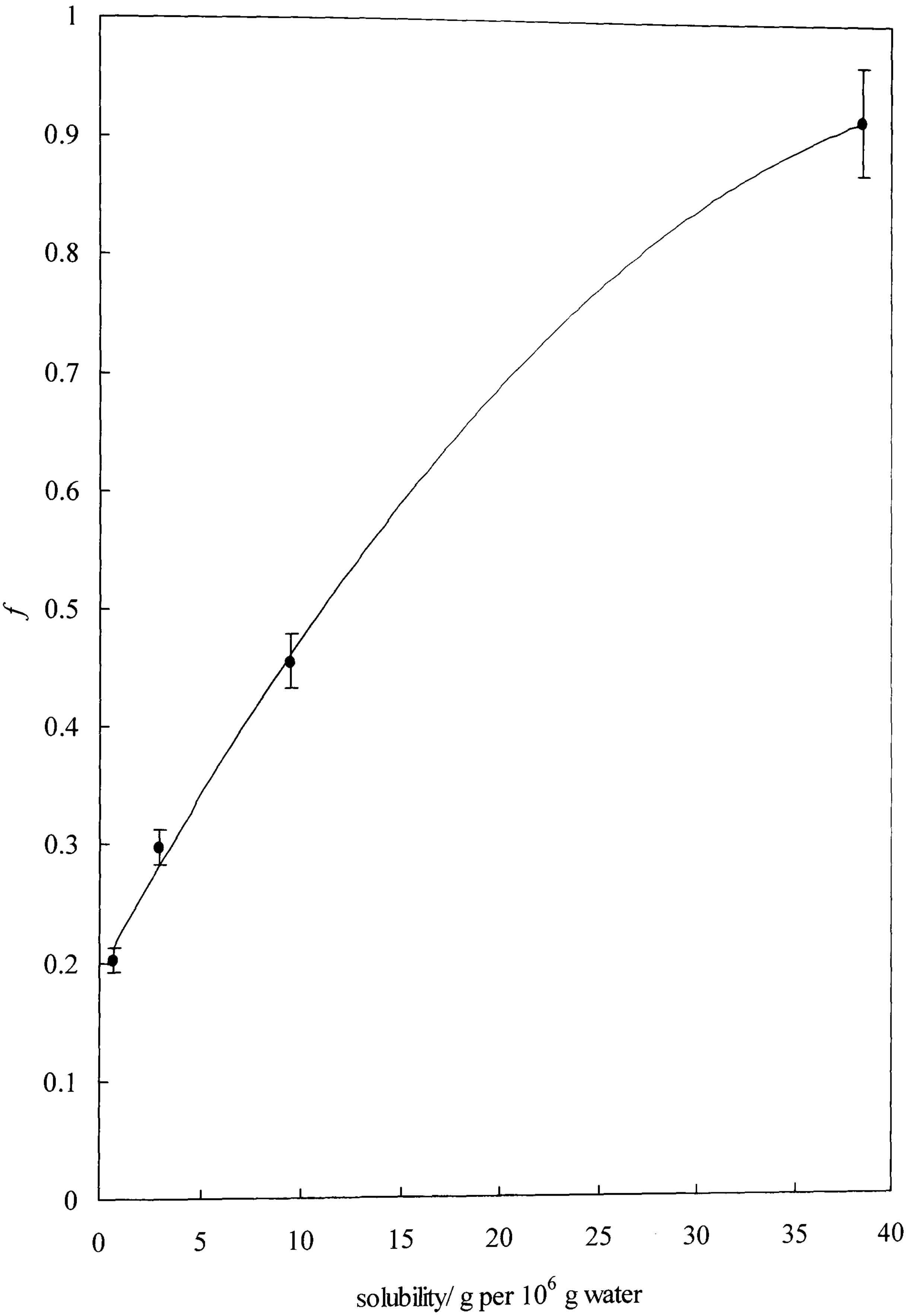

Figure 5.7 ***Variation in f with oil solubility in water at 25.0°C for the emulsions shown in Figure 5.6.***

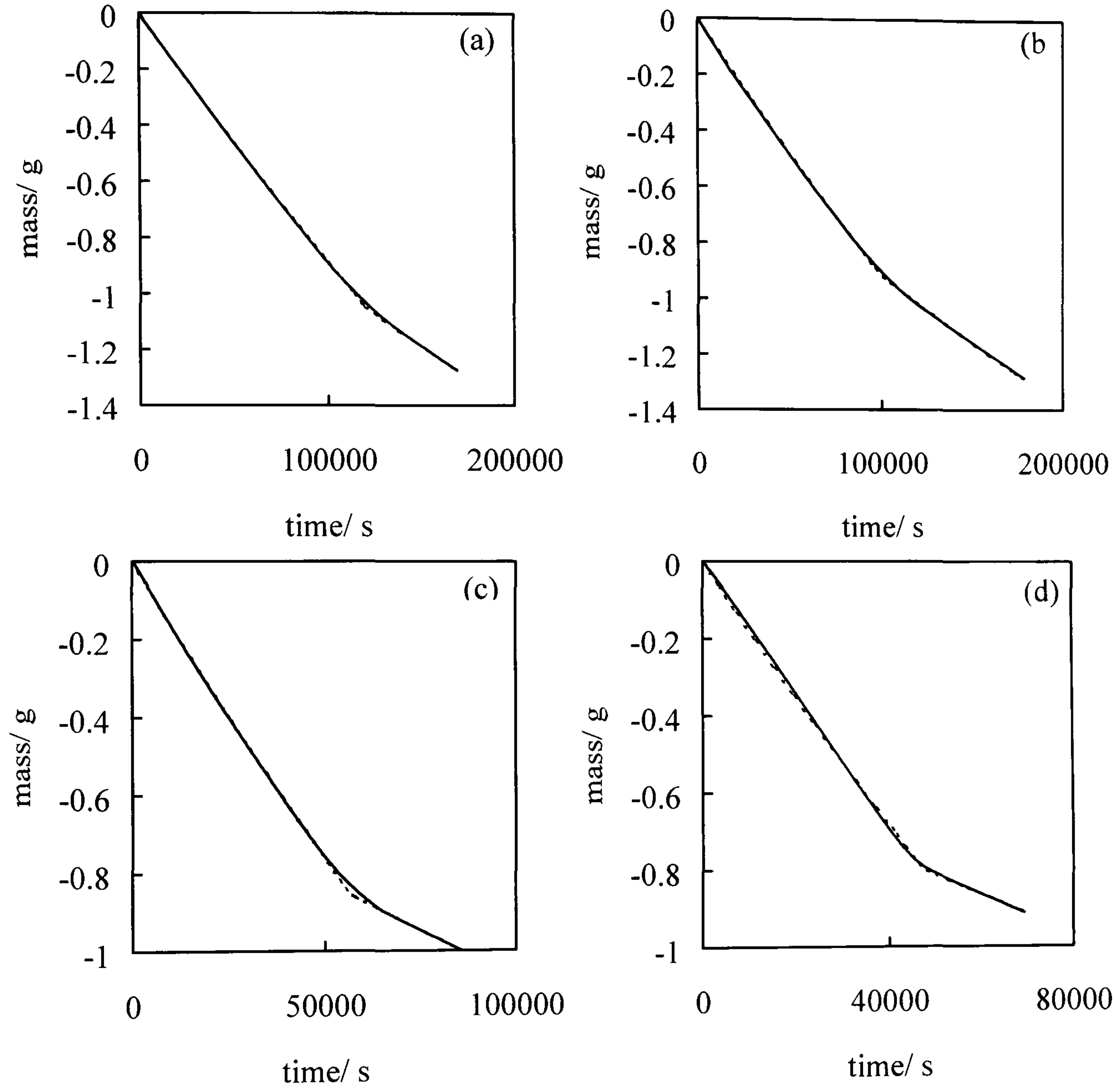

Figure 5.8 ***Mass versus time plots for approximately 20 vol% creamed n-heptane – in – water emulsions stabilized with 20 mM surfactant, measured at 25°C and 1920 ml min^{-1} nitrogen gas flow rate. The surfactants used were (a) CTAB, (b) SDS, (c) AOT and (d) $C_{12}E_6$. The dashed lines represent the theoretical fit obtained as described in the text. The solid lines are the experimental data. All parameters to calculate the theoretical fit are given in Tables 5.1, 5.3 and 5.4.***

The variation in *f* with surfactant type is shown in Figure 5.9.

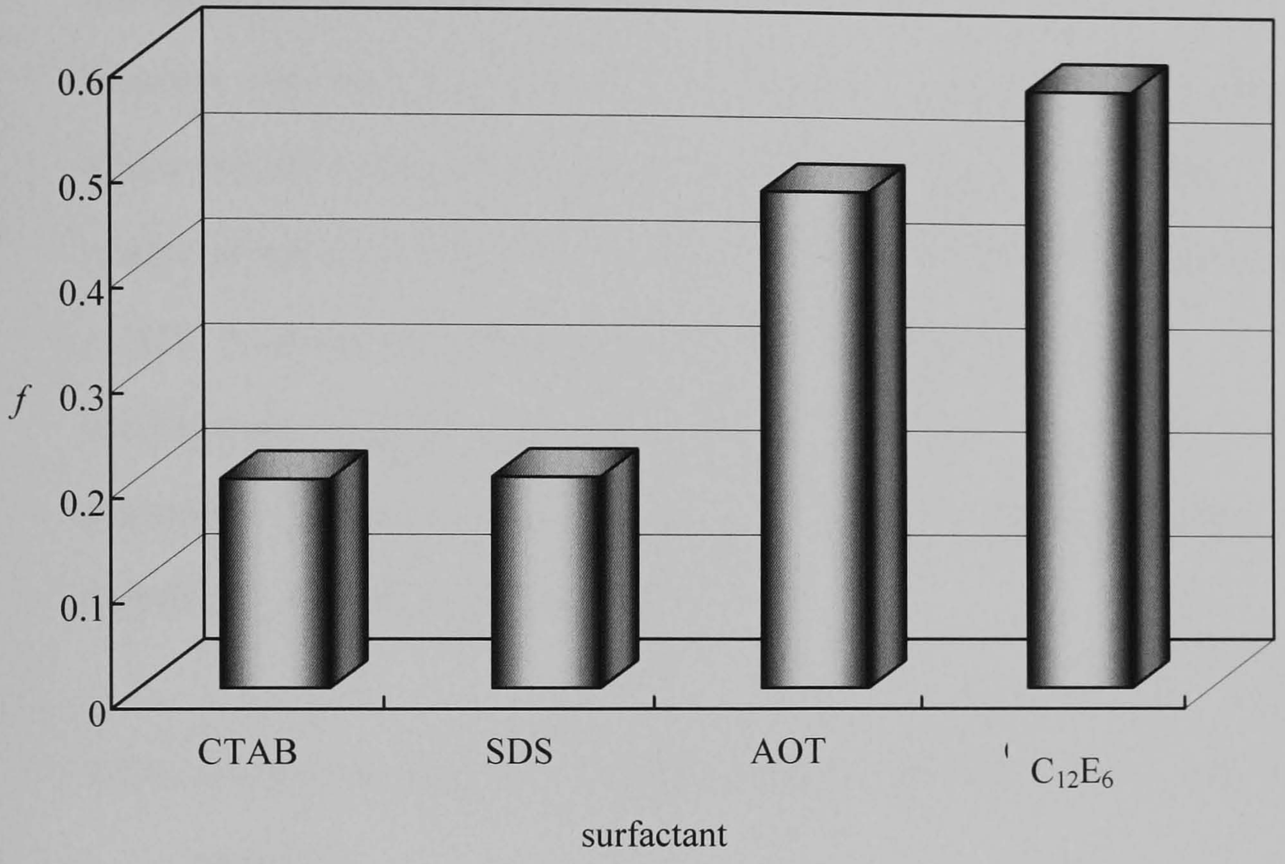

Figure 5.9 ***Variation in f with surfactant for the emulsions shown in Figure 5.8***

The value of *f* is very similar for the single-tail cationic surfactant, CTAB and the single-tail anionic surfactant, SDS. The twin-tail anionic surfactant AOT gives a larger *f* value, with the highest *f* being shown by the non-ionic $C_{12}E_6$. This can be explained qualitatively by consideration of electrostatic interactions for each surfactant. The value of *f* is expected to be highest for thin films and to decrease as the film thickens. For CTAB and SDS, large repulsion forces between the like-charged surfactant headgroups in the surface monolayer and those surrounding the oil droplets are expected. Therefore, the film thickness is expected to be relatively large and *f* is expected to be small.

For $C_{12}E_6$, the surfactant headgroups are uncharged. The repulsive forces are smaller than in the case of ionic surfactants and a thinner film and higher *f* is expected. The high *f* seen in the case of AOT can be partially explained by steric effects. For AOT, the area occupied by the tailgroup is large relative to the headgroup and the repulsive force per unit area is likely to be lower than in the case of SDS. A thinner film is therefore predicted. This explanation is not comprehensive since film thickness is dependent on the balance of capillary pressures and colloidal forces across the film [9,10], but does provide a plausible explanation for the trend seen in *f* values.

5.2.4 Effect of foaming on the evaporation rates of creamed oil – in – water emulsions

An interesting practical problem arises in the preparation of emulsions containing oils with very high vapour pressures. During emulsification, evaporation of the oil leads to a decrease in volume. When the volume falls below a critical level, the homogeniser pulls air into the emulsion, and the net effect is a "lifting" of the surface and foam formation. Figure 5.10 shows the mass versus time plot for a 20 vol% hexane – in – water emulsion stabilised with CTAB where foam has formed on the emulsion surface. There are significant deviations between the predicted and experimental plots. In particular, the value of *f* required to obtain a similar initial evaporation rate is higher than expected. For this emulsion system *f* = 0.500, whilst the corresponding emulsion stabilised with SDS has an *f* value of 0.298.

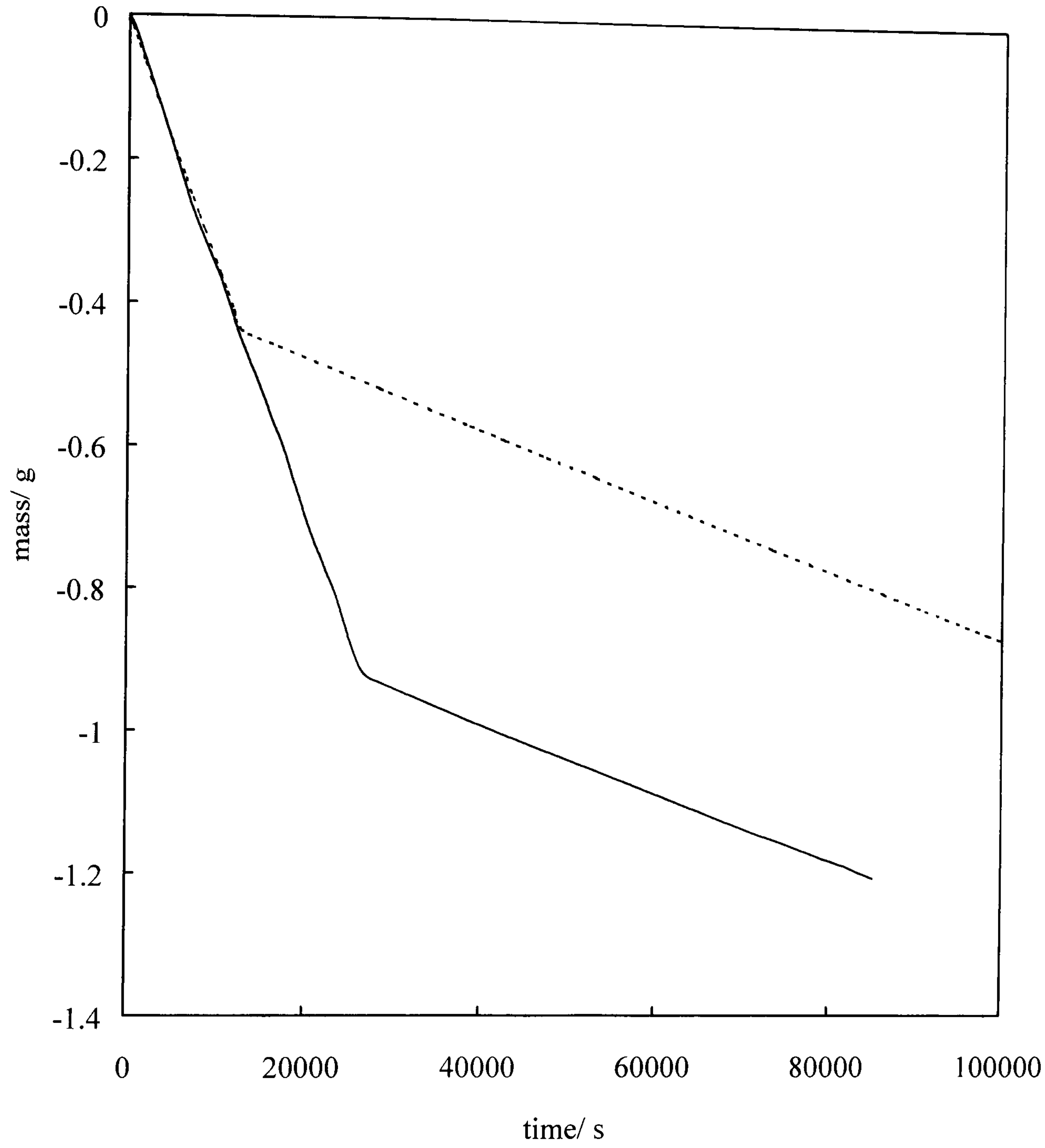

Figure 5.10 ***Mass versus time plot for a foaming approximately 20 vol% n-hexane in water emulsion stabilized with 20 mM CTAB solution. The solid line is the experimental data, whilst the dashed line is the theoretical fit calculated as described in the text. Parameters for the theoretical fit are given in Table 5.1. In addition, $m_{o,d}$ = 0.3720 g, $m_{o,c}$ = 3.0671 g and f = 0.500.***

In addition, the mass at which the rate changes from the creamed to the continuous rate is much larger than predicted. The evaporation rate model fails to account for this data because it assumes that the stagnant layer thickness can be accurately calculated from the volume of continuous and dispersed phases in the emulsion system. When foaming occurs, there is a decrease in stagnant layer thickness and a corresponding increase in the evaporation rate of the continuous phase.

5.2.5 Effect of oil volume fraction on the evaporation rates of creamed oil – in – water emulsions

Figure 5.11 shows a series of experimental and calculated mass versus time plots for a family of hexane – in – water emulsions stabilised with the sugar surfactant n-decyl-β–D- glucopyranoside. The parameters used to calculate the theoretical fits are given in Table 5.5.

Table 5.5 Parameters used to calculate the theoretical mass versus time plots shown in Figure 5.11.

Vol% hexane	$m_{o,d}/g$	$m_{o,c}/g$	f
19	0.4284	2.7721	0.505
26	0.5977	2.6028	0.495
29	0.6898	2.5950	0.574
47	1.2284	2.0811	0.605
67	1.7432	1.2909	0.536

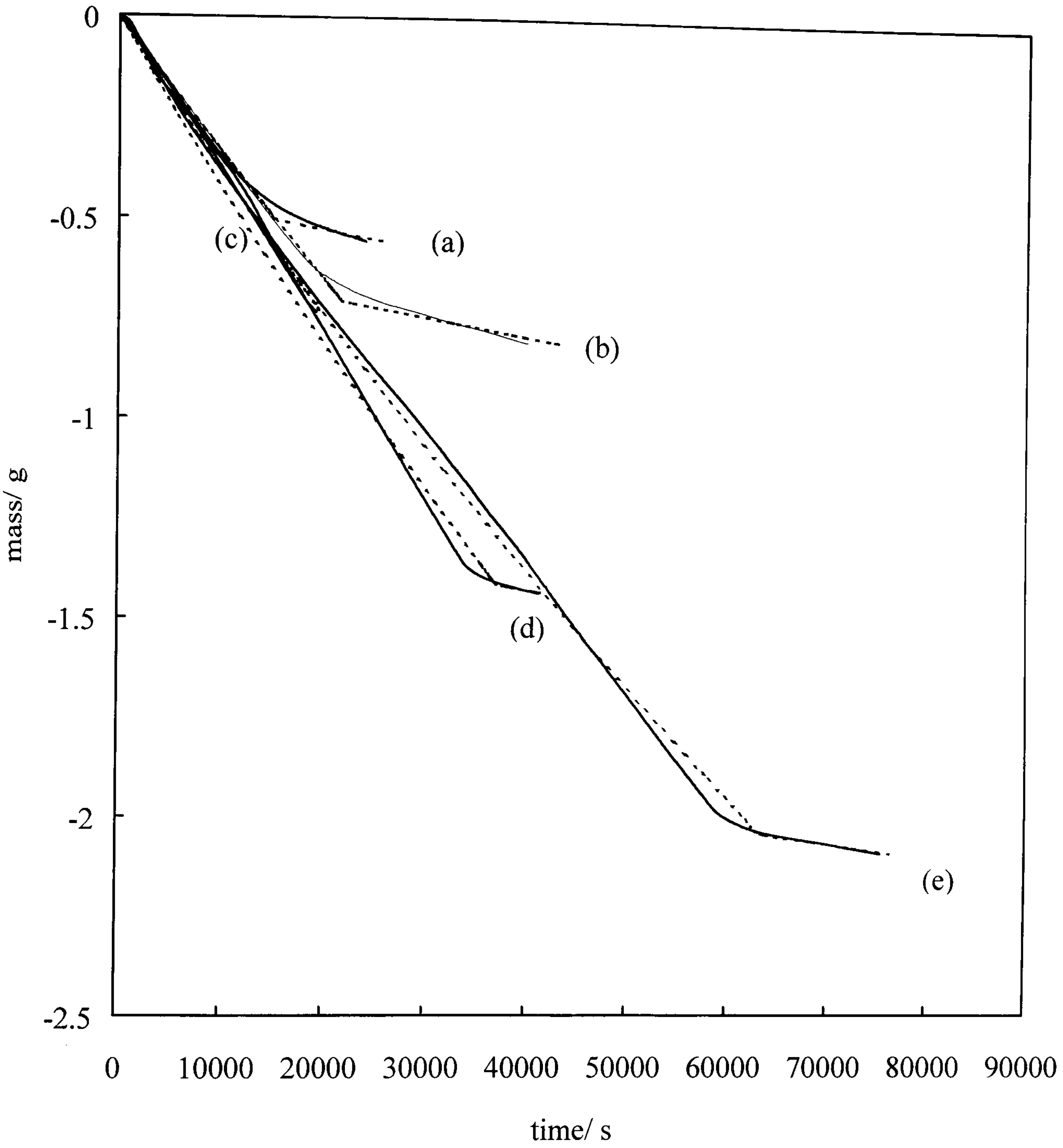

Figure 5.11 *Mass versus time plots for different oil volume percent n-hexane – in – water emulsions stabilised with 20 mM β-decyl gluco-pyranoside evaporated at 25°C and 1920 ml min^{-1} nitrogen gas flow rate. The oil contents of the emulsions are (a) 19%, (b) 26%, (c) 29%, (d) 47% and (e) 67%. Calculation of the theoretical fits (shown as dashed lines) was carried out using the parameters given in Tables 5.2 and 5.5.*

It can be seen that variation of the overall volume fraction of oil in the emulsion produces no significant change in *f*. The poor comparison between theoretical and experimental plots and the minor differences in *f* values seen can be attributed to foam formation on the emulsion surface. Visual investigation of the emulsion samples showed that an increase in volume fraction of oil is accompanied by an increase in volume of the creamed layer. Both results indicate that a non-foaming emulsion would show no change in *f* with volume fraction. Recent experiments in which foaming problems have been eliminated have confirmed this finding[11].

5.3 Evaporation rates of sedimented oil – in – water emulsions

For an emulsion in which the dispersed phase is more dense than the continuous phase, sedimentation occurs. In the case of a volatile oil, a typical mass versus time curve is expected to be the opposite of that seen for creamed oil – in – water emulsions. In this section, the model is modified for application to sedimented systems and some preliminary measurements are reported.

5.3.1 Modification of the model to predict the evaporation rate of a sedimented oil – in – water emulsion

For a sedimented emulsion system, the relationship between mass and time for the upper layer is given by

$$t = \frac{RT\left(h_x - \left(m_{o,d}\,\rho_d / A\right)\right)}{M_c A D_c P_c z_c}\left(m_{o,c} - \left(m_{o,c} + m_{e,b}\right)\right) - \frac{RT}{2\rho_c M_c A D_c P_c z_c}\left({m_{o,c}}^2 - \left(m_{o,c} + m_{e,b}\right)^2\right)$$

[5.26]

which is analogous to Equation [5.2]. Equation [5.26] is valid until the upper layer of the emulsion has evaporated. This does not correspond to the complete loss of the continuous phase, however, since the sedimented layer contains both dispersed and continuous phase. The mass of continuous phase within the sedimented layer, $m_{c,s}$ is given by

$$m_{c,s} = (1 - \phi)m_{o,d} \qquad [5.27]$$

where ϕ is the volume fraction of oil in the sedimented layer. Therefore, the critical mass at which Equation [5.26] becomes invalid is given by the expression

$$m_{e,b}' = -\left(m_{o,c} - \left((1 - \phi)m_{o,d}\right)\right) \qquad [5.28]$$

Substitution of Equation [5.28] in Equation [5.26] gives t_s for a sedimented emulsion

$$t_s = \frac{RT\left(h_x - \left(m_{o,d}\rho_d / A\right)\right)}{M_c A D_c P_c z_c}\left(m_{o,c} - \left(m_{o,c} + m_{e,b}{}'\right) - \frac{RT}{2\rho_c M_c A D_c P_c z_c}\left(m_{o,c}{}^2 - \left(m_{o,c} + m_{e,b}{}'\right)\right)^2\right) \qquad [5.29]$$

Beyond t_s, the evaporation of the emulsion is given by the sum of the evaporation of continuous phase and dispersed phase using a slightly modified version of Equation [5.18].

Figure 5.12 shows the mass versus time and evaporation rate versus time plots for a 50 vol% 1-bromobutane in water emulsion stabilised with SDS. The plots are characterised by a slow initial evaporation rate corresponding to the loss of the less volatile continuous phase and a faster rate when the oil-rich layer is depleted. The agreement between the experimental data and the calculated fit is poor in comparison to that for creamed emulsions. The differences can be seen more clearly in the rate versus time plot, where there are two notable features. Firstly, the change between the rate for the continuous and sedimented layers is more gradual than predicted. The explanation for this is not immediately obvious. The fact that the same phenomenon is not seen for the layered systems discussed in Section 5.1 indicates that the effect is not due simply to diffusion of 1-bromobutane into the water layer. Further investigation is required to fully explain these results.

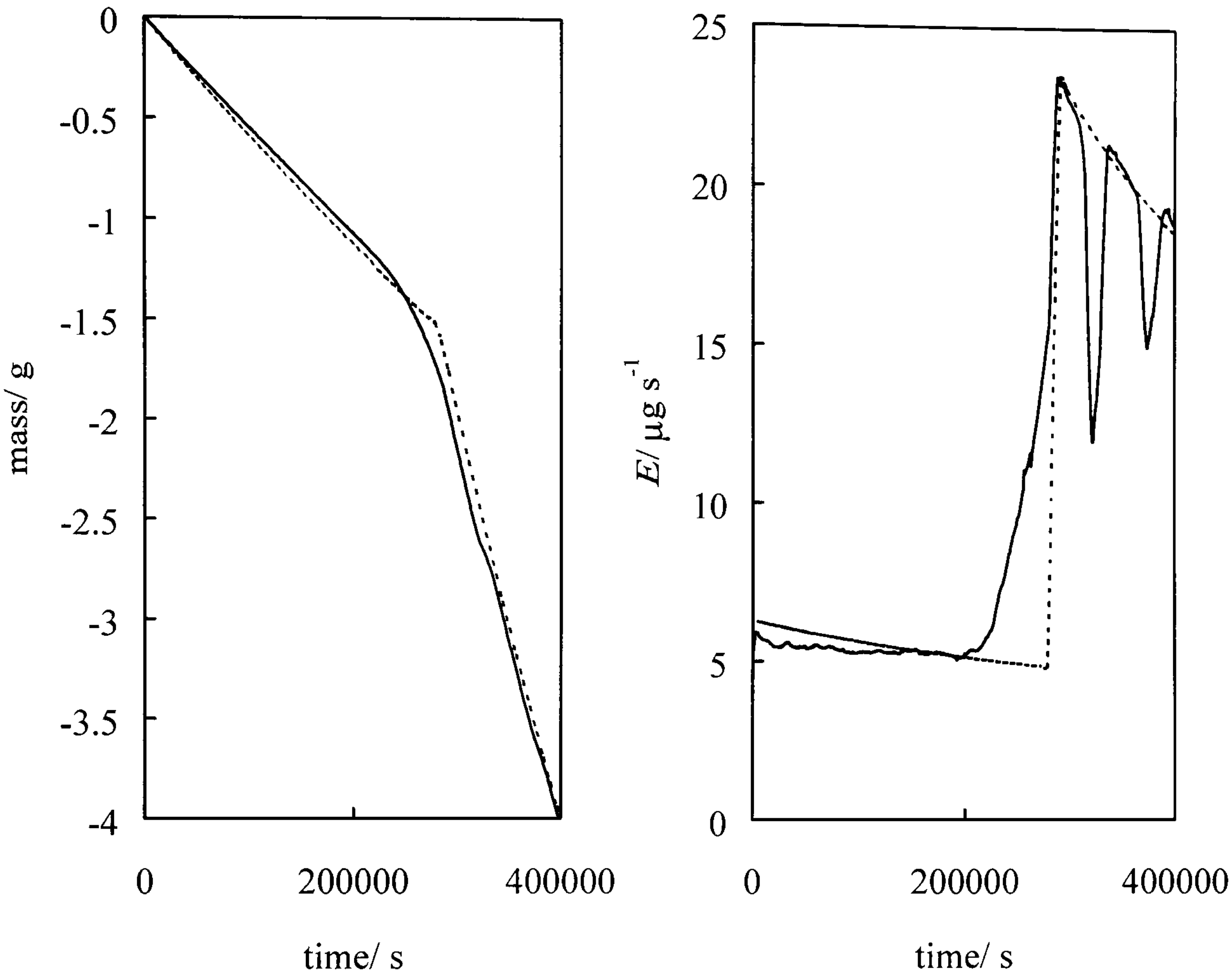

Figure 5.12 ***Mass versus time and evaporation rate versus time plots for a sedimented 50 vol% 1 – bromobutane in water emulsion stabilized with 20 mM sodium dodecyl sulphate, evaporated at 25.0 °C. The full lines are the experimental data, whilst the dashed lines are the calculated fit obtained for Equations [5.18] and [5.29]. The values of $m_{o,c}$ and $m_{o,d}$ were 2.0089 g and 3.1718 g respectively. D_c was 2.15×10^{-5} m^2 s^{-1} and D_d was 7.15×10^{-6} m^2 s^{-1}. The molar masses, densities and vapour pressures for the two components can be found in Table 5.1. Best fit values of ϕ and f were 0.85 and 1 respectively.***

Secondly, the evaporation rate of the lower layer is characterised by a series of peaks. The reason for this is not apparent, but it is likely that this is related to the stability and structure of the sedimented layer. Visual investigation of these emulsion samples revealed that the sedimented layer appeared to have "cracks" containing continuous phase only. It is postulated that the drops in evaporation rate seen correspond to these cracks. The fact that the evaporation rate does not fall to that of the pure continuous phase may be due to a large amount of solubilised 1-bromobutane in the liquid contained in these regions. This theory is supported by the fact that the "troughs" in the plot correspond to higher evaporation rates at longer times. A similar stratification process has been reported for sedimenting clay suspensions[12].

It is interesting to note that the best-fit f value in this case is equal to 1, indicating that the sedimented emulsion does not experience a significant barrier to evaporation. The high solubility of 1-bromobutane in water (58.5 g per 10^6 g as compared to 47.3g per 10^6 g for toluene[13], which has an f value of 0.918) may explain this observation. In addition, the best fit value of ϕ is higher than 0.74, the volume fraction expected for close-packing of spherical, monodisperse droplets[14]. This suggests that the oil droplets experience deformation within the sedimented layer.

5.3.2 Effect of oil volume fraction on the evaporation rate of sedimented oil – in – water emulsions

Figure 5.13 shows a series of experimental and calculated mass versus time curves for different oil volume fraction 1- bromobutane in water emulsions stabilised with SDS. The additional parameters required to calculate the theoretical fit are given in Table 5.6.

Table 5.6 Parameters used to calculate the theoretical mass versus time plots shown in Figure 5.13.

Volume fraction 1-bromobutane	$m_{o,d}/g$	$m_{o,c}/g$	ϕ	f
0.40	2.0458	2.4994	0.81	0.90
0.55	3.1718	2.0089	0.85	1.00
0.71	3.6792	1.2005	0.90	0.93
0.80	4.0683	0.8011	0.91	0.94
0.83	4.5676	0.7303	1.00	1.00

It is interesting to note that it is possible to prepare emulsions of very high volume percentage oil in which the oil droplets must undergo deformation. The preliminary nature of these experiments is reflected both in the variation of ϕ with volume fraction and in the behaviour of the 83 vol% emulsion.

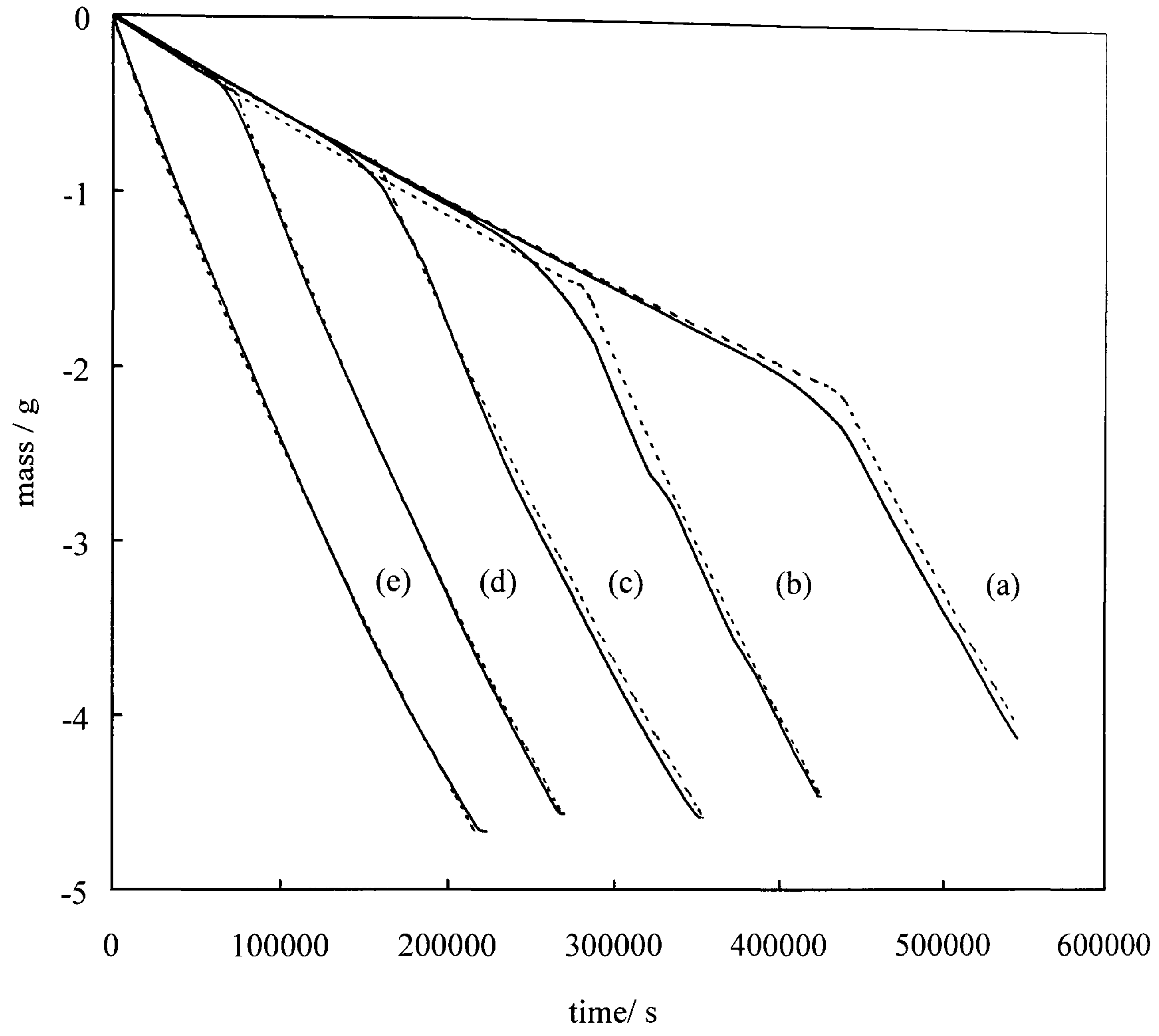

Figure 5.13 ***Experimental and calculated mass versus time plots for a family of different oil volume percent 1- bromobutane in water emulsions stabilised using 20 mM sodium dodecyl sulphate evaporated at 25.0°C and 1920 ml min^{-1} nitrogen gas flow rate. The full lines are the experimental data and the dashed lines the calculated fits. The oil contents of the emulsions are (a) 40%, (b) 55%, (c) 71%, (d) 80% and (e) 83%. The calculated fits were obtained using the parameters given in Tables 5.2 and 5.6. Diffusion coefficients for 1- bromobutane and water are as given for Figure 5.12.***

Here, the oil-rich region of the emulsion has the same evaporation rate as pure 1-bromobutane and the best theoretical fit is obtained when ϕ and f are set to 1. Further work is necessary to fully understand these systems. However, the variation in f is small relative to the effects seen for different oil solubilities in creamed emulsions. It is likely that evaporation rate is independent of volume fraction of oil in the emulsion.

5.3.3 Delayed release of a volatile species by water evaporation

The work reported in sections 5.1 and 5.3 shows that the evaporation of a volatile species denser than water can be delayed in a controllable manner. By using several sample tubes containing mixtures of different compositions, complex but predictable evaporation rate profiles can be obtained in which rates increase after a timed delay. This is highly unusual in conventional systems. Figure 5.14 shows the experimental arrangement used to investigate this idea. The single sample tube used for most measurements is substituted by two smaller tubes.

The mass versus time and evaporation rate versus time plots for a system consisting of two tubes, one containing an 80 vol% 1-bromobutane in water emulsion and the other containing the same volume of 17 vol% 1-bromobutane in water emulsion, are shown in Figure 5.15. The theoretical fit is obtained by adding the expected plots for the individual tubes. Parameters required for the calculation are given in Table 5.7.

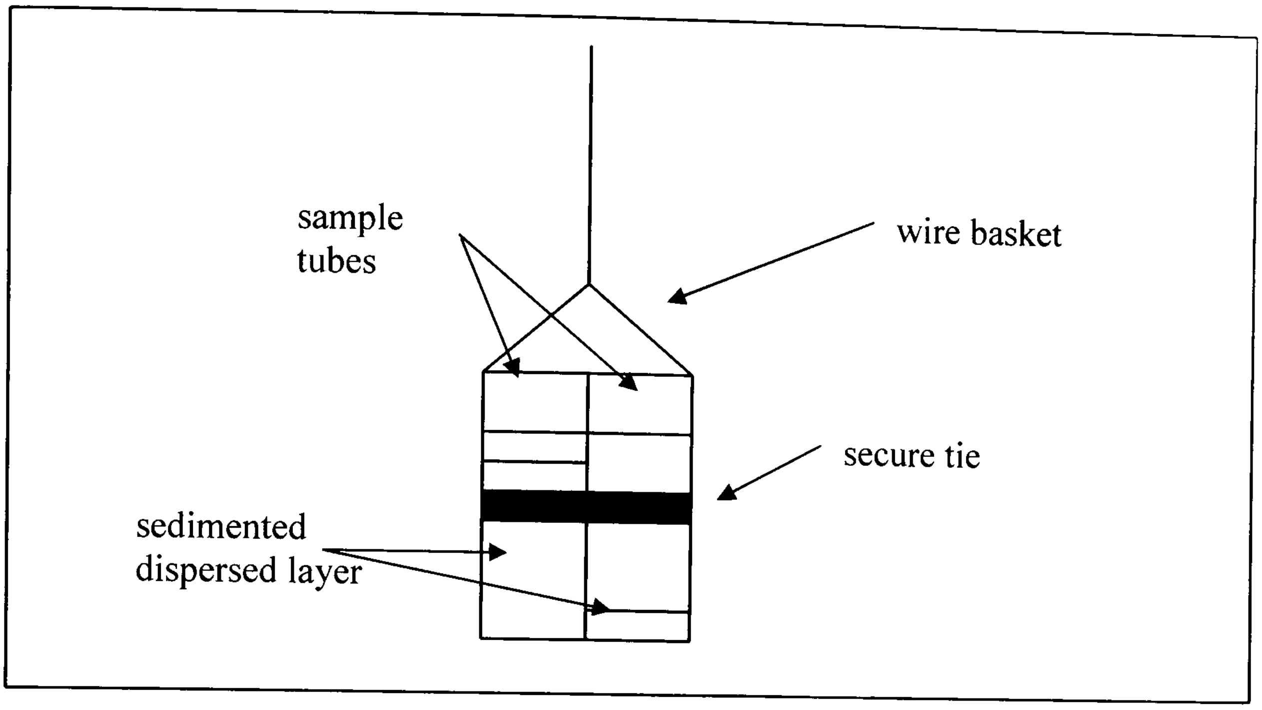

Figure 5.14 ***Schematic diagram showing the two sample tube arrangement used for the time delay sequenced evaporation.***

Table 5.7 ***Parameters used to calculate the theoretical mass versus time plots shown in Figure 5.15.***

Vol% 1-bromobutane	$m_{o,d}/g$	$m_{o,c}/g$	ϕ	f
17	0.3097	1.5120	0.92	1.00
80	1.4574	0.3643	0.85	1.00

The model predicts that the initial evaporation rate will be that of water evaporating from an area equal to the sum of the areas of the two tubes. In practice, the initial evaporation rate is intermediate between that expected for water and that of 1-bromobutane.

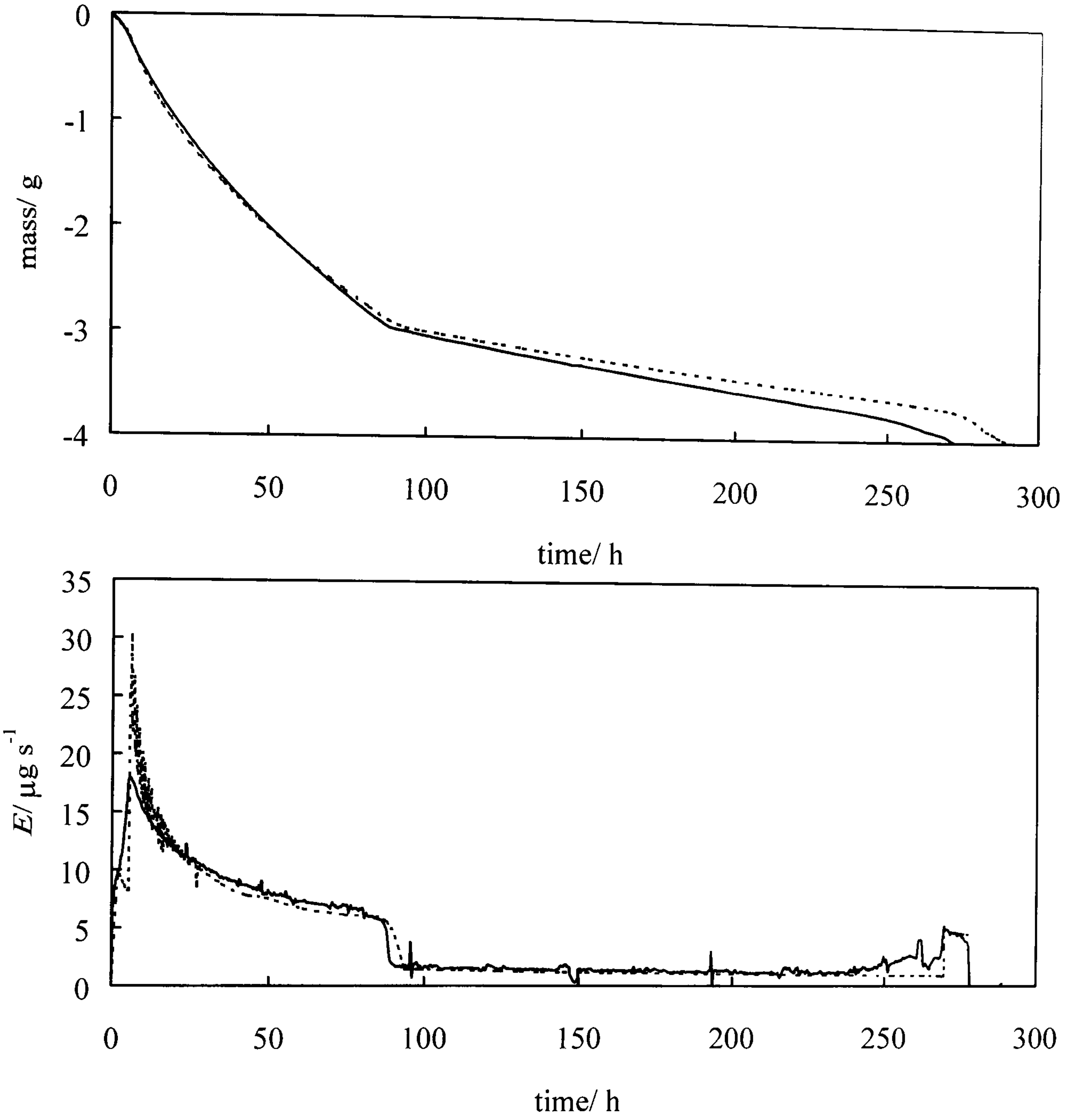

Figure 5.15 ***Mass versus time and evaporation rate versus time plots for a two tube arrangement containing an 80 vol% and a 17 vol% 1-bromobutane in water sedimented emulsion. The full lines are the experimental data, whilst the dashed lines are the calculated fits obtained as described in the text. Parameters required for the calculation are given in Tables 5.3 and 5.7. Diffusion coefficients for 1-bromobutane and water are as given for Figure 5.12. Both sample tubes had h_x = 37.30 mm and A = 5.64 x 10^{-5} m^2.***

The rate increases gradually over the first 5 hours of the experiment. This corresponds with the time taken to deplete the upper layer of the 80 vol% emulsion. At this point, the evaporation rate is approximately equal the sum of the rates for pure 1-bromobutane from one tube and water from the second tube. The evaporation rate falls as predicted until 90 hours have passed, when the sedimented layer of the 80 vol% emulsion has been depleted. From 90 to 250 hours the evaporation rate is low, and corresponds to loss of the continuous phase from the 10 vol% emulsion. Beyond 250 hours, the rate gradually increases until it reaches that of pure 1-bromobutane. This corresponds to complete depletion of the upper layer. Evaporation continues at this rate until both tubes are empty.

The preliminary model offers an approximation of the evaporation rate profile, but further investigation of transport mechanisms in sedimented emulsions is necessary to improve accuracy. It is worth noting here that the model would be expected to show greater accuracy if the experiments were repeated using the layered systems discussed in Section 5.1.

5.4 Evaporation rate of a gelled emulsion

It is well documented that the release of an active component from a gelled emulsion is significantly slower than from an ungelled emulsion containing the same dispersed and continuous phases [15, 16]. Gelling prevents the sedimentation and creaming processes, and gives a more uniform release.

In the final section of this chapter, a simple model for the prediction of the evaporation profile of a gelled emulsion is compared against experimental data obtained for a oil – in – water emulsion which has been gelled with carrageenan. The carrageenan swells as it takes up the continuous phase and eventually forms a homogeneous colloidal solution. The emulsion droplets are dispersed throughout this gel network. In contrast to ungelled emulsion where the continuous phase experiences no barrier to evaporation, the evaporation of both the continuous and dispersed phases are likely to be limited by the time taken for diffusion through the gel structure. It is worth noting that the liquid depth should vary only slightly throughout the evaporation process. Therefore, the vapour flux of both oil and water should remain approximately constant with time.

5.4.1 Modification of the model to predict the evaporation rate of a gelled emulsion

For a gelled emulsion, loss of both the continuous and dispersed phases occurs initially. The evaporation rate of the emulsion is given by the sum of these two losses. In this model, *h* is assumed not to vary throughout the evaporation process. Thus, the evaporation of the emulsion is given by

$$E_{em} = \left(\frac{-f_c dm_c}{dt} - \frac{f dm_d}{dt} \right) = \left(\frac{f_c M_c A D_c P_c z_c}{h_x RT} + \frac{f M_d A D_d P_d z_d}{h_x RT} \right) \qquad [5.30]$$

where f_c is the evaporation barrier experienced by the continuous phase.

Equation [5.30] is valid until the dispersed phase has been completely depleted. The evaporation rate after this time is due only to the loss of the continuous phase and is given by

$$E_{em} = f_c\left(\frac{-dm_c}{dt}\right) = f_c\frac{M_c A D_c P_c z_c}{h_x RT} \qquad [5.31]$$

Integration of Equations [5.30] and [5.31] will give the relationship between between $m_{e,b}$ and t for the gelled emulsion.

Before the dispersed phase is depleted

$$t = \frac{f' h_x RT m_{e,b}}{M_d A D_d P_d z_d + M_c A D_c P_c z_c} \qquad [5.32]$$

where f' is a combination of the evaporation barriers experienced by the continuous and dispersed phases.

After depletion of the dispersed phase

$$t = \frac{f_c h_x RT(m_{e,b} - m_d^o)}{M_c A D_c P_c z_c} + t_c \qquad [5.33]$$

where t_c is the time at which the dispersed phase has fully evaporated.

Figure 5.16 shows the evaporation rate versus time and mass versus time plots for a gelled 20 vol% n-hexane – in – water emulsion stabilised with 20 mM SDS. The evaporation rate versus time plot shows an approximately constant rate up to 200,000 s (approximately 2.5 days). This supports the theory that there is no significant change in emulsion height throughout the evaporation. In this region, $f' = 0.16$.

Beyond this time, (assumed to be t_c), the evaporation rate first falls and then stabilises at a value of $f_c = 1.63$. It is notable that the evaporation rate in this region is significantly higher than that of the pure continuous phase. This would indicate that the rate reduction does not correspond to full depletion of the volatile oil. It is possible that the evaporation of the continuous phase causes the gel to "shrink". Both oil and water diffusing from the shrunken gel would have a more tortuous diffusion path and therefore the evaporation rate would decrease.

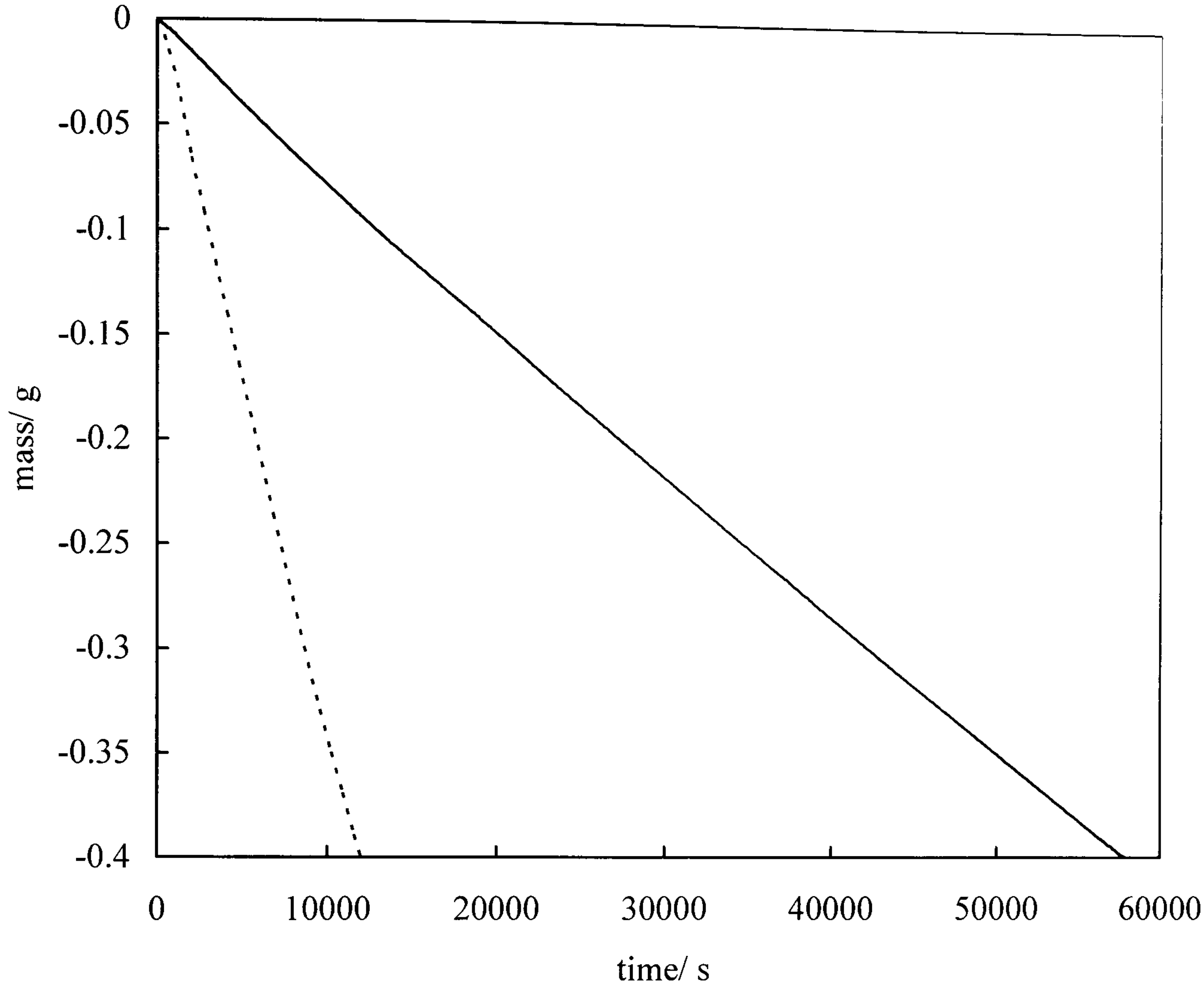

Figure 5.16 ***Mass versus time plot for a gelled n-hexane – in – water emulsion stabilised with 20 mM sodium dodecyl sulphate evaporated at 25.0°C and 1920 ml min^{-1} nitrogen gas flow rate. The solid lines are the experimental data, whilst the dashed lines are calculated using Equations [5.30] – [5.34]. For n-hexane, $m_{o,d}$ = 0.5238 g. All other parameters are given in Table 5.1. Values of f' and f_c were found to be 0.159 and 1.620 respectively.***

It is interesting to compare the behaviour of the gelled emulsion system with that of the n-hexane gels described in Chapter 4, where no significant reduction in evaporation rate was seen until long times. The structures of the two gels are very different. In the n-hexane gels, silica particles form a separate and immiscible phase. In the emulsion gels both evaporating species are held within a rigid three-dimensional gel structure. It is the high degree of structure which causes the lowering in evaporation rate.

This preliminary experiment has shown that the evaporation rate of an emulsion is significantly slowed by gelling. However, further work is required to develop a model which accurately predicts the evaporation profile for a gelled system.

5.5 Conclusions

For immiscible layered systems, the evaporation rates of both components are limited by vapour diffusion rates across the stagnant layer. The less dense liquid behaves as a physical barrier to the evaporation of the more dense liquid.

A model has been developed which predicts the evaporation rate of a creamed oil – in – water emulsion. The evaporation rate of the aqueous continuous phase is virtually identical to that of pure water, whereas the rates for dispersed oil drops may be retarded. Rates for different emulsified oils are consistent with a mechanism in which the oil drops remain separated from the vapour phase by a thin water film at the emulsion surface. Oil transport from the emulsion drops to the vapour occurs by diffusion of dissolved oil across the water film. The thickness of the water film is determined by the colloidal forces. Therefore, the evaporation rate of creamed oil drops is influenced primarily by the solubility of the oil and the nature of the surfactant.

For sedimented systems, the upper layer of continuous phase acts as a physical barrier to the evaporation of the volatile oil. For the 1-bromobutane emulsions studied here a gradual increase in evaporation rate is seen as the lower layer is approached, which may be attributed to solubilisation of the oil in surfactant micelles. Combinations of sedimented systems can be used to engineer complex evaporation profiles.

Gelling significantly lowers the evaporation rate of creamed oil – in – water emulsions. The diffusion of the continuous and dispersed phases is hindered by the gel structure.

5.6 References

1. "*Selected Values of Properties of Hydrocarbons and Related Compounds*". Thermodynamics Research Centre, AP144, Texas A&M University, 1978.
2. "*CRC Handbook of Chemistry and Physics*", CRC Press Inc., Boca Raton, 62nd edn., 1981.
3. G. A. D. McD. Cummings and A. R. Ubbelohde, *J. Chem. Soc.*, 1953, 3751.
4. R.C. Reid, J. N. Prautsnitz and T. K. Sherwood, "*The Properties of Liquids and Gases*", 3rd edn., McGraw-Hill, 1977.
5. S. E. Friberg and I. Kayali, *J. Pharm. Sci.,* 1989, **78**, 639.
6. S. E. Friberg and B. Langlois, *J. Dispersion Sci. Technol.,* 1992, **13**, 223.
7. B. R. C. Langlois and S. E. Friberg, *J. Soc. Cosmet. Chem.,* 1993, **44,** 23.
8. R. Aveyard, B. P. Binks, P. D. I. Fletcher, T. G. Peck and C. E. Rutherford, *Adv. Colloid Interface Sci.,* 1994, **48**, 93.
9. L. Lobo and D. T. Wasan, *Langmuir*, 1998, **9**, 1668
10. V. Bergeron, M. E. Fagan and C. J. Radke, *Langmuir*, 1993, **9**, 1704.
11. I. Aranberri, K. J. Beverley, B. P. Binks, J. H. Clint and P. D. I. Fletcher, *Langmuir*, 2002, **18**, 3471..
12. W. H. Brewer, *Clays Clay Miner.* 1884, **13**, 395.
13. http://www.flash.net/~defilip1/solubility.htm. Louis DeFilippi, Louis DeFilippi, LLC; all rights reserved
14. http://www.math.lsa.umich.edu/~hales/countdown/

15. K. G. Das (Ed.), "*Controlled Release Technology*", John Wiley and Sons Inc., New York, 1983.

16. Eric Dickinson, "*An Introduction to Food Colloids*" Oxford University Press, 1992.

CHAPTER 6

CONCLUSIONS AND SUGGESTIONS FOR FURTHER WORK

In this study, a new experimental technique for the measurement of the evaporation rates of volatile species from a wide range of formulations has been developed and tested. The experimental apparatus has been shown to provide accurate and reproducible results for a range of pure liquids. The evaporation rate of a pure liquid is limited by diffusion through a stagnant vapour layer at the liquid surface. and is easily predicted using Fick's Laws of Diffusion.

The combination of the equation developed to predict the evaporation rate of a pure liquid with the Kelvin Equation enables the quantitative comparison of the evaporation rates of water contained in different pore size solid particles for the first time. In the simple systems reported here, the evaporation rate of water is limited by diffusion through the stagnant vapour layer at the liquid surface. The vapour pressure of a liquid under a curved surface is reduced from that under a flat surface, and a consequent lowering in the evaporation rate is seen. The prediction of evaporation rate could be made more relevant to the assessment of hazards arising from volatile liquid spillages which have been absorbed onto porous solids by replicating the experiments using liquids with a range of contact angles and volatilities.

The work reported on the evaporation of squalane/ alkane mixtures shows that the evaporation rate is again limited by diffusion across the stagnant vapour layer at the liquid surface. Mixing within the liquid mixture is rapid relative to this process. The evaporation rate of the mixtures has been shown to be proportional to the vapour pressure of the mixture, and is therefore composition dependent.

The evaporation rate of n-hexane gelled with silica particles is similar to that of pure ungelled hexane. The vapour pressure of hexane is uninfluenced by the addition of the silica particles. The evaporation rate deviates slightly from that of the pure liquid as the measurement proceeds. These deviations are likely to arise from (i) the presence of loose silica powder on the liquid surface and (ii) lowering of the vapour pressure of hexane contained in highly curved liquid bridges between the silica particles.

Water evaporation rates from mixtures with the non-ionic surfactant $C_{12}E_6$ have been measured. The rates are seen to be reduced to approximately 10% of the rate predicted for a mechanism where diffusion through the stagnant vapour layer is rate-limiting. This reduction is likely to be the result of the development of concentration gradients in the liquid mixture. The time taken for the concentration gradients to relax is slow relative to the time taken for diffusion through the vapour layer. No correlation has been found between the reduction in evaporation and the mesophase structure.

Previous work has shown that bulk evaporation from thin layers is slowed by the presence of a lamellar liquid crystal mesophase[1]. It would be interesting to compare the evaporation characteristics of an emulsion system from a thin layer with the results obtained using the experimental apparatus detailed in this thesis. A combination of the two methods may yield a quantitative measure of the retarding effect of the lamellar liquid crystal phase.

The evaporation rates of two-component immiscible liquid mixtures have been modelled and determined experimentally. The rate of the upper layer is limited by diffusion through the stagnant vapour layer at the liquid surface. The less dense liquid acts as a physical barrier to the evaporation of the more dense liquid. For a mixture where the more volatile species is more dense than the less volatile species, the mutual solubility of the two liquids may influence the evaporation rate of the mixture as the lower layer is approached. Currently, there is no experimental evidence to support this hypothesis.

A model has been developed which predicts the evaporation rate of a creamed oil – in – water emulsion. This model has allowed quantification of the barrier to evaporation experienced by oil drops in emulsions for the first time.

The evaporation rates for different emulsified oils are consistent with an evaporation mechanism in which the oil drops remain separated from the vapour phase by a thin water film at the emulsion surface. Oil transport from the drops to the vapour occurs by diffusion of dissolved oil across the water film. The thickness of the water film is determined by the colloidal forces. Therefore, the evaporation rate of oil from a creamed emulsion is influenced primarily by the solubility of the oil and the nature of the surfactant. The evaporation rate of the continuous phase is virtually identical to that of bulk water. Since the experimental work for this thesis was completed, further studies have quantified the barrier to evaporation/in terms of the oil solubility, water film thickness and oil diffusion rate through the water film[2]. Studies into the evaporation rates of emulsions stabilized with solid particles are ongoing.

Early work on evaporation from sedimented emulsions has yielded some promising results. The experiments indicate that the upper layer of continuous phase acts as a physical barrier to the evaporation of the oil-rich phase. For the 1-bromobutane emulsions studied here, a gradual increase in evaporation rate is seen as the lower layer is approached. This may be attributed to the high solubility of the oil in the continuous phase. Further work is needed to obtain an better understanding of the evaporation mechanism for these emulsions.

Preliminary results for gelled emulsions indicate that the gelling process significantly lowers the evaporation rate of an oil – in – water emulsion. Both dispersed and continuous phases experience a barrier to evaporation which is likely to result slow diffusion through the gel structure. Further work may establish how oil drops are released from gelled emulsions.

As yet, water – in – oil emulsions have not been studied. The mechanisms for water drop release from such systems are likely to be very different to the mechanisms for oil drop release from oil – in – water emulsions. It would be interesting to extend the study reported here to cover this class of emulsions.

6.1 References

1. B. R. C. Langlois and S. E. Friberg, *J. Soc. Cosmet. Chem.*, 1993, **44**, 23.2.
2. I. Aranberri, K. J. Beverley, B. P. Binks, J. H. Clint and P. D. I. Fletcher. *Langmuir*, 2002, **18**, 3471.

APPENDIX 1

1. SoftwareWedge^{TM}

The SoftwareWedge^{TM} software provides a simple method of connecting any RS232 instrument to a PC and reading from or writing to the instrument from within any Windows application.

1.1 Configuring a Precisa 125A Balance to a 486 PC using SoftwareWedge^{TM} with EXCEL to log and plot mass versus time curves.

1.1.1 Balance settings

In order to connect the balance and computer, it is necessary to have a cable (25 pin female to 25 pin male) connected from the COM2 port of the PC to the RS232 connector of the balance. The pins used in the cable connections are shown in Table 1.1.

Table 1.1: Pin connections from balance to PC

Male pin number (balance)	Female pin number (PC)
2	3
3	2
6	20
7	7

1.1.2 Balance Settings

Exact balance displays vary from model to model, but for the Precisa 125A Balance, the following settings should be used. Details on how to configure the balance can be found in the Precisa manual[1].

Balance unit	Unit1g
Calibration	cal ext
Baud Rate	9600 bdr
Parity	PAr odd
Print	Print UST
Combined print function	Prt-ALL on
Delayed printout	Prt-dEL off
Good laboratory practice	Glp-off
Last digit	LASt d on
Auto zero	A-ZEro oFF
Date setting	SEt D+T
Anti-theft coding	SetPrO TEC
Auto standby mode	A-Stby off
Menu latch	LAtch off
Status print	StAtUS Prt

1.13 Automatic running of SoftwareWedge^{TM}

The EXCEL file used to run the data logging and plotting in PRELOG.xls, which contains the correct VBA module to automatically run SoftwareWedge^{TM}. The directory containing PRELOG.xls must also contain the EXCEL template file PRECISA2.xlt.

VBA Module PRELOG.xls

```
Public Const MyPort$ = "Com2"

Sub getdata()
   Range("a11", "b2000").Value = ""
   Static RowPointer As Long, ColPointer As Long
   RowPointer = 11: ColPointer = 1
   dt = [$C$11]
   time0 = Timer
   timelast = Timer
100 timec = Timer
   STO$ = INKEY$
   If STO$ = Chr$(27) Then GoTo 300
   If (timec - timelast) > dt Then GoTo 200 Else GoTo 100
200 ChannelNum = DDEInitiate("WinWedge", "Com2")
   Application.DDEExecute ChannelNum,
"[SENDOUT('P0',13,10)]"
   Application.Wait Now + TimeValue("00:00:01")
   F1 = DDERequest(ChannelNum, "Field(1)")
   WedgeData$ = F1(1)
   DDETerminate ChannelNum
   Sheets("Sheet1").Cells(RowPointer, ColPointer).Formula =
(Timer - time0)
   Sheets("Sheet1").Cells(RowPointer, ColPointer +
1).Formula = WedgeData$
   RowPointer = RowPointer + 1
   timelast = Timer
   GoTo 100
300 RowPointer = 11
   ColPointer = 1
```

```
End Sub

Sub Auto_Open()
   Toolbars("Standard").Visible = False
   Toolbars("Formatting").Visible = False
   On Error GoTo ErrorHandler
   AppActivate "Software Wedge-" + MyPort$
   On Error GoTo 0
   AppActivate Application.Caption
   Exit Sub
ErrorHandler:
   RetVal = Shell("C:\WINWEDGE\WINWEDGE.EXE
C:\WINWEDGE\Precisa.SW1", 4)
   If RetVal = 0 Then
   Beep
   MsgBox ("Cannot find WinWedge.Exe")
   Exit Sub
   Else
   Application.Wait Now + 0.00002
   End If
   Resume Next
End Sub

Sub Auto_Close()
   Toolbars("Standard").Visible = True
   Toolbars("Formatting").Visible = True
   On Error Resume Next
   chan = DDEInitiate("WinWedge", MyPort$)
   DDEExecute chan, "[Appexit]"
End Sub
```

2. VBA Macros generating theoretical data.

2.1 Macros used for the evaluation rates of $C_{12}E_6$/ water mixtures.

2.2.1 Raw data binning program.

The experiments carried out on the $C_{12}E_6$/ water mixtures described in Chapter 4 generated a large number of data points. A visual basic program was written to ‘bin’ the data to make them more manageable.

```
Function bin()
nbin = [g3]
ndata = 2635

'For x = 1 To ndata Step 1
'Range("sheet1!e" & (5 + x)).ClearContents
'Range("sheet1!f" & (5 + x)).ClearContents
'Next x

stopm = (ndata / nbin)
For m = 1 To stopm Step 1
bintime = 0
binmass = 0
For n = 1 To nbin Step 1
bintime = bintime + Range("sheet1!c" & (5 + (m - 1) * nbin +
n)).Value
binmass = binmass + Range("sheet1!b" & (5 + (m - 1) * nbin
+ n)).Value
Next n
Range("sheet1!e" & (5 + m)).Value = bintime / nbin
Range("sheet1!f" & (5 + m)).Value = binmass / nbin
Next m
End Function
```

2.2.2 Calculation of the activity coefficient of water in the $C_{12}E_6$/ water mixtures

```
Function gammaw(Xw)
startbreak = 0.8203
endbreak = 0.809
actbreak = 0.84492
If Xw <= 1 And Xw >= startbreak Then GoTo 100
If Xw <= startbreak And Xw >= endbreak Then GoTo 200
If Xw <= endbreak And Xw >= 0.08 Then GoTo 300
100 gamma = 115.2611 * Xw ^ 4 - 446.2241 * Xw ^ 3 +
640.7014 * Xw ^ 2 - 404.9035 * Xw + 96.16506
GoTo 500
200 gamma = actbreak / Xw
GoTo 500
300 gamma = 20.14592 * Xw ^ 5 - 57.55524 * Xw ^ 4 +
65.21757 * Xw ^ 3 - 37.02639 * Xw ^ 2 + 10.36538 * Xw +
0.027823
GoTo 500
500 gammaw = gamma
End Function
```

2.2 Macros used for the evaporation rates of oil and water layered mixtures

The VBA macro tmcalc calculates the time taken for the evaporation of both layers of an oil and water mixture.

```
Function tcalc(deltam, mwupper, rupper, pupper, moupper, dupper,
          mwlow, rlow, plow, molow, dlow)
R = [a4]
T = [b4]
A = [f4]
ht = [e4]
patm = 101325
mwupper = mwupper / 1000
mwlow = mwlow / 1000
moupper = moupper / 1000
molow = molow / 1000
deltam = deltam / 1000
mupper = moupper + deltam
zupper = ((patm / pupper) * Application.Ln(1 / (1 - (pupper /
patm))))
htupper = ht - (molow / rlow) / A
If -deltam > moupper Then GoTo 100
```

```
tcalc = ((((R * T * htupper) / (mwupper * A * dupper * pupper *
  zupper)) * (moupper - mupper))) - ((((R * T) / (2 * rupper *
mwupper * A ^ 2 * dupper * pupper)) * (moupper ^ 2 - mupper ^2)))
GoTo 500


100 tupper = ((((R * T * htupper) / (mwupper * A * dupper * pupper
 * zupper)) * (moupper))) - ((((R * T) / (2 * rupper * mwupper * A ^
2 * dupper * pupper)) * (moupper ^ 2)))
mlow = moupper + molow + deltam
zlow = ((patm / plow) * Application.Ln(1 / (1 - (plow / patm))))
tcalc = tupper + ((((R * T * ht) / (mwlow * A * dlow * plow * zlow))
 * (molow - mlow))) - ((((R * T) / (2 * rlow * mwlow * A ^ 2 * dlow
            * plow)) * (molow ^ 2 - mlow ^ 2)))


500 End Function
```

2.3 Macros used in the calculation of the evaporation rates of emulsions.

Macros were written to calculate the evaporation rate versus time and the mass loss versus time data for creamed oil – in – water emulsions.

2.3.1 VBA Macro for the calculation of the evaporation rate versus time data for a creamed oil – in-water emulsion.

```
Function ecalc(m, f, ro, rmo, difo, po, zo, moi, rw, rmw, difw, pw, zw, mwi)
A = [c6]
ht = [d6]
R = [a6]
T = [b6]
alpha = rmw * difw * pw * zw
beta = rmo * difo * po * zo * f
mo = moi + ((beta * m) / (alpha + beta))
mw = mwi + m - ((beta * m) / (alpha + beta))
h = ht - (mo / (ro * A)) - (mw / (rw * A))
'calculates emulsion rate when oil is present
If mo < 1E-23 Then GoTo 100
ecalc = 1000000000# * (A * (alpha + beta)) / (h * R * T)
```

```
GoTo 500
'calculate emulsion rate when oil has all gone
100 ecalc = 1000000000# * (A * alpha) / ((ht - ((mwi + m+moi) / (rw * A))) * R * T)
500 End Function
```

2.3.2 VBA Macro for the calculation of the mass loss versus time data for a creamed oil in water emulsion

```
Function tmcalc(m, f, ro, rmo, difo, po, zo, moi, rw, rmw, difw, pw, zw, mwi)
A = [c6]
ht = [d6]
R = [a6]
T = [b6]
alpha = rmw * difw * pw * zw
beta = rmo * difo * po * zo * f
mo = moi + ((beta * m) / (alpha + beta))
mw = mwi + m - ((beta * m) / (alpha + beta))
b = (R * T) / (A ^ 2 * (alpha + beta))
c = moi / ro
d = beta / (2 * ro * (alpha + beta))
e = mwi / rw
```

```
j = 1 / (2 * rw)
g = beta / (2 * rw * (alpha + beta))
h = A * ht
i = (R * T) / (alpha * rw * A ^ 2)
x = -(moi * (alpha + beta)) / (beta)
tc = (b * x) * (c + (d * x) + e + (j * x) - (g * x) - h)

'calculates the time taken for emulsion to lose m when oil is present
If mo < 1E-23 Then GoTo 100
tmcalc = (b * m) * (c + (d * m) + e + (j * m) - (g * m) - h)
GoTo 500

'calculates the time taken for emulsion to lose m when oil has been depleted
100 tmcalc = i * ((m * moi) + (m * mwi) + (m ^ 2 / 2) - (m * ht * rw * A) - (x * moi) - (x * mwi) - (x ^ 2 / 2) + (x * ht * rw * A)) + tc
500 End Function
```